MONOBODY BINDING PROTEINS AS BIORECOGNITION ELEMENTS FOR ELECTROCHEMICAL BIOSENSORS

By

Sunanda Dey

A DISSERTATION

Submitted to
Michigan State University
in partial fulfillment of the requirements
for the degree of

Chemical Engineering – Doctor of Philosophy

2024

ABSTRACT

The burden of poor prognosis and high mortality rates associated with complex and aggressive diseases can be reduced with early detection. Biomarker sensing provides a dynamic approach to early diagnosis. However, the lack of a single diagnostic biomarker that can be correlated to a specific disease, there is a need to create a biosensing platform that can detect multiple targets which vary in size and complexity.

To address the need to use stable biorecognition elements for sensing, we have explored the utility of synthetic binding proteins, which are like antibodies in function, except much smaller in size. Small synthetic proteins derived from human fibronectin, also known as monobodies, can act as powerful and highly modular biorecognition elements. Using computational tools such as homology modeling and protein-protein docking, we have identified monobodies with a unique chemistry that have strong binding affinity for specific targets of interest.

In this work, we have developed an innovative electrochemical biosensor that harnesses the modularity of monobodies for the detection of large biomolecules. We used lysozyme as our model target due to its clinical relevance, cost efficiency, and ease of availability. As these monobodies cannot inherently generate any signal on binding with the target, we have functionalized them using NHS-EDC chemistry and electrochemically grafted them on the surface of the electrode. These modifications help generate a readable signal when the biosensor comes into contact with the target of interest.

Immobilization of the monobodies on the surface of the electrode has created a non-conductive layer that impedes electron transfer, thus enabling the selective detection of target molecules. Our findings indicate that this biosensor exhibits high specificity, negligible non-specific adsorption, and exceptional electrical stability, making it a promising tool for accurate

biomolecule detection in complex physiological fluids like serum.

This method offers the potential for multiplexing, enabling the creation of a versatile, adjustable biosensor that can support more accurate prognosis through detecting a range of disease-related biomarkers. The development of this novel protein-electrode interface opens exciting possibilities for improving the performance and reliability of portable diagnostic devices, with significant implications for clinical and analytical applications.

Dedicated to Doll, my sister, the reason why my childhood was beautiful.

জানি দেখা হবে...

ACKNOWLEDGEMENTS

Embarking on my PhD journey was filled with challenges, yet it was immensely gratifying. I have been extraordinarily fortunate to have the support and guidance of wonderful individuals along the way—people I've had the pleasure to meet, collaborate with, and call friends. First, a big thank you to my advisors, Dr. David P. Hickey, and Dr. Daniel R. Woldring. Their guidance was invaluable, not just in my research, but in helping me grow as an individual. Their patience, kindness, and enthusiasm for science inspired me. I couldn't have asked for better mentors.

I want to express my gratitude to my doctoral committee: Dr. Scott C. Barton and Dr. Alex R. Dickson. Their insights, feedback, and mentoring were crucial in helping me navigate through my PhD milestones and I could not thank them enough for all the invaluable advice over the years. I would like to thank the Chemical Engineering and Material Science Department for their resources and support, especially through the ChEMS Graduate Student Association. Being in the GSA was a fantastic way to grow and connect within the MSU community. I am grateful to my wonderful lab mates at both Woldring and Hickey labs. You guys are not only great engineers and scientists but also amazing people! I would also like to thank the Leadership Fellowship Program, where I had the pleasure of working with Dr. Meg Moore. I deeply connected with the program, reflected on my leadership skills, and had the pleasure of making amazing friends outside my program.

I want to express my special thanks to my family away from home; Haritha, Konika, Navya, Avirup, Joydeep, Bismark, Ankita, Dhimaan, Samik Da, Rupa Di, Bharath, Sharmila, Mehrsa and Samriddhi. I will always be thankful for the constant support and love that I received from them throughout the last 4.5 years. Michigan felt warmer because of y’all!

Last, but not least, a big thank you to my parents, my grandmom, and my fiancé and best friend, Souvik. Their love has kept me rooted through all ups and downs. The Ph.D. program has taught me persistence, critical thinking, the value of collaboration, and most importantly patience. I am excited for the opportunities that lie ahead and hopefully can contribute in my own small ways to the scientific community.

Thank you,

Sunand Dey

TABLE OF CONTENTS

LIST OF SYMBOLS & ABBREVIATIONS

A260	Absorbance At 260 Nm
A488	Absorbance At 488 Nm
A647	Absorbance At 647 Nm
ACV	Alternating Current Voltammetry
ADP	Adenosine Diphosphate
ALP	Alkaline Phosphatase
ATP	Adenosine Triphosphate
B1	Binder 1
B2	Binder 2
BD	Becton Dickinson And Co
BLAST	Basic Local Alignment Search Tool
BSA	Bovine Serum Albumin
CDR	Complementarity-Determining Regions
CEA	Carcinoembryonic Antigen
CH_2Cl_2	Methylene Chloride
CH_3CN	Acetonitrile
CV	Cyclic Voltammetry
D_0	Diffusion Coefficient of Oxidized Species
D_2O	Deuterium Oxide
DARPin	Designed Ankyrin Repeat Proteins
DCM	Dichloromethane

DET	Direct Electron Transfer
DM - JLFTET	Dielectric Modulated Junctionless Tunneling FET
DMSO	Dimethyl Sulfoxide
DNA	Deoxyribonucleic Acid
DPV	Differential Pulse Voltammetry
E_0	Standard Potential
EC	Electrochemical-Chemical
ECC	Electrochemical-Chemical-Chemical
ECL	Electrogenerated Chemiluminescence
EDC	1-Ethyl-3-(3-dimethylaminopropyl)carbodiimide
EE	Electrochemical–Electrochemical
EIA	Enzyme Immunoassays
EIS	Electrochemical Impedance Spectroscopy
ELISA	Enzyme Linked Immunosorbent Assays
ENL	Electrochemical–Enzyme Label
ENN	Electrochemical–Enzymatic–Enzymatic
ESI	Electrospray Ionization
FACS	Fluorescence-Activated Cell Sorting
FAD	Flavine Adenine Dinucleotide
$FADH_2$	Flavin Adenine Dinucleotide-Hydrogen
FASTA	Fast Adaptive Shrinkage Threshold Algorithm
FCA	Ferrocene Carboxylic Acid
FET	Field Effect Transistors

FITC	Fluorescein Isothiocyanate
FL063	Lysozyme Binding Monobody
FN3	Fibronectin Type III
FPLC	Fast Protein Liquid Chromatography
GCE	Glassy Carbon Electrode
GMQE	Global Model Quality Estimate
GO_x	Glucose Oxidase
GS	Gly And Ser Residues
HPCC	High Performance Computing Cluster
HRP	Horseradish Peroxidase
IDTDNA	Integrated DNA
ISFET	Ion-Sensitive Field Effect Transistor
K_D	Dissociation Constant
K_M	Michaelis-Menten Constant
LB	Lysogeny Broth
LOD	Detection Limit
LOQ	Quantification Limit
M	Molarity
MB	Methylene Blue
MC	Monte Carlo
MCH	Methylcyclohexane
MET	Mediated Electron Transfer
MWCNT	Multi-Walled Carbon Nanotubes

MX1	Resuspension Buffer
MX2	Lysis Buffer
MX3	Neutralizing Buffer
NAD(P)H	Nicotinamide Adenine Dinucleotide
NHS	N-Hydroxysuccinimide
NMR	Nuclear Magnetic Resonance
NN	Enzymatic–Enzymatic
OD600	Optical Density At 600 Nm
OECT	Organic Electrochemical Transistors
PAGE	Polyacrylamide Gel Electrophoresis
PBS	Phosphate-Buffered Saline
PBSA	2-Phenylbenzimidazole-5-Sulphonic Acid
PCR	Polymerase Chain Reaction
PDB	Protein Data Bank
POCT	Point-Of-Care Testing
PSA	Polar Surface Area
QMEAN	Qualitative Model Energy Analysis
QSQE	Quaternary Structure Quality Estimate
RED	Activity Of the Reduced Species
RNA	Ribonucleic Acid
SCE	Saturated Calomel Electrode
SDS	Sodium Dodecyl Sulfate
SELEX	Systematic Evolution of Ligands by Exponential Enrichment

SG	Sg Yeast Media
SH	Src Homology
SH2	Src Homology 2 Domain
SMTL	Swiss-Model Template Library
SOB	Super Optimal Broth
SOC	Super Optimal Broth with Catabolite Repression
SPE	Solid Phase Extraction
SPR	Surface Plasmon Resonance
SWV	Square Wave Voltammetry
TEER	Transepithelial/Transendothelial Electrical Resistance
THH	Tetra hexahedral
TNF	Tumor Necrosis Factor
V_0	Initial Reaction Rate
VEGF	Vascular Endothelial Growth Factor
VPS	Vinyl Polysiloxane Impression Material
VSP	Voltage-Sensitive Phosphatase
WS	Wash Buffer
XPS	X-Ray Photoelectron Spectroscopy
YPD	Yeast Peptone Dextrose

1. REVIEW OF THE CURRENT TRENDS OF ELECTROCHEMICAL BIOSENSORS

1.1 INTRODUCTION

A biosensor is an analytical tool that combines a biological component (e.g., enzyme, antibody, living organism) with a transducer to produce a signal that is proportional to the concentration of a specific analyte. This union provides a means to convert a biological response into a readable signal, allowing for the detection and quantification of various target molecules. The primary advantage of biosensors is their ability to detect analytes with high sensitivity and specificity in complex matrices, such as blood, urine, or food samples.[1]

Electrochemical biosensors, a subclass of biosensors, harness the principles of electrochemistry to transduce biorecognition events. These biosensors often involve the immobilization of a bio-recognition element, like an enzyme or antibody, on an electrode surface.[1] When the target analyte interacts with the biological component, it induces a change in the electrical properties of the electrode. These electrical responses are typically measured as a current, voltage, or impedance change, as depicted in Figure 1.1. Due to their inherent sensitivity, simplicity, and capability for miniaturization, electrochemical biosensors have garnered significant attention for various applications.

The history of electrochemical biosensors can be traced back to the early 1960s, with the development of the first glucose oxidase enzyme-based biosensor by Leland C. Clark and Champ Lyons.[2] This seminal work paved the way for the commercialization of glucose monitoring devices and has transformed the personal management of diabetes. The principle behind this biosensor is the enzymatic conversion of glucose to gluconic acid and hydrogen peroxide, with the latter being electrochemically detected. Over the years, this basic concept has been refined, miniaturized, and

integrated into the disposable glucose strips and continuous glucose monitoring systems widely used today.[3]

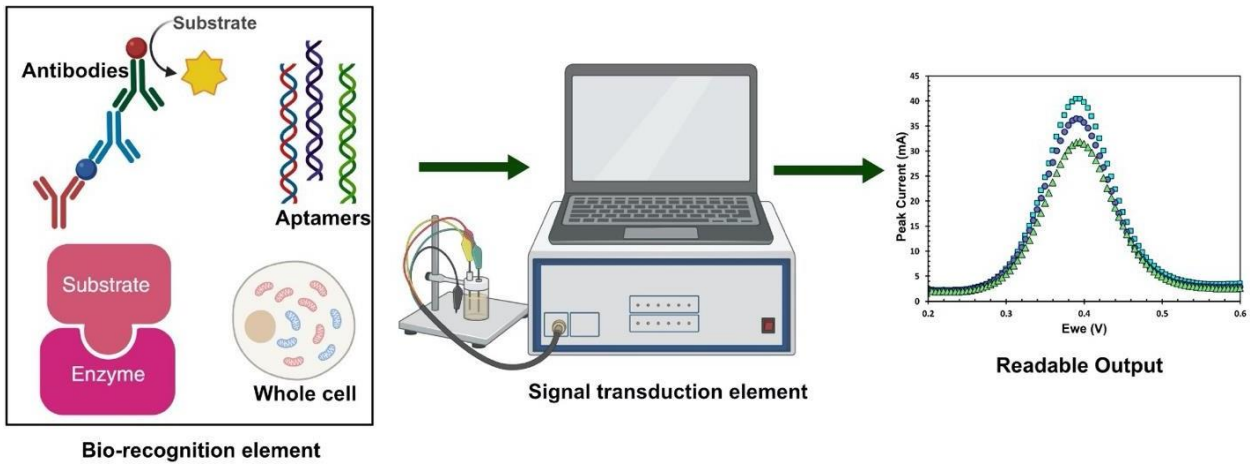

Figure 1.1 Schematic of an electrochemical biosensor illustrating the integration of biological recognition elements with electrochemical signaling element to convert biological responses into readable electrical outputs.

Electrochemical biosensors can be further categorized based on the type of electrochemical transduction, the bio-recognition element, or the target analyte. Recent advances in nanotechnology and materials science have expanded the possibilities, with innovations including nanoparticle-enhanced electrodes or graphene-based sensors pushing the boundaries of detection limits, specificity, and versatility. Electrochemical biosensors have evolved significantly since their inception. The fusion of biology and electrochemistry has created powerful tools that are now indispensable in various sectors, from medical diagnostics to food safety and environmental monitoring. Upon delving deeper into electrochemical biosensors development and applications, a comprehensive understanding of their various types becomes pivotal. The following section will discuss a diverse array of electrochemical biosensors, categorizing them based on their bio-recognition elements and underlying detection mechanisms.

1.2 TYPES OF ELECTROCHEMICAL BIOSENSORS BASED ON BIO- RECOGNITION ELEMENTS

Electrochemical biosensors are versatile analytical devices that rely on the integration of biological recognition elements with electrochemical transducers. This synergy enables the detection and quantification of specific analytes with high sensitivity and selectivity. The bio-recognition element selected will define both the functionality and application of the electrochemical biosensor. This section details several categories of electrochemical biosensors defined by the bio-recognition elements they employ. These elements include antibodies, enzymes, and oligonucleotides, each offering distinct advantages and tailored capabilities for biosensing applications.

1.2.1 Antibody-Based Electrochemical Biosensors

Antibody-based electrochemical biosensors, often referred to as immunosensors, leverage the remarkable specificity of antibodies to detect target analytes.[4,5] These biosensors involve the immobilization of antibodies onto the electrode surface or within a matrix. When the target molecule interacts with the immobilized antibody, it triggers a series of molecular events leading to a measurable electrochemical signal change. The high affinity and selectivity of antibodies make immunosensors well-suited for applications such as clinical diagnostics, environmental monitoring, and food safety.[6]

1.2.1.1 Basic Principles of Immunosensors

Antibodies, also known as immunoglobulins (Ig), are specialized glycoproteins with a unique ability to identify antigens precisely. These proteins are structured in a distinct “Y” shape, consisting of two heavy chains (each approximately 50 kDa) and two light chains (each about 25 kDa), linked by a single disulfide bond between each heavy and light chain pair.

Antibodies are categorized into monoclonal and polyclonal types based on their interaction with epitopes (i.e., the specific regions on antigens they bind to). Monoclonal antibodies are highly specific, capable of targeting a single epitope and reducing cross-reactivity risks. In contrast, polyclonal antibodies can attach to multiple epitopes, offering a varied immunological response. The choice between monoclonal and polyclonal antibodies is dependent on their intended analytical application.[6]

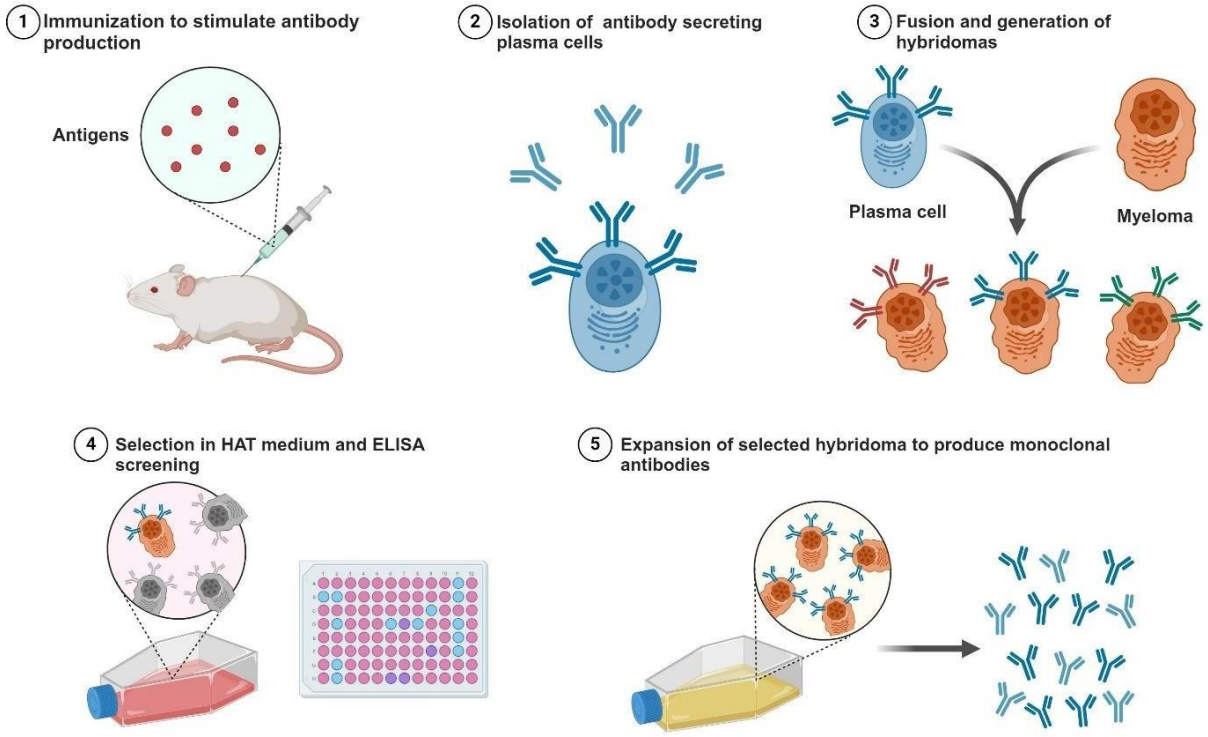

Figure 1.2 Step by step schematic of monoclonal antibody production using the hybridoma method.

An immunosensor is a form of bio-affinity biosensor. These employ antibodies to capture antigens which could be biological agents like toxins, bacteria, viruses, and proteins with molecular weights typically over 1.5 kDa. The binding affinity between antigen and antibody is a reflection of interaction strength and can be significantly influenced by minor changes in the antigen's molecular structure. Generally, these interactions exhibit high association constants,

sometimes reaching values as high as 1.0 x 10^{15}, under standard conditions of pH, temperature, and buffer solution. [7]

In vitro observation of antigen-antibody interactions is not always straightforward. Historically, radioimmunoassay, utilizing radioactive labels, was the first choice due to their high sensitivity. However, restrictions on radioactive materials led to alternative labeling methods like enzyme immunoassays (EIA), enzyme linked immunosorbent assays (ELISA), chemiluminescent, and fluoroimmunoassays. ELISAs are particularly popular and features two forms of interaction (1) sandwich and (2) competitive binding.[8] The sandwich format, despite its efficacy, requires the analyte to have multiple antibody binding sites. Necessitating multiple antibody binding sites poses design limitations but functional advantages.

In a basic ELISA setup, the antigen is fixed onto a solid surface, followed by the introduction of a specific antibody linked to an enzyme. The final step involves adding the enzyme's substrate, which triggers a reaction, often resulting in a color change for optical detection. In sandwich ELISA, the antigen is enclosed between two antibodies (primary and enzyme-linked secondary), amplifying the detection signal. For sandwich-type immunosensors, primary antibodies are typically anchored on an electrode surface, forming an immunocomplex with detection antibodies.[6,9]

Immunosensors stand out for their excellent sensitivity and specificity. They also allow for the real-time monitoring of immunoreactions on detector surfaces. These sensors are categorized based on their detection method: optical (i.e., luminescence and SPR), electrochemical, calorimetric, and mass variation (e.g., electrochemical quartz crystal microbalance). In electrochemical transducers, immunoreactions prompt responses in potential, current, and impedance.[10,11] These transducers are favored for their compactness, affordability, robustness, and

rapid response. They are ideal for mass production and require minimal analyte volumes, making them a popular choice especially in pharmaceutical and environmental applications.[6] However, the high molecular weight of many analytes in environmental, pharmaceutical, and food sectors poses challenges. Thus, selecting markers with high sensitivity, stability, strong antibody binding affinity, and cost-effectiveness is crucial. Ideal immunosensors would detect target species reversibly, continuously, and selectively; unfortunately, this desired performance is frequently prevented by the strong and often irreversible nature of antibody-antigen interactions.

1.2.2 Enzyme-Based Electrochemical Biosensors

Enzyme-based electrochemical biosensors rely on the catalytic activity of enzymes to convert a specific substrate into a detectable product. The immobilized enzyme on the electrode surface facilitates the conversion, and the resulting electrochemical signal change is proportional to the concentration of the target analyte.[12] Enzyme-based biosensors are widely recognized for their accuracy and sensitivity. Notably, the pioneering glucose oxidase enzyme-based biosensor, as described in Section 1.1, revolutionized the field of glucose monitoring, and serves as a cornerstone for enzyme-based biosensing applications, which is discussed later in this chapter. Enzyme-based labels have been established in the fields of biosensors and bioassays for signal amplification. However, the past decade has witnessed the rise of nanomaterial-enhanced ultrasensitive biosensors. The enduring preference for enzyme labels, particularly those involving horseradish peroxidase (HRP) and alkaline phosphatase (ALP), is a result of their unique ability to generate consistent, robust, and reproducible signal boosts.[12,13] Despite this, enzyme-triggered signal enhancement often falls short in ultrafine detection of biomolecules, critical for early and swift disease diagnosis. To bridge this gap, enzymatic reactions are augmented with additional amplification strategies, such as redox cycling, or by employing multiple enzyme labels per probe

for heightened signal boost. [12,13]

Redox cycling is a natural phenomenon instrumental in transforming chemical species. It involves the continuous generation or utilization of signaling entities (e.g., molecules or electrons) in the presence of reversible redox agents. These cycling processes, comprised of oxidation and reduction reaction, can be catalyzed enzymatically, chemically, or electrochemically. Integrating redox cycling with enzymatic amplification is straightforward and only requires the introduction of an extra chemical, enzyme, or an additional electrode in electrochemical assays.[14]

The application of multienzyme-based branched DNA assays is employed in ultrasensitive detection of DNA and RNA. Although these assays can be mechanized, their complex nature limits their applicability as an ultrasensitive biosensor technology. In response, recent advancements have led to the creation of multienzyme label-driven electrochemical biosensors that utilize nanomaterials as carriers. These biosensors achieve remarkable signal amplification as a result of the high enzyme-to-carrier ratios, while maintaining simplicity in detection akin to traditional enzyme-based electrochemical biosensors.[14]

Electrochemical detection is particularly compatible with redox cycling. Redox cycling enhances detection by regenerating consumed signaling species and maintaining high, stable electrochemical signals. Often neglected aspects of electrochemical biosensors are the stability and precision of small-scale electrochemical instruments, which reliably provide steady voltage and current measurements.[15] This stability significantly reduces variability in biosensor results. Consequently, merging redox cycling with electrochemical detection is poised to play a pivotal role in developing highly sensitive, reliable biosensors, especially beneficial for point-of-care testing applications.[16] Numerous redox-cycling methods feature variable advantages and limitations. A comprehensive representation of these methods is summarized in Figure 1.3.

The first approach (Figure 1.3a) involves the use of redox enzymes like HRP and glucose oxidase in redox cycling. In contrast, the other methods (Figure 1.3b to Figure 1.3h) do not use enzyme labels that are redox enzymes, as interactions between such enzyme labels and redox cycling can be problematic. In these scenarios, enzymes like ALP and β-galactosidase, which are not redox enzymes, are typically employed and require the addition of reactive substances, enzymes, or an extra electrode compared to conventional methods. [17] This increased complexity can lead to undesired reactions and may reduce signal strength or increase background noise, consequently diminishing the signal-to-background ratio. Selecting a redox-cycling system with slow side reactions is crucial for ultra-sensitive detection. Additionally, using oxygen-resistant chemicals and enzymes, and electrodes (or electrode potentials) where oxygen reduction is slow, is important to maintain good signal-to-background ratios. [18]

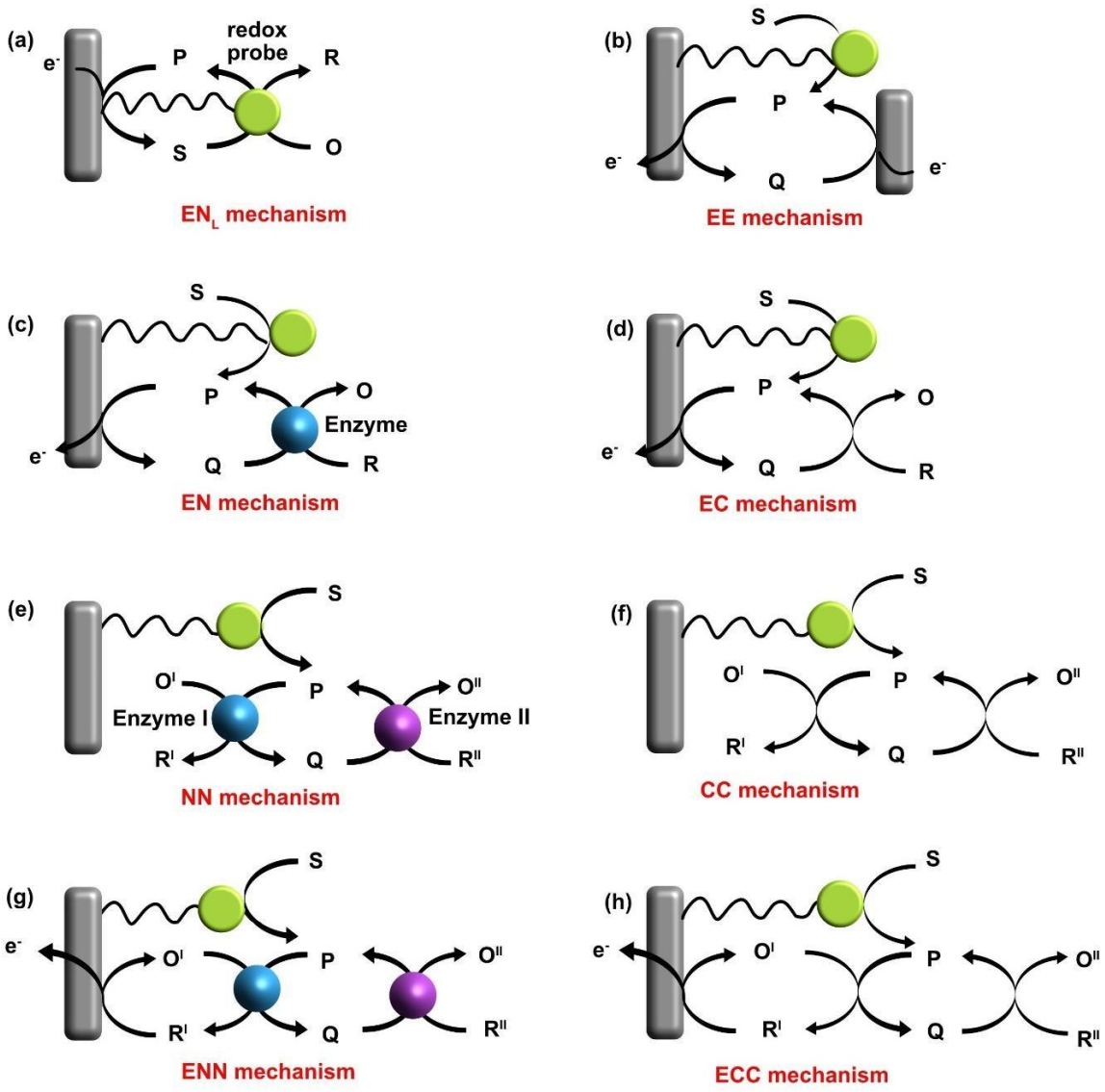

Figure 1.3 Illustrated overview of redox-cycling methods, including: (a) electrochemical with enzyme label, (b) dual electrochemical, (c) electrochemical paired with enzymatic, (d) electrochemical with chemical, (e) enzymatic-enzymatic, (f) chemical -chemical, (g) electrochemical-enzymatic-enzymatic, and (h) electrochemical- chemical- chemical mechanisms. The abbreviations P = product, S= substrate, O = oxidized form, R = reduced form, Q = oxidized form of P, O^1= oxidant, R^{II}= reductant, O^{II} = oxidized form of R^{II}, R^{II}= reduced form of O^I.

The standard type of redox cycling, illustrated in Figure 1.3a, is electrochemical–enzyme label (ENL) redox cycling. Here, a product of an enzymatic reaction is electrochemically reduced back to a substrate, which then re-enters the enzymatic cycle. However, in sandwich-type biosensors, this method only provides modest signal amplification, as the quantity of enzyme label on the sensing surface is limited, particularly at low target concentrations. The most extensively researched method is electrochemical–electrochemical (EE) redox cycling, involving two closely spaced electrodes. Interdigitated array electrodes with narrow gaps are commonly used to boost signal amplification. Despite its popularity, recent years have seen a shift from EE redox cycling to systems using two electrodes separated by a nanogap for ultra-high signal amplification of electroactive species. Other forms of redox cycling include electrochemical–enzymatic (EN), enzymatic–enzymatic (NN), and electrochemical–enzymatic–enzymatic (ENN), respectively. These methods rely on redox enzymes for rapid and selective reactions with specific chemicals. Although EN redox cycling has been both theoretically and experimentally implemented using ALP as a label and diaphorase as a redox enzyme, its application in protein and DNA detection remains limited. [17] Redox cycling can also be achieved without additional enzymes including electrochemical–chemical (EC), chemical–chemical (CC), and electrochemical–chemical–chemical (ECC) redox cycling, respectively. These have been increasingly applied in biosensors. Crucially, these redox-cycling strategies can be implemented by simply adding one or two chemicals to traditional enzyme-based biosensors.

1.2.2.1 Direct and mediated electron transfer

An enzymatic reaction is typically a two-step process. Initially, there is a reversible formation of an enzyme-substrate complex (E-S), which can be expressed as:

$$E + S \leftrightarrow ES \qquad \textbf{Eq. 1.1}$$

Subsequently, the product(s) (P) is released from the enzyme at a constant rate denoted by k_2:

$$ES \rightarrow E + P \qquad \textbf{Eq.1.2}$$

The rate of this reaction is defined by the Michaelis-Menten constant (K_M), a key concept in enzymatic kinetics. This relationship is captured in the Michaelis-Menten equation[19]

$$V_0 = \frac{V_{max}\,[S]}{K_M + [S]} \qquad \textbf{Eq.1.1}$$

In this equation, V_0 is the initial reaction rate, V_{max} the maximum reaction rate, and [S] the initial substrate concentration. The K_M value indicates the substrate concentration needed for the enzyme to reach half of its maximum reaction rate. Extending these principles to electrochemical reactions, we derive a similar equation that relates to the steady-state currents (I_{ss}) in amperometric measurements for successive substrate additions:

$$Iss = \frac{(Imax \times [S])}{(K_M(apparent) + [S])} \qquad \textbf{Eq.1.2}$$

Here, I_{ss} represents the steady-state current, I_{max} is the maximum current achievable under saturated substrate conditions, and K_M (apparent) the apparent Michaelis-Menten constant, reflecting the combined action of the enzyme and electrode.[20] The K_M (apparent) value, which can be determined by finding the substrate concentration at half the maximum current, is a measure of concentration. Lower K_M values suggest a stronger affinity of the enzyme for the substrate, leading to a faster reaction rate at a given substrate concentration. Conversely, a higher K_M value implies less efficient substrate binding, requiring more substrate to achieve the maximum reaction velocity. Factors such as the immobilization technique and the choice of solid surfaces for enzyme loading can influence these rates. The chosen surface should possess suitable conductivity, chemical

stability, and compatibility with biomolecules for optimal electron transfer.

Additionally, the physical properties of the substrate, like hydrophobicity or hydrophilicity, might need adjustment to facilitate the correct orientation of the enzyme for efficient electron transfer. Carbon-based nanomaterials and gold nanostructures are particularly effective as solid substrates due to their high conductivity and enzyme-friendly characteristics. These materials can also be easily functionalized with various chemical compounds, allowing customization based on the preferred enzyme immobilization technique.

1.2.2.2 Types of enzymatic bioreceptor

The pivotal role of enzymes in sensor development lies in their specific affinity for certain molecules, a crucial aspect for biosensor selectivity. Enzymes are sizable molecules, typically ranging from 10 to 400 kDa. Broadly, they are categorized into six principal groups based on their action on organic substrates (Table 1.1):

Table 1.1 Principal groups of enzymes based on their substrates.

Organic Substrate	Description
Oxidoreductases	Enzymes responsible for catalyzing oxidation-reduction reactions
Transferases	Facilitate the transfer of molecular groups from one molecule to another
Hydrolases	Enzymes involved in the hydrolysis of molecules
Lyases	Break C-C, C-O, or C-N bonds and add functional groups to molecules
Ligases	Couple two molecules together
Isomerases	Enzymes catalyze rearrangement of molecules into isomeric forms

Among these, oxidoreductases, including glucose oxidases and glucose dehydrogenases, are particularly noteworthy for their commercial appeal and will be the focus of extensive discussion in this chapter. Each enzyme category encompasses a range of subgroups, which are elaborated in a subsequent flowchart. Despite their potential, these subgroups are infrequently used in sensing techniques. Recent literature on enzyme inhibition-based biosensors highlights numerous studies

on methyltransferase, a subgroup of transferase, that has been leveraged for DNA analysis.[21] Similarly, glutathione-s-transferase has been used for detecting captan, a substance that inhibits the enzyme's catalytic activity.[22] Another subgroup, hexokinase, is instrumental in phosphorylating hexoses and has been effectively utilized in amperometric and conductometric techniques for adenosine triphosphate (ATP) detection.[21] This principle has also been applied to glucose detection using spectrochemical methods.

Following oxidoreductases, hydrolases have garnered significant attention in enzymatic electrochemistry. A notable application is the detection of organophosphate pesticides using enzymes like acetylcholinesterase, organophosphorus hydrolase receptors, or alkaline phosphatase, based on the concept of enzyme inhibition. Proteases, another hydrolase subgroup, are considered in identifying various proteins, including HIV-related proteins or DNA, through biosensors designed around enzyme inhibition. [21] DNA analysis has also been conducted using ligases-based electrochemical biosensors. However, biosensors based on lyases are less common, with a few instances like the ion-selective sensor for citrate detection using citrate lyase. Isomerases have not been directly used in sensing applications, but their potential is recognized, particularly in studies involving glucose isomerase in combination with glucose oxidase.[16]

Enzyme performance in biosensing is influenced by factors like pH, temperature, and the type and amount of enzyme used. However, a critical aspect in enzymatic electrochemistry is the chemical cofactor that enhances the enzyme's functionality. Oxidoreductases are prominent in this field, facilitated by various coenzymes. Oxidoreductases catalyze oxidation/reduction reactions by transferring electrons between reductants and oxidants. These enzymes act on various functional groups, often utilizing both inorganic and organic cofactors. In most oxidation processes, electrons are ultimately transferred to convert ADP to ATP. Cofactors, either nonprotein chemical

compounds or metallic ions, are essential for enzyme activity. Organic cofactors, or coenzymes, include several well-known types, with vitamins being a major group.

Key cofactors like nicotinamide adenine dinucleotide (NAD(P)H), flavin adenine dinucleotide-hydrogen ($FAD(H_2)$), and heme are vital for the catalytic processes of enzymes and are extensively studied in electrochemistry. NAD(P)H, abundant in all living cells, is involved in both oxidation and reduction reactions with over 400 oxidoreductase enzymes.[17] In plants and liver tissues, electron transfer reactions catalyzed by NAD(P)H are fundamental in various metabolic processes.[23] Other important cofactors include molybdopterin, iron-sulfur (Fe-S) clusters, and glutathione. Glutathione-dependent enzymes have been reviewed extensively, though there are limited studies on glutathione-based enzymatic reactions. Hemoglobin, a well-known heme-containing protein, has been utilized for oxygen detection through electrochemical procedures.[24] The role of other cofactors in catalytic reactions by dehydrogenase and reductase enzymes is also noteworthy. Less prominent cofactors like coenzyme Q and lipoamide are also relevant. Quinone derivatives, integral to coenzyme Q, are of particular interest in electrochemistry due to their distinct redox characteristics. However, some cofactors like coenzyme A, though significant in biochemistry, are not conducive to electrochemical tracking as they facilitate acetyl group transfer rather than electron transfer.

The widespread application of oxidoreductases in biosensing over the past three decades is attributable to the catalytic capabilities provided by coenzymes, enabling detectable reactions. The relevance of substrates catalyzed by oxidoreductases in indicating diseases in the human body is another factor. Advancements in biological and electrochemical sciences have led to the development of various modified electrodes through chemical interactions for efficient electron transfer. Significant progress in instrumentation, including atomic force microscopy, scanning

electron microscopy, and other spectroscopic techniques, has enhanced the study of modified surfaces, enabling effective immobilization or orientation of biomolecules on electrodes.

In electron transfer by enzymes, there are two perspectives: direct and indirect. Direct electron transfer (DET) can occur with or without an observable electrochemical signal from the enzyme's cofactor. Indirect or mediator-based electron transfer (MET) involves an external chemical mediator. While chemical mediators can enhance electron transfer kinetics, DET is favored for its simplicity and stability, despite ongoing challenges in its characterization.[25]

1.2.2.3 The Evolution of Glucosensors

The journey of electrochemical glucose biosensors, a foundational category in the field of biosensors, commenced with groundbreaking work by Dr. Leland Clark and Cham Lyons[26]. In the late 1950s and early 1960s, they developed the Clark oxygen electrode, later enhancing it by integrating the enzyme glucose oxidase under a protective membrane. This biosensor consisted of a platinum working electrode and an Ag/AgCl reference electrode, enveloped by an outer dialysis membrane housing the glucose oxidase and an inner membrane permeable to oxygen. Its operation hinged on a series of reactions:

- Glucose reacts with glucose oxidase (GOx) that contains flavine adenine dinucleotide (FAD), converting glucose to gluconic acid and reducing FAD, Eq. 1.6.
- Oxygen is then reduced to hydrogen peroxide, concurrently re-oxidizing FAD, Eq. 1.5.
- Finally, hydrogen peroxide is further oxidized into oxygen and electrical current, measured under an applied voltage, Eq. 1.7.

These reactions can be represented as follows:

$$\text{glucose} + \text{GOx(FAD)} \rightarrow \text{gluconic acid} + \text{GOx}(FADH_2) \qquad \textbf{Eq. 1.5}$$

$$H_2O_2 \rightarrow O_2 + 2H^+ + 2e^- \quad \textbf{Eq. 1.7}$$

$$GOx(FADH_2) + O_2 \rightarrow GOx(FAD) + H_2O_2 \quad \textbf{Eq. 1.6}$$

This initial type of glucose biosensor, relying on oxygen penetration, was commercialized in 1975 by the Yellow Springs Instrument Company as the Model 23A YSI analyzer.[27] Despite its innovative design, it was primarily suited for laboratory use due to its size, cost, and the complexity of the assay process. The first-generation glucose biosensors faced challenges such as susceptibility to interference from blood compounds like ascorbic acid and performance issues under restricted oxygen conditions. Subsequent developments led to the second generation of glucose biosensors, which replaced oxygen with electron mediators such as ferrocene, ferricyanide, and quinones. These mediators, housed within membranes that prevent the entry of interfering substances, enhanced the biosensor's resistance to redox-active compounds.[3]

The concept of the third generation of glucose biosensors emerged, featuring direct electron transfer between the enzyme and the electrode/membrane. This generation often utilizes composite and nanomaterial components or substitutes glucose oxidase with enzymes like glucose dehydrogenase.[28] The absence of electron mediators simplifies the fabrication process and avoids using materials that might be hazardous. A further advancement is the fourth generation of glucose biosensors,[15] where the biological recognition element (enzyme) is replaced by artificial structures with similar catalytic and specific properties. For example, Dayakar et al. replaced glucose oxidase with a CeO_2 nanostructure on a CuO core-shell in their electrochemical assay.[29] Other materials, such as mesoporous metal oxides and graphene composites, have also been employed. The fourth generation's advantage is chemically derived recognition elements, offering better uniformity and reproducibility compared to biotechnologically produced enzymes,

though specificity may be compromised.[30] Note that the distinctions between these biosensor generations are not rigidly defined and should be viewed as approximate rather than strictly accurate classifications. Furthermore, belonging to a "higher" generation does not necessarily equate to superior analytical performance. Evaluating new biosensor technologies requires a critical assessment of various factors, including analytical capabilities and economic feasibility. The progression of glucose biosensor generations is summarized in a comprehensive table.

Table 1.2 Different generations of glucosensors highlighting their advantages and limitations.

Generation	Description	Characteristics	Ref.
First-Generation Glucose Biosensors	Utilize the process of converting oxygen to hydrogen peroxide.	Potential interference from blood constituents like ascorbic acid. Original electrodes were costly.	[31]
Second-Generation Glucose Biosensors	Employ electron mediators replacing oxygen in the reaction, coupled with improved membrane technologies.	Reduced sensitivity to blood interferents like ascorbic acid.	[32]
Third-Generation Glucose Biosensors	Characterized by direct electron transfer from enzyme to membrane/electrode, eliminating electron mediators and utilizing conductive membranes.	Similar analytical properties to the second generation with simpler fabrication. Environmentally safer due to the absence of certain mediators.	[28]
Fourth-Generation Glucose Biosensors	Replace the enzyme with an artificial structure mimicking the enzyme's catalytic and specificity properties.	Easier mass production and improved uniformity and reproducibility. Specificity needs thorough verification.	[15,33]

The rapid advancement of biosensor technology, particularly in areas like miniaturized lab-on-a-chip devices, innovative wearable electronics, and user-friendly point-of-care systems, has catalyzed the emergence of novel enzyme-based biosensors. While research on biosensors incorporating multienzyme systems is gaining momentum, there are several hurdles to overcome in their development and practical deployment. One primary challenge lies in the biosensor's sensitivity to various substances. Biosensors that rely on multiple enzymes react to the substrates

of each enzyme, complicating the measurement of individual substrates in mixed samples.[3,12,16,30] A potential solution involves carefully selecting the multienzyme system to ensure it only reacts with the target substrate. Another approach is to design multiplexed systems or arrays of biosensors, each tailored to detect a specific substance, allowing for comprehensive analysis of all components in a sample. The diverse optimal immobilization conditions required by different enzymes poses another challenge. In multienzyme biosensors, the immobilization conditions need to strike a balance that suits all enzymes, which can sometimes lead to reduced enzyme efficiency. Although techniques like layer-by-layer immobilization exist, the more commonly used method is co-immobilization of enzymes in a single matrix or carrier. Ensuring that all enzymes in the biosensor function effectively under uniform conditions, such as pH, buffer type, and the presence of cofactors, is also difficult. Compromising on the composition of the working buffer to accommodate all enzymes might lead to decreased enzyme activity. The development process for these biosensors is typically more extensive and intricate. This involves extra experimentation to address the challenges mentioned above and to determine the most effective ratios of enzymes for the biosensor's optimal function.

The shelf life of a multienzyme biosensor is determined by the enzyme with the least stability. For example, while glucose oxidase may retain its activity for several months, hexokinase may become inactive within 1-2 months, thus limiting the biosensor's overall shelf life. The response time of multienzyme biosensors is generally longer, particularly in systems with sequential reactions. This delay is also evident in coupled enzyme assays, where there is an initial lag phase before reaching a steady state of maximum reaction rate.[14] Finally, the manufacturing complexity and cost for multienzyme biosensors are higher compared to their single-enzyme counterparts. The plethora of enzyme combinations adds to this complexity, necessitating a careful consideration of

cost-effectiveness and practicality in their design. While these sophisticated multienzyme biosensors hold promise, their development must balance innovation with practicality, ensuring they meet real-world needs in terms of affordability, ease of manufacture, and longevity.[16,30]

1.2.3 Oligonucleotide-Based Electrochemical Biosensors

Oligonucleotide-based electrochemical biosensors, also known as DNA or RNA biosensors, utilize synthetic or natural nucleic acids to recognize complementary sequences or specific genetic markers. These biosensors offer exceptional selectivity in the detection of nucleic acid-based targets, making them invaluable in genomics research, pathogen detection, and the diagnosis of genetic diseases. Oligonucleotide-based biosensors often employ hybridization events or DNA strand displacement to trigger electrochemical responses upon target binding.[34]

The emergence of nucleic acid aptamers as innovative biological receptors has revolutionized the field of affinity-based electrochemical sensors. Aptamers, derived from the Latin terms 'aptus' (meaning 'to fit') and 'meros' (meaning 'particle'), are short RNA or single-stranded DNA synthetic oligonucleotides. They also include peptides known for their high affinity, selectivity, and specificity in binding to target molecules. These artificial bioreceptors were first discovered in 1990 by Ellington and Szostak, and Tuerk and Gold, who developed RNA molecules capable of binding to organic dyes and T4 DNA polymerase, respectively.[35] Peptide aptamers, introduced by Colas et al. in 1996, are short peptide structures capable of recognizing specific proteins such as cyclin-dependent kinase 2. [35] However, in the context of this discussion, the term ‘aptamer’ will refer specifically to those based on nucleic acids.[36]

Aptamers are created through a process known as "systematic evolution of ligands by exponential enrichment" (SELEX). This method involves repetitive cycles of incubating a random pool of oligonucleotide sequences with a target molecule, separating bound and unbound

sequences, and then amplifying the target-bound sequences. Over the past decades, numerous variations of the SELEX process have been developed to produce aptamers more efficiently and with higher affinity, although these variants are beyond the scope of this chapter.[37]

Aptamers stand out as bioreceptors due to several unique characteristics, some of which rival or even surpass those of antibodies, making them highly effective in biosensing and other applications like biomedical imaging and targeted drug delivery.[37] One of the primary advantages is their method of production. Aptamers are synthesized in vitro, a process that is more cost-effective, simpler, and more reproducible than the animal or cell line-dependent antibody production. This method also allows for the creation of aptamers for targets that are typically challenging in antibody technology, such as low molecular weight, toxic compounds, or antigens with epitopes similar to host animal proteins with antibodies.[38]

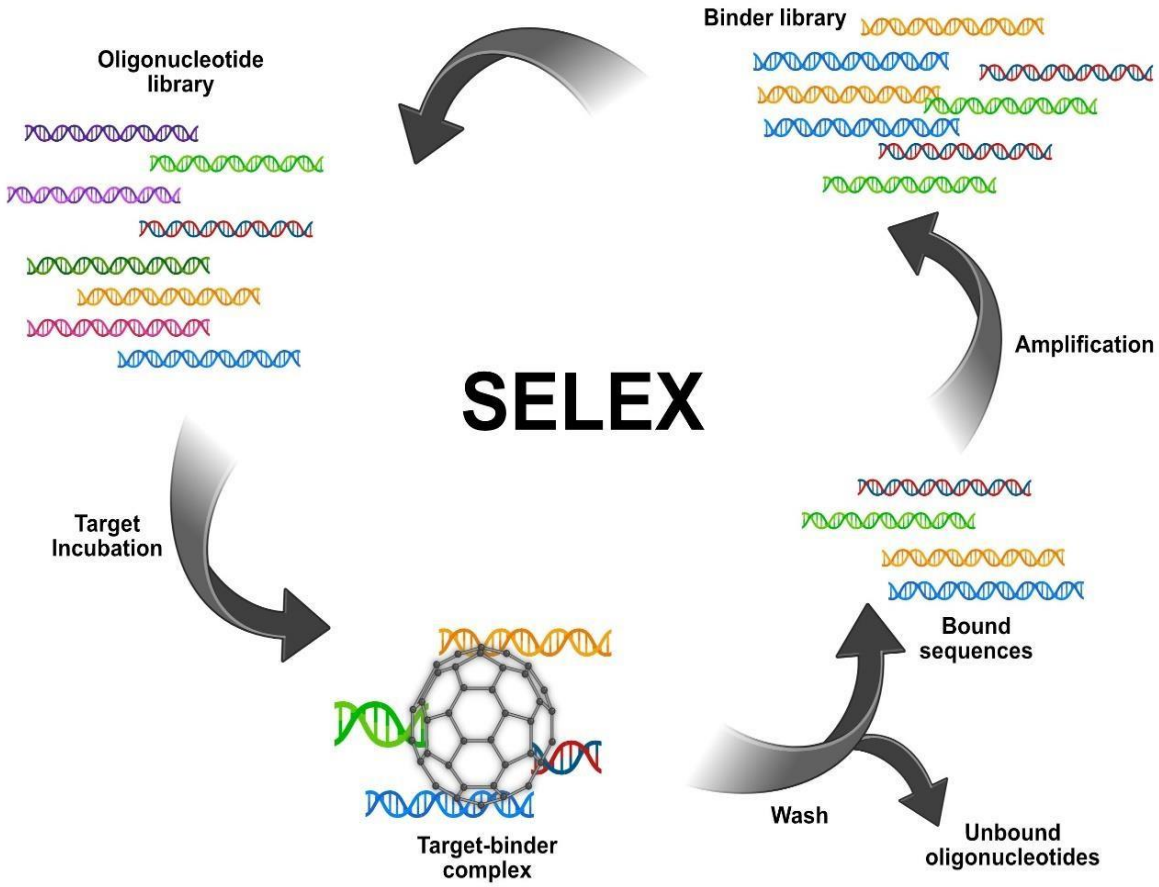

Figure 1.4 Schematic of the SELEX process for synthesizing aptamers. [38]

Their affinity binding capacity is another significant feature. Aptamers bind to their targets through a variety of noncovalent interactions, facilitated by conformational changes in their structure. This results in highly stable complexes with dissociation constants that are on par with or even better than those of monoclonal antibodies. Additionally, aptamers can be chemically modified more easily than antibodies. They can be synthesized with reactive groups at either end, enabling stable and oriented immobilization on electrode surfaces, a process that is comparatively more challenging. [39]

Table 1.3 Aptamer-based electrochemical biosensors detecting clinically relevant targets.

Target	ctrochemical Technique	Strategy	Linearity Range	tection Limit	Reference
Thrombin	CV	Au-PANI-Gra hybrid	1.0 pM–30 nM	5.6 × 10−13 M	[40]
Thrombin	DPV, CV, EIS	Au electrode	5.0 pM−50 nM	0.9 pM	[41]
Thrombin	EIS	Graphene oxide/double-stranded DNA nanocomposite	0.1–100 nM	0.06 nM	[42]
Thrombin	SWV, CV	Aptamer-target-aptamer sandwich structure	1–600 nM	170 pM	(Wang et al., 2017)
Thrombin	DPV, CV, EIS	TiO2/MWCNT/CHIT/SB	0.00005–10 nM	1.0 fM	[44]
Thrombin	DPV	MnPP-catalyzed aerobic oxidation of l-cysteine	0.1–25 nM	0.02 nM	[45]
Thrombin	ACV	"Signal-on/off'' aptasensor based on the biobarcoded amplification	0.003–30 nM	1.1 pM	(Wang et al., 2017)
C-reactive protein	CV, EIS, SWV	Gold surface	1–100 pM	–	[47]
Activated protein C	DPV, CV, EIS	(PS/SPE)	5–12.5 μg mL−1	0.74 μg mL−1 (buffer medium), 2.03 μg mL−1 (serum)	[48]
VEGF	CV	DNA-templated Ag/Pt bimetallic nanoclusters	6.0–20 pM	4.6 pM	[49]
VEGF	PEC	g-C3N4/Au NPs/HT/S1+S2 aptamer/S2+S3 aptamer/MB/target	100 fM–10 nM	30 fM	[50]
PDGF-BB	ACV	Self-assembling ferrocene-labeled aptamer onto Au electrode	20 pg mL−1–200 ng mL−1	10 pg mL−1	[51]
PDGF-BB	DPV	Catalase-functional DNA-PtNPs dendrimer	50 fM–35 nM	20 fM	[52]
PDGF-BB	EIS	Co3(PO4)2-based nanocomposites	0.5–100 ng mL−1	61.5 pg mL−1	[51]
PDGF-BB	ECL	MoS2-AuNPs/Apt1/MCH/PDGF-BB/QDs-Apt2/GCE	0.01–100 pM	1.1 fM	[53]
MUC1	DPV, EIS	Au nanoparticle/thiolated aptamer/MUC1 protein/graphite SPE	2.5–15 ng mL−1	3.6 ng mL−1	[54,55]
MUC1	CV	MB-anti-MUC1 aptamers/gold electrode	Up to 1.5 μM	50 nM	[55]
MUC1	DPV	ITO	1.0 pg mL−1–50 ng mL−1	0.40 pg mL−1	[34]
MUC1	Photoelectrochemical (PEC)	TiO2 NT/aptamer/c-DNA@QD/MUC1	0.002–0.2 μM	0.52 nM	[37]
MUC1	EIS	SPE/carbon nanotube/aptamer/MUC1	0.1–2 U mL−1	0.02 U mL−1	[56]
PSA	ESI Amperometric	11-Amino alkanethiol/Au nanoparticle/SH-aptamer/MCH or FcSH/PSA	1–10 pg mL−1	10 pg mL−1	[57]
PSA	DPV	GE/gold nanospheres/aptamer-MB/PSA	0.125–200 ng mL−1	50 pg mL−1	[58]
CEA	DPV	GE/aptamer I/CEA/aptamer II-AuNPs	1–200 ng mL−1	0.5 ng mL−1	[5]
Lysozyme	SWV	Aptamer modified with Fc	1–30 nM	0.45 nM	(Chen et al., 2013)
Lysozyme	EIS	Comparison of two different aptamers (COX and TRAN)	0.1–0.8 μM/25 nM–0.8 μM	100 nM/25 nM	(Ocaña et al., 2015)
Lysozyme	CV, DPV, EIS	Signal-off architecture	7–30 nM	0.45 nM	(Chen et al., 2013)
Lysozyme	SWV	Aptamer/tetrahexahedral (THH) Au NCs/GCE	0.1 pM−10 nM	0.1 pM	[62]

Furthermore, aptamers exhibit remarkable thermal and conformational stability. Unlike antibodies, which can undergo irreversible unfolding and aggregation upon thermal treatment, aptamers are highly stable single-stranded nucleic acids capable of reverting to their active conformation after thermal denaturation. Their ability to fold into various 3D structures upon binding to their target molecule is another beneficial property. This characteristic allows for the development of innovative label-free and single-step biosensing strategies, which can be further optimized through the aptamer's rational design. [63]

The exploration and quantification of small molecules, ranging from natural to pharmaceutical origins, are crucial in various fields such as biology, pharmacology, environmental science, and food safety. The key to designing sensitive and specific sensing platforms lies in the choice of the recognition element. While antibodies have been the go-to for biomolecular recognition, they pose challenges in developing sensors for small molecules, primarily due to their complex preparation process, low thermal stability, pH sensitivity, and high cost. In contrast, aptamers, often referred to as "chemical antibodies," offer comparable affinity and specificity. Their advantages include in vitro selection, chemical synthesis, diverse modifications, and robust stability. Consequently, aptamer-based sensing platforms have emerged as a significant tool for detecting various small molecules across different applications.[64]

Point-of-Care Testing (POCT) with portable or onsite detection is particularly beneficial in healthcare, environmental safety, and food quality assessment. These tests are invaluable in resource-limited settings where specialized laboratory equipment and expert operators are scarce. The importance of detecting diverse small molecules, coupled with the limitations of laboratory-based detection in areas lacking resources and the need for onsite detection, underscores the significance of developing aptamer-based POCT for a variety of small molecules.[30]

Different sensing models, including direct aptamer-target binding, sandwich models, target-induced conformation change models, and competitive binding models, have been integrated with portable devices like Personal Glucose Meters (PGM), pH meters, thermometers, pressure meters, Lateral Flow Strips (LFS), Microfluidic Paper-based Analytical Devices (μPADs), Surface Plasmon Resonance (SPR) devices, electrochemical devices, and smartphones. The design of these sensors is a crucial initial step in developing a comprehensive POCT platform, with a primary focus on achieving specificity and sensitivity. Another critical aspect is converting the target signal into a detectable signal by the POCT device, where aptamers play a pivotal role. When considering the final detection device, factors like equipment size, operational complexity, and cost become crucial.[65] Moreover, simplifying manual operation steps, enhancing operation simplicity, and enabling onsite detection are achievable through the integration of different portable devices.

Despite the development of numerous devices for detecting various small molecules, challenges remain. These include the need for more aptamer selections against different small molecule targets, improvement in aptamer selection methods, and exploration of more efficient affinity detection methods. [66] Simplifying the detection operations of aptamer based POCT is essential, especially since many POCTs, while portable, often require complex procedures unsuitable for in-home diagnostics or in situ monitoring in emergencies.[67] Additionally, there is a need for comprehensive studies on the simultaneous detection of multiple small molecules and high-throughput sample analysis. The design and construction of dual- or multiple-aptamer sensing platforms integrated with POCT devices are highly sought after for practical applications. The advancement of bioinformatics and computational biology has fueled research into optimizing nucleic acid libraries based on computer simulation technology. This approach aids in library design and candidate sequence selection, improving the effectiveness of selected aptamers.

Establishing a comparison scale for different affinity measurement methods would benefit researchers by providing a standardized approach for affinity evaluation. Furthermore, considering the impact of actual sample matrices on analysis and detection, strategies like anti-matrix effect aptamer selection, aptamer engineering design modifications, and changes in the interface structure of aptasensors should be considered to improve applicability in complex sample matrices.[36]

Although aptamer based POCTs for sensitive detection of small molecules are highlighted in this review, their commercialization and routine use still have a long way to go. In fields like environmental monitoring and food safety, where working conditions are challenging and lack experimental facilities and expert operators, the development of miniaturized devices that integrate reaction and signal output is crucial. [68] In health monitoring, integrating aptasensors into emerging wearable technologies is a future trend for long-term health monitoring and disease management.

1.3 TYPES OF ELECTROCHEMICAL BIOSENSORS BASED ON DETECTION MECHANISM

Electrochemical biosensors operate by converting biologically driven changes in chemical concentration or activity into electrical signals. The versatility of these devices arises from their ability to exploit a variety of electrochemical techniques, each offering its unique advantages in terms of sensitivity, selectivity, and application range. In this section, we explore the predominant detection mechanisms employed by electrochemical biosensors.

1.3.1 Voltammetry, Amperometry and Potentiometry

Voltammetry and potentiometry are integral electrochemical techniques in the realm of biosensing and analytical applications, each offering unique insights and functionalities. Cyclic Voltammetry (CV), a cornerstone of voltammetry, systematically varies the potential at a working

electrode relative to a reference electrode, capturing the resultant current from redox reactions at the electrode surface. This method illuminates the electroactivity of biomolecules, with the peak intensities in the voltammogram (CV signal) depending on the rate at which the analyte reaches the electrode surface. CV's ability to distinguish various redox-active species and provide quantitative data makes it a staple in sensors designed for complex biological systems.

In linear sweep voltammetry, the potential is swept in one direction, culminating at a set endpoint like E_f at time $t = t_1$. This sweep can be either positive or negative, with initially variable sweep speeds. In contrast, CV reverses the sweep direction at $t = t_1$, fluctuating between a minimum potential (E_{min}) and a maximum potential (E_{max}), thereby creating cycles with multiple sweeps. Analyzing a cyclic voltammogram involves assessing the initial potential (E_i), initial sweep direction, sweep speed (ν), maximum potential (E_{max}), minimum potential (E_{min}), and final potential (E_f). The voltammogram reveals a faradaic current (If) from electrode reactions and a capacitive contribution (I_c) from changes in the electrical double layer's charge (Cd) during potential sweeping. The capacitive element increases with sweeping speed, influencing the technique's sensitivity. The potential in CV follows the Nernst equation: [69]

$$E = E0 + \left(\frac{RT}{nF}\right) * \ln\left(\frac{[OX]}{[RED]}\right) \qquad \textbf{Eq. 1.1}$$

where E is the cell potential, E_0 is the standard potential, R is the universal gas constant, T is the temperature, n is the number of electrons involved, F is the Faraday constant, [RED] is the activity of the reduced species, and [OX] is the activity of the oxidized species. Due to certain limitations, CV is generally used for exploratory purposes rather than precise quantitative determinations. Potentiometry, a static interfacial method, is commonly used in analytical applications, exemplified by pH meters based on glass membrane electrodes. Potentiometric biosensors typically involve ion-selective electrodes constructed from glass, solid, or liquid membranes,

tailored for specific ions such as F^{-}, Ag^{+}, Cl^{-}, $S2^{-}$, H^{+}, K^{+}, Na^{+}, NH^{+}, and Ca^{+}. [70] These electrodes can be integrated into clinical analyzers for blood electrolyte detection and adapted for detecting enzymes, nucleic acids, or proteins by integrating a biological element or linking biorecognition events with ionic reactions.

Solid-contact ion-selective electrodes, made from solvent polymeric membranes without internal solutions, offer robustness and easy fabrication. These electrodes enable protein and nucleic acid analysis through ions released from nanoparticle-tagged probes, allowing, for example, the detection of DNA at femtomolar levels in micro-volume samples. All-solid-state ion-selective electrodes, constructed with conducting polymers or nanomaterials, are implemented in commercial portable devices for point-of-care detection of electrolytes and blood gases. Additionally, paper-based potentiometric biosensors and wearable devices like 'smart wristbands' demonstrate the versatility of these electrodes in real-time biofluid analysis.

Chronoamperometry, another potentiostatic technique, measures the current at a working electrode over time under a constant potential, correlating the current flow with the concentration of oxidized or reduced species on the electrode surface. The current in chronoamperometry follows the Cottrell equation: [71]

$$i = \frac{nFA\left(\frac{C_0}{D_0^{0.5}}\right)}{\pi} * \frac{t^{-0.5}}{2} \qquad \textbf{Eq. 1.2}$$

where i is the current at time t, n is the number of electrons, F is Faraday's constant, A is the electrode area, c_0 is the concentration of the oxidized species, and D_0 is the diffusion coefficient of the oxidized species.

In both amperometric and voltammetric biosensors, which utilize a three-electrode system, the focus is on quantifying targets. [70] These systems comprise a biosensor as the working electrode (WE) for target recognition, a counter electrode as the power source, and a reference electrode for stable potential application. The generated current signals from electrochemical reactions on the WE highlight the differences between the two: amperometric biosensors maintain constant potential, while voltammetric biosensors vary it. Techniques under voltammetry include cyclic voltammetry, differential pulse voltammetry, square wave voltammetry, and anodic stripping voltammetry.

Amperometric biosensors are notably effective for detecting metabolites such as glucose, lactate, and uric acid, employing target-specific enzymes like glucose oxidase (GO_x) immobilized on the working electrode for target oxidation. These biosensors, simple in construction, offer high sensitivity and selectivity, making them ideal for wearable technologies. Nanomaterials like metallic nanoparticles, carbon nanotubes, and graphene are integrated into the biosensing interface to enhance sensitivity due to lower metabolite concentrations in non-blood fluids.

Affinity sensors, needed for detecting biomarkers like proteins and nucleic acids, require electroactive labels for target sensing via voltammetric techniques. These sensors typically involve immobilizing capture biomolecules on the WE, enabling protein or nucleic acid detection through sandwich assays. However, complex procedures often required for these devices pose challenges in device integration. Automated fluidic systems and microfluidics have been implemented to overcome these hurdles, facilitating continuous, high-throughput detection of trace analytes in

complex samples. While commercial electrochemical biosensing devices for chip-based or cartridge-based detection exist, cost-effective alternatives like paper-based microfluidics combined with amperometric or voltammetric biosensors offer multiplex sensing capabilities.

Proximity binding-based affinity electrochemical biosensors, suited for protein biomarker detection, transform protein immunoassays into DNA detection. These sensors employ antibody-DNA affinity probes for dual recognition of target proteins, leading to proximity ligation products that initiate DNA assembly on the electrode surface. These developments in electrochemical biosensing, from detailed redox analysis in voltammetry to direct target detection in potentiometry and chronoamperometry's time-dependent current measurement, underscore the field's continuous evolution and significant impact on various analytical and diagnostic applications.

1.3.2 Square wave voltammetry

Square Wave Voltammetry (SWV) stands as a rapid and highly sensitive pulse voltammetry technique, rivaling the detection limits of chromatographic and spectroscopic methods. [69] This technique's exceptional sensitivity and strong rejection of capacitive currents stem from its unique potential-current curve, shaped by applying potentials of a specific height (ΔE, pulse amplitude), which vary according to a defined potential step (E_{step}) and duration (τ). In SWV, the pulse width ($\tau/2$) is marked as t, with the frequency of pulse application denoted by f, calculated as (1/t). The electric currents are measured at the end of both direct (I1) and reverse (I2) pulses, with the differential current (ΔI) constituting the signal. This precise measurement is preceded by an initial time (t_i), where the working electrode is polarized at a non-reactive potential.

The current-potential curves in SWV typically exhibit well-defined, symmetrical profiles, as currents are measured only at the end of each semi-period and variations in pulse height and width remain constant within a determined potential range. This consistency allows electrochemical

techniques to contribute significantly to the synthesis and characterization of materials through voltammetric methods, correlating current to electric potential in an electrochemical cell. In amperometric sensors, a constant electric potential is applied to the cell, generating a current due to redox reactions at the working electrode's surface. This current provides a means to quantify the reactions involved. Amperometric sensors, often operated through CV, offer a powerful technique for synthesizing and characterizing various electroactive species, establishing the relationship between current and potential for each oxidation or reduction reaction. Generally, voltammetric sensors are employed in detecting species involved in redox reactions within the electrochemical cell.

The SWV technique has been instrumental in developing sensors and biosensors, highly valued for its sensitivity and selectivity. [72] It has garnered significant interest in pharmaceuticals, environmental monitoring, and other sectors for detecting disease biomarkers, environmental pollutants like heavy metals, and various chemical contaminants. For example, SWV has been employed to quantify pheniramine in pharmaceutical formulations using a glassy carbon electrode modified with Multi-Walled Carbon Nanotubes (MWCNTs) in the presence of sodium lauryl sulfate. [69] The results revealed an electrocatalytic effect of pheniramine in anionic surfactant solutions, significantly increasing the peak current, with a detection limit of 58.31 μg mL^{-1} and a linear response range from 200–1500 μg mL^{-1}.

In clinical and medical contexts, SWV's quantitative determination capabilities extend to industries, agriculture, environmental science, medicine, food, and life sciences. It successfully detects various organic and inorganic substances with redox properties. For instance, Du et al. designed an electrochemical DNA sensor utilizing a ratiometric mechanism, employing methylene blue (MB) as a reporter probe for conformational changes in hairpin (HP) DNA, while ferrocene

(Fc) served as a control probe. [69] This SWV-based method efficiently determined conformational changes triggered by target DNA, revealing a decrease in MB's peak current and a consistent Fc current with increasing target DNA concentration.

Yu et al. developed a novel strategy for prion protein detection based on a competitive host-guest interaction regulated by protein biogate.[73] In their system, an MB-tagged prion aptamer was integrated into multi-walled carbon nanotubes-β-cyclodextrins composites through host-guest interactions. The presence of prion protein led to the formation of a protein biogate, sealing the β-cyclodextrin cavity and preventing the displacement of MB. This specific interaction increased the oxidation peak current of MB while decreasing that of ferrocene carboxylic acid (FCA) with rising prion concentration. This SWV-based approach achieved a low detection limit for prion protein, demonstrating the technique's prowess in sensitive biomarker detection.

1.3.3 EIS (Electrochemical Impedance Spectroscopy)

Electrochemical Impedance Spectroscopy (EIS) is a nuanced, yet immensely powerful technique. It subjects a system to varying frequency electrical signals and measures the system's impedance. In biosensors, minute alterations at the electrode interface, such as those arising from biomolecular binding events, produce noticeable changes in impedance.[71] Given its non-invasive nature and the ability to provide data without the need for external reagents or markers, EIS is increasingly being incorporated into state-of-the-art biosensing platforms.

In a standard electrochemical cell, the interaction of matter (specifically redox species) with electrodes encompasses several key aspects: the concentration of electroactive species, charge-transfer, mass transfer from the solution to the electrode surface, and the electrolyte's resistance. Each of these aspects is symbolized by an electrical circuit component (i.e., resistances, capacitors, or constant phase elements) arranged either in parallel or in series to create an equivalent circuit.

Electrochemical Impedance Spectroscopy (EIS) utilizes this framework to investigate mass-transfer, charge-transfer, and diffusion processes, thus capable of probing intrinsic material properties or specific processes that affect the conductance, resistance, or capacitance of an electrochemical system.

Impedance differs from resistance, primarily observed in DC circuits, where Ohm's Law is directly applicable. In EIS, a small signal excitation is applied to measure the impedance response. The electrochemical cell exhibits a pseudo-linear response where a phase-shift occurs as the current response to a sinusoidal potential is also sinusoidal but at the applied frequency. The excitation signal over time is represented as follows:

$$E(t) = E0 \cdot \sin(\omega t) \qquad \textbf{Eq. 1.10}$$

where E(t) is the potential at time t, E0 is the amplitude of the signal, and ω is the radial frequency. The relationship between the radial frequency (ω) and the applied frequency (f) is given by:

$$\omega = 2\pi f \, \omega = 2\pi f \qquad \textbf{Eq. 1.11}$$

In a linear system, the signal experiences a phase shift (Φ) and differs in amplitude from I0:

$$I(t) = I0 \sin(\omega t + \Phi) \qquad \textbf{Eq. 1.12}$$

From this, the impedance of the entire system is derived:

$$Z = EI = Z0ei\Phi = Z0(\cos\Phi + i \sin\Phi) \qquad \textbf{Eq. 1.13}$$

In this equation, Z represents impedance, E is the potential, II is the current, ω is the frequency, and Φ is the phase shift between E and I. Impedance is expressed in terms of a magnitude (Z) and a phase shift (Φ). When the applied sinusoidal signal is plotted on the X-axis against the sinusoidal response signal (I) on the Y-axis, a "Lissajous Plot" is formed. Before modern EIS instrumentation, Lissajous analysis was the primary method for impedance measurement.

EIS-based biosensors, integrating antibodies or aptamers, have emerged as potent tools for detecting specific biomarkers. These biosensors exhibit high selectivity due to the precise biomarker recognition by antibodies or aptamers. Typically, self-assembling monolayers are functionalized onto gold electrodes, followed by immobilizing primary antibodies or aptamers using carbodiimide cross-linking chemistry. EIS-based biosensors have achieved remarkable detection limits for biomarkers like interleukin (IL)-6 and tumor necrosis factor (TNF)-α. For instance, secondary antibodies linked to enzymes are used to detect analytes, with substrates like H2O2 being reduced and electrons released proportionally to the analyte concentration.[74]

Electrodes also play a crucial role in characterizing Organ-on-a-Chip (OoC) models, including barriers like the blood-brain barrier, lung-on-a-chip, eye-on-a-chip, and gut-on-a-chip models. [68] Assessing the barrier function and integrity is essential in culturing endothelial or epithelial layers, for which Transepithelial/Transendothelial Electrical Resistance (TEER) measurement is widely employed. TEER offers a label-free, rapid, and sensitive assessment of barrier integrity and has been used for real-time monitoring of biological function and drug responses.[68] For instance, integrating TEER-measuring electrodes into a Blood-Brain Barrier (BBB) platform has enabled the monitoring of dynamic changes in TEER across a BBB layer over extended culture periods. This integration of EIS in various biosensing and OoC applications signifies its versatility and potential in both diagnostics and research, contributing significantly to advancing biomedical technologies and understanding complex biological processes. [71]

1.3.4 FET (Field Effect Transistors)

Field Effect Transistors (FETs) introduce a semiconductor approach to biosensing. These devices modulate the conductivity between a source and drain electrode using an external electric field applied via a gate electrode. Any change in surface potential, often arising from molecular interactions or binding events near the gate area, dramatically influences the device's conductivity. This change can be seamlessly read out, making FETs a promising platform, especially when miniaturization or integration into electronic devices is desired. FET-based biosensors, like the ISFET (Ion-Sensitive Field Effect Transistor), have already shown their mettle in pH sensing and real-time DNA detection.[75]

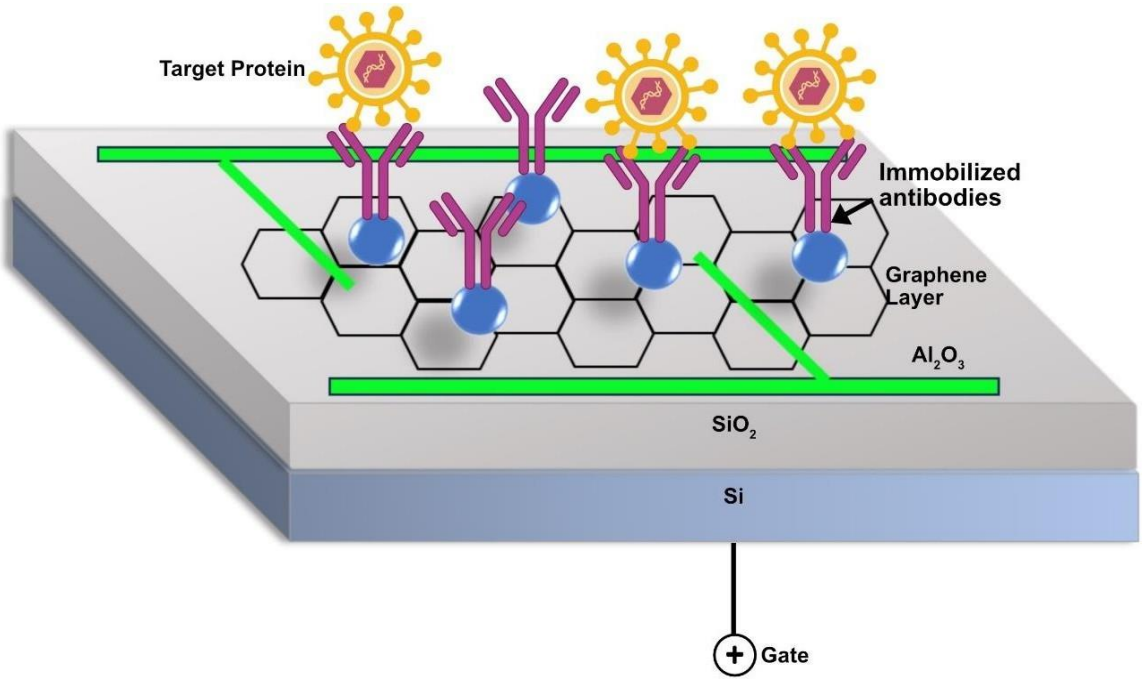

Figure 1.5 Schematic of a FET-based biosensor with immobilized biorecognition element.

Field-Effect Transistor (FET)-based biosensors consist of three electrodes: source, drain, and gate. The region between the drain and source acts as a biological recognition element, interacting with and sensing the presence, concentration, and electrical activity of target analytes or biomolecules. These biosensors convert biological information directly into measurable electrical

signals. Depending on the application, the generated signal can then be displayed, amplified, stored, processed, or transmitted to the cloud for further analysis. The working principle of FET-based biosensors involves: a change in analyte concentration leading to a change in charge near the sensor interface (represented as (Δq)), this charge shift induces a change in effective gate voltage (V_{EG}), and this alteration in gate voltage results in changes in the drain current ((ΔI_D)), observable in the I–V characteristics. The sensor's sensitivity is mathematically represented as a function of changes in analyte concentration ((Δc)), charge density at the sensor's surface ($(\Delta q\ )$), and the change in drain current ($(\ \Delta I_D)$), against a steady state drain current ($(\ I_D)$) when the sensor is exposed to a reference sample.[76]

$$\frac{dI_D}{I_D} = (dc\,\frac{d\rho}{dc})(\frac{dV_{EG}}{dp})(\frac{dI_D}{dV_{EG}} \cdot \frac{1}{I_D}) \qquad \textbf{Eq.1.3}$$

FET biosensors detect analytes based on charge interaction and permittivity shift effects. Innovations in their structural design have improved sensor performance and broadened their application scope. For example, a charged-plasma base gate underlap dielectric modulated junctionless tunneling FET (DM-JLTFET) offers high sensitivity and cost-effectiveness for biomedical sensor development. Material properties like high charge mobility or mechanical strength have diversified FET biosensors. Graphene FET-based biosensors, known for their high carrier mobility and optical transparency, offer high throughput and a wide detection range. Nanowire FETs also provide broad detection limits with high sensitivity. [76] Organic Field-Effect Transistors (OFETs) and Organic Electrochemical Transistors (OECTs) have enabled integration with flexible and wearable electronics, leading to the development of devices like sweat sensors that measure ion concentration for healthcare monitoring.[77]

However, challenges like poor reliability during large-scale fabrication and homogeneity issues impede FET biosensors' commercialization. The characteristics of the Si-SiO_2 interface, for

instance, directly affect a biosensor's reliability. Damages like hot carrier-induced or stress-induced damage at this interface, along with issues within the oxide such as traps and defect generation, can reduce device reliability and optimization. Structural changes, like extended-gate FETs with a metal sensing layer on the sensor surface, could improve reliability. Addressing these challenges can pave the way for developing new generations of FET-based biosensor technologies, leading to scientific and commercial success. Such advancements would benefit both industries and consumers, promoting the integration of these sensors into a range of applications, including wearable devices.

1.4 OVERVIEW OF INCLUDED WORKS

Electrochemical biosensors represent a rapidly advancing field that continues to yield innovative sensing strategies with immense potential to make precision medicine, environmental monitoring, and biodefense more accessible. However, ongoing research efforts are still needed to fully realize their benefits through improving reproducibility, stability, sensitivity, and integration with electronics. The future translation of electrochemical biosensors from proofs-of-concept to viable commercial devices will rely on optimizing the choice of biorecognition elements, nanomaterials, immobilization chemistries, and assay formats for the target application. More interdisciplinary collaborations and technology transfers between academic labs and industry partners can accelerate the development of field-deployable electrochemical biosensing tools that are simple, fast, and cost-effective.

2. PROTEIN ENGINEERING ENABLED THE DEVELOPMENT OF MONOBODIES AS BIORECOGNITION ELEMENTS FOR BIOSENSING

2.1 INTRODUCTION TO VARIOUS SYNTHETIC BINDING PROTEINS

Synthetic binding proteins are artificially engineered proteins designed to target specific molecules. The immune system's remarkable ability to produce antibodies capable of binding to a wide range of antigens, along with an understanding of the molecular processes behind this, has spurred the creation and advancement of the field dedicated to designing and engineering these synthetic binding proteins. [78] Similar to the process of generating various antibodies by modifying parts of the immunoglobulin molecule, these synthetic proteins are typically produced by modifying certain sections of a structurally stable but functionally passive protein, known as a protein scaffold [79][Figure 2.1]. The overarching goal in developing synthetic binding protein systems is to create proteins that can bind to a multitude of targets, rather than being limited to a single specific target.[80] These proteins are synthetic because they do not occur naturally; they are polypeptides composed of naturally occurring amino acids and are synthesized using the regular protein production processes. [81]

In the last few decades, the hurdle of creating a highly effective molecular recognition interface via a protein scaffold has been largely resolved. The focus is now shifting towards whether these synthetic binding proteins can broaden the horizons of basic research and drug discovery, surpassing the capabilities offered by traditional antibodies. A primary driving force behind the ongoing advancement of synthetic binding proteins is their potential in therapeutic applications. Synthetic binding proteins are typically created by introducing numerous mutations, often between 10 and 20, into a protein scaffold. Techniques like molecular display, particularly those employing directed evolution strategies, allow for the efficient creation of a large library of mutated versions.

Variants that bind with high affinity to the target molecule can be identified from those libraries. The initial scaffold systems are selected with the goal of yielding synthetic binding proteins that have desirable functional and biophysical properties. These include creating effective molecular recognition interfaces for a variety of targets, compact size, robust stability, ease of production, and suitability for use in fusion proteins. Various successful platforms have been developed, and for a comprehensive understanding, extensive reviews on this topic, including additional scaffold systems and molecular details, are recommended.

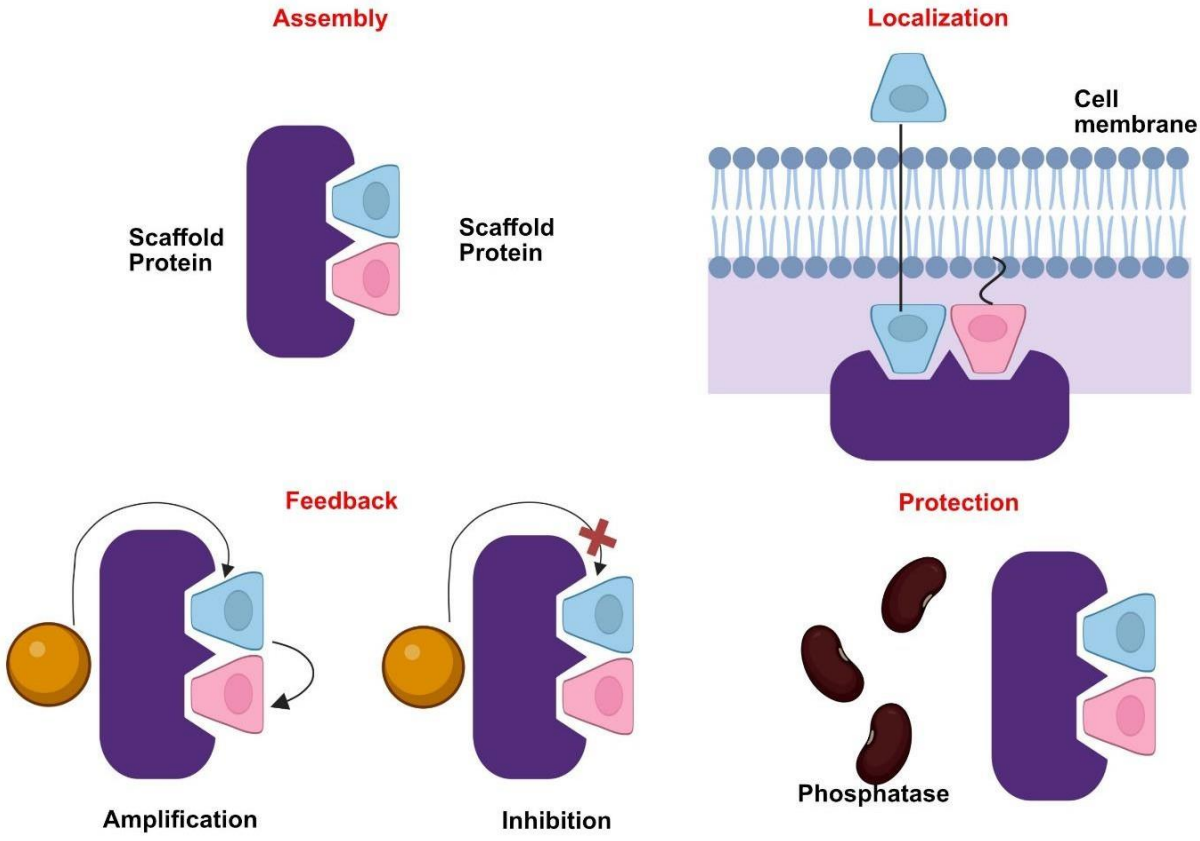

Figure 2.1 Scaffold proteins serve multiple roles, including assembling and localizing signaling pathway components, regulating feedback signals, and shielding active intermediates from phosphatase deactivation.

Prominent examples of synthetic binding protein platforms include Affibodies, [82] Anticalins, Monobodies, and DARPins. Affibodies are derived from the Z domain of Staphylococcus aureus' protein A. They feature three α-helices, lack disulfide bonds, and are among the smallest characterized synthetic binders (approximately 6 kDa). Anticalins, based on lipocalins, possess a β-barrel structure with an attached α-helix. Although some lipocalins contain disulfide bonds, they are chosen for their innate capacity to bind small molecules through their barrel and loops, a trait exploited in Anticalin libraries. Monobodies are designed from the fibronectin type III (FN3) domain, which has an immunoglobulin fold but lacks disulfide bonds. Following the success of Monobodies and their industry equivalence, several 'Monobody mimics' have been effectively developed, proving the reliability of the FN3 scaffold for creating synthetic binding proteins. Designed ankyrin-repeat proteins (DARPins) utilize repetitive structural units to form an extended binding surface. Despite lacking disulfide bonds, DARPins show high thermodynamic stability. Although these platforms are based on proteins with distinct structural configurations, they have all yielded high-performance synthetic binding proteins against varied targets, demonstrating the collective achievement of the field in developing effective scaffold systems. [83]

Ubiquitin, a 76-residue protein involved in numerous intracellular regulatory processes, stands out as a noteworthy addition. Several enzymes in ubiquitin-dependent pathways bind ubiquitin with relatively low affinity. Combinatorial phage-display libraries of ubiquitin variants have been created, yielding high-affinity (KD in the 1–100 nM range) and specific variants for particular ubiquitin-interacting proteins. [84]This success exemplifies how a promiscuous, low-affinity binding protein can evolve into a highly selective and effective one, akin to antibody maturation. Ubiquitin-based binding proteins have also been developed for targets such as the extradomain B of fibronectin, a protein not typically associated with ubiquitin interactions. However, the general

efficacy of ubiquitin-based single-domain binding proteins for broad applications remains to be seen, as their potency currently appears limited.[85]

When developing a scaffold system, designers usually envision a specific mode of interaction. For instance, the original Monobody system introduced amino acid diversity in loops at one end of the molecule, similar to diversified positions in natural immunoglobulins.[86] Structural analyses of monobody-target complexes revealed that in addition to the planned target interaction via diversified loops, an unexpected interaction mode was observed, where (unaltered) residues on the β-sheet surface contributed to target recognition. This led to the creation of a new library where β-sheet residues were diversified [Figure. 2.2]. Monobodies from this 'side' library presented a concave surface for recognition, as opposed to the convex surfaces typically seen in monobodies from the original 'loop' libraries. This approach allowed two distinct libraries to demonstrate preferences for differently shaped surfaces: the loop library tends to favor concave epitopes, while the side library is more suited to flatter surfaces. For instance, in an unbiased selection experiment against the Abl SH_2 domain, a dominant monobody clone from the loop library bound to the concave, peptide-binding groove, whereas a dominant clone from the side library bound to a flat surface on the opposite side of the SH_2 domain. [87] Similar library designs have been reported for other FN3-based systems like Centyrin, though details on the epitopes of resultant molecules are not available. These examples show how different surfaces can be utilized for presenting amino acid diversity, thereby expanding the types of epitopes that can be effectively recognized.

In a similar yet contrasting development, a new library for the DARPin system expanded binding site topography. The original DARPin libraries diversified positions mainly on α-helices, presenting a concave surface. The new 'LoopDARPin' library introduced significant diversity in loops lining one edge of the scaffold. This design created protruding loops, complementing the

original library's approach. High-affinity DARPins were identified from this new library after just one round of selection, highlighting the library's effectiveness. Structural analysis of anticalins has led to a second-generation library where amino acid diversity presentation positions have been refined for targeting large antigens like proteins, underscoring the benefits of structure-guided improvement in combinatorial libraries.

2.1.1 Monobodies: Structure, function, therapeutic applications

Proteins that bind to specific targets, such as antibodies and engineered binding proteins, are essential and powerful tools in both biological research and medical applications. These proteins, often referred to simply as 'binders,' are valuable in two primary aspects: firstly, as instruments for interfering with biological processes; and secondly, as facilitators in successful crystal formation. The fields of structural biology and the development of binders are deeply interconnected. Binders are instrumental in enabling the structural determination of complex systems, often referred to as 'harvesting high-hanging fruit.' Furthermore, the detailed structures of complexes formed by binders and their targets are crucial in understanding the molecular basis of target recognition and contribute to the advancement of binder technologies.

Monobodies are a type of synthetic binding protein constructed using the tenth type III domain of human fibronectin (FN3) as their foundational structure.[88] Since their first introduction, numerous designs of monobody libraries and similar systems like adnectin, centyrins, and tenascins have emerged in both academic and industrial settings. In the realm of structural biology, monobodies are the most prevalent among FN3-based binders, with 47 PDB entries for monobody-target complexes, compared to only six structures reported for other FN3-based systems. [89]

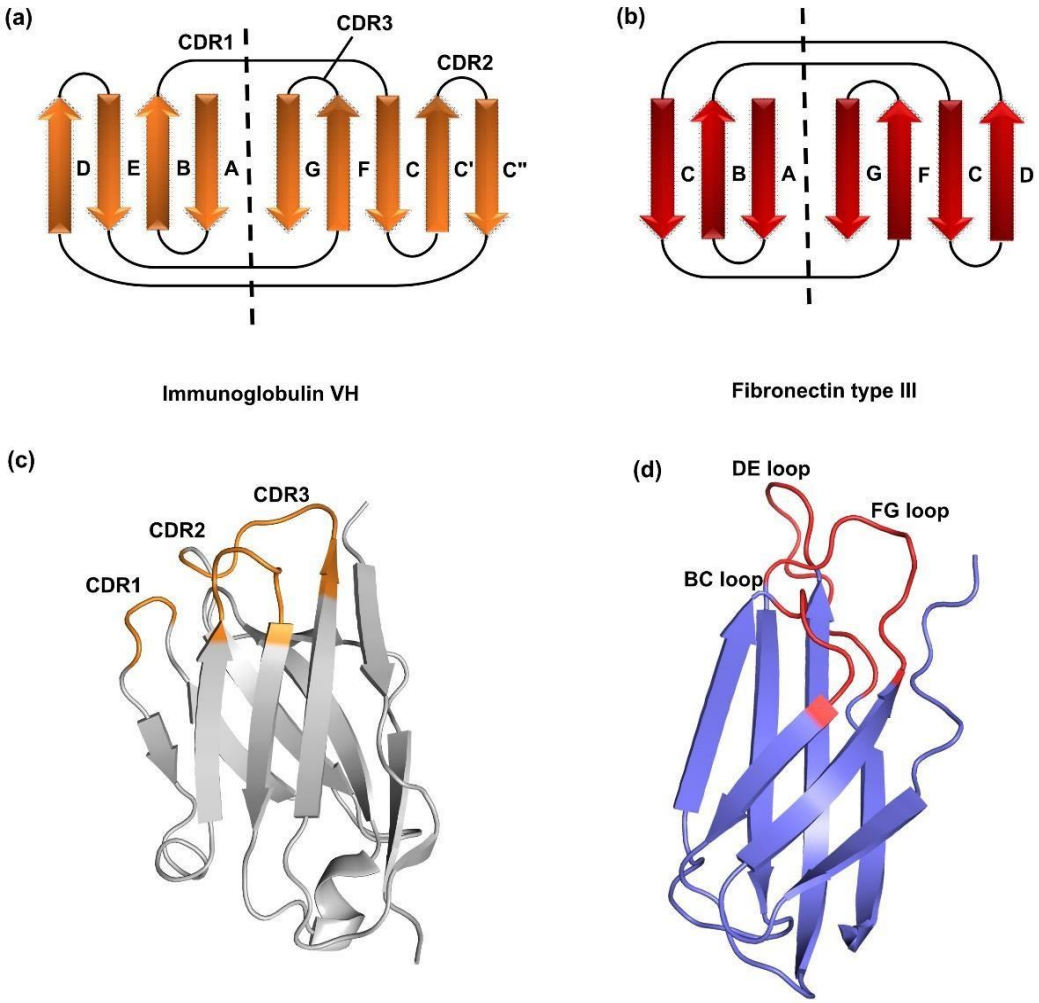

Figure 2.2 Illustrations of the fibronectin type III domain ((b) and (d)) and the immunoglobulin VH domain from the anti-lysozyme antibody D1.3 ((a) and (c)) showcase the β-strand and loop topology. These illustrations highlight the positions of the complementarity-determining regions (CDRs) on D1.3 and the binding region located on the Fn3 monobody.

Recent advancements in monobody technology have led to the development of two distinct types of combinatorial phage-display libraries, each characterized by its unique strategy for diversification. The first type of library focuses on diversifying three loops, akin to the complementarity-determining regions (CDRs) found in antibodies. [88] The second type diversifies

two loops at opposing ends of the FN3 scaffold, along with the intermediate β-sheet surface. This approach has enabled monobodies to exhibit an extensive variety of target-binding surface topography, ranging from convex to concave formations. This versatility significantly broadens the array of epitopes that monobodies can effectively target and bind to. In their role as crystallization chaperones, monobodies are generally engineered without a predetermined preference for any specific epitope. Nevertheless, additional methodologies, such as negative selection with blocking agents or decoy mutants, can be employed to selectively favor monobodies that bind to particular sites. These site-specific monobodies have proven to be exceptionally useful in dissecting and understanding mechanistic details of molecular interactions.[90,91] Typically, monobodies are produced and purified using *Escherichia coli*. However, their flexible production allows them to be expressed in various systems, including cultured cells and in vivo animal models. [92] This adaptability facilitates functional testing and analysis across different biological environments, further highlighting their applicability and utility in diverse scientific contexts.

2.2 MATERIALS AND METHODS

2.2.1 Protein Structure Modeling

In the field of comparative modeling, [93] a target protein's 3D structure is predicted by leveraging experimental data from a structurally similar, evolutionarily related protein, which acts as a reference template. The default workflow in SWISS-MODEL [94–96] includes these primary stages:

- Input Data: Lysozyme binding fibronectin type III monobody protein sequences in various FASTA format was provided to the web server.
- Template Search: The input data is used to find related protein structures in the SWISS-MODEL Template Library (SMTL) using BLAST for closely related templates and HHblits

for remote homology. [97]

- Template Selection: Post search, templates are ranked based on potential model quality, evaluated by Global Model Quality Estimate (GMQE) and Quaternary Structure Quality Estimate (QSQE) metrics. The best templates are chosen, considering their conformational states and coverage areas on the target protein. [94]
- Model Building: For each chosen template, a 3D model is created. This involves transferring conserved atomic coordinates, modeling loops for insertions/deletions, and constructing non-conserved amino acid side chains. This process is powered by OpenStructure and ProMod3.
- Model Quality Estimation: The QMEAN scoring function assesses the model's accuracy, using statistical potentials and pairwise distance constraints from all template structures to provide global and per-residue quality estimates. [94–96]

An alternative and powerful approach for the protein structure prediction is using AlphaFold, [98] a blend of bioinformatics and physical principles that leverages physical and geometric biases without heavily relying on manually crafted features, such as a specific scoring function for hydrogen bonds. This approach allows AlphaFold to efficiently learn from the Protein Data Bank (PDB) despite its complexity and diversity, including scenarios with incomplete physical context or structures dependent on specific conditions, like the presence of ligands or ions. The design enables it to predict structures that align with constraints that can be inferred from the sequence alone, thereby demonstrating significant utility in molecular replacement and the interpretation of cryogenic electron microscopy maps. With its capability to directly output protein coordinates within a short time frame, AlphaFold paves the way for proteome-scale structure prediction. This advancement is crucial, as it complements the rapid growth of genomic sequencing by potentially bridging the gap in structural knowledge, underscoring its importance as a tool in modern biology

and structural bioinformatics.

2.2.2 Protein-protein interaction studies using docking

RosettaDock,[99] operating on a Monte Carlo (MC) methodology, is a multi-scale docking algorithm that combines a low-resolution, centroid-mode, coarse-grain phase with a high-resolution, all-atom refinement phase. This process is aimed at optimizing the orientation of rigid bodies and the conformation of side chains. The algorithm aligns with the biophysical theory of encounter complex formation, transitioning to a bound state. It either begins with a random orientation of the protein partners (global docking) or a perturbed orientation from a predetermined pose (local perturbation). In this initial phase, proteins are represented with centroids replacing side chains. This phase involves a 500-step Monte Carlo, adjusting rotational and translational steps dynamically to achieve a 25% acceptance rate. The scoring function predominantly comprises a 'bump' term, a contact term, and residue environment and residue-residue pair-wise potentials specific to docking. [100]

After completing the centroid-mode, the algorithm selects the structure with the lowest energy from this stage for high-resolution refinement. In this phase, the pseudo-atoms of the centroids are substituted with the side-chain atoms in their original unbound conformations. This involves 50 MC steps, where the rigid-body position undergoes perturbation in a random direction and magnitude, defined by a Gaussian distribution centered around 0.1 Å and 3.0°. [101] Subsequent steps include energy minimization of the rigid-body orientation and optimization of side-chain conformations using Rotamer Trials, followed by Metropolis criteria evaluation. Every eight steps, the algorithm performs an additional combinatorial optimization of side chains using a full packing algorithm, which is also subject to Metropolis criteria. To increase efficiency, energy minimization is omitted if a rigid body move leads to a score change greater than +15. The all-atom scoring

function in this stage primarily includes Van der Waals forces (attractive and repulsive), a solvation term, an explicit hydrogen bonding term, residue-residue pair-wise interaction term, internal side-chain conformational energy, and an electrostatic term. For specific targets, RosettaDock utilizes various sampling strategies to enhance the likelihood of precise structure prediction. In scenarios lacking prior structural or biochemical information about the protein interaction, global docking is employed to generate randomized initial docking poses. [102] These are then processed through score filters and clustering to identify feasible low-energy structure clusters for further refinement. When some information about the complex is available, either from similar protein complexes or from biochemical or bioinformatics data indicating likely interaction regions, users can manually set the starting pose for local docking perturbations. Moreover, distance-based filters can be applied to bias the sampling towards docking poses that align with predefined constraints. In cases where backbone conformational changes are expected, appropriate strategies for backbone sampling are adopted to accommodate these changes.

2.2.3 Yeast surface display to check protein target binding [103]

Yeast cells are cultured at 30ºC in 10mL YPD broth until they reach mid-log phase, which is indicated by a cell density of approximately $5x10^6 – 2x10^7$ cells/ml or an OD600 of 0.8-1.0. All subsequent steps are performed at room temperature. The cells are then centrifuged at 500g for 4 minutes, and the supernatant is discarded. The cell pellet is washed with 10 mL of EZ 1 solution, followed by a second centrifugation and supernatant removal. The pellet is then resuspended in 1 mL of EZ 2 solution. At this stage, the competent cells can be used immediately for transformations or stored at temperatures at or below -70ºC. For storing, slow freezing is crucial, achieved by wrapping the aliquoted cells in 2-6 layers of paper towels or placing them in a Styrofoam box before storage in the freezer. It is important to avoid snap-freezing using liquid nitrogen.

For the transformation process, which applies to both freshly prepared and thawed frozen competent yeast cells, a mixture of 10-50 µl of competent cells and 0.5-2 µg of DNA (in a volume less than 5 µl) is prepared, to which 500 µl of EZ 3 solution is added and mixed thoroughly. This mixture is then incubated at 30°C for 45 minutes, vigorously mixing by flicking or vortexing 2-3 times during the incubation. After incubation, the cells are centrifuged at 1500g for 3 minutes, resuspended in PBSA, and then centrifuged again. The resulting pellet is resuspended in 3 mL of YPD and shaken at 30°C for 1 hour. Following this, the cells are pelleted again, the supernatant is removed, and the cells are resuspended in 1 mL of PBSA, pelleted, and the supernatant removed. The cells are then resuspended in 5 mL of SD media. 50 µl of the transformation mixture is spread on an SD plate for quantification of transformation efficiency and clonal storage. The 5 mL SD culture is outgrown for 16-24 hours, and protein expression is induced using SG media while ensuring the OD remains below 6.

The plates are incubated at 30°C for 2-4 days to allow growth of transformants. The OD of the liquid culture is monitored after approximately 12-18 hours. The culture is then washed and resuspended in SG media to induce protein expression. Growth of transformants is facilitated by incubating the plates at 30°C for a period of 2-4 days. Meanwhile, the OD of the liquid culture is monitored after roughly 12-18 hours, followed by washing and resuspending in SG media to trigger protein expression.

For the flow cytometry binding check, a series of solutions are prepared. Initially, 198 µL of PBSA is combined with 1.86 µL of streptavidin-Alexa647 to create a 333 nM solution. Concurrently, 1 µM stocks of biotin-(Target) are prepared. Secondary reagents, comprising 36 µL PBSA, 2 µL strep-Alexa647, and 0.5 µL GαM-FITC, are also prepared and stored in the dark at 4º. Yeast cells containing the plasmid are pelleted at 1000g for 1 minute, with the supernatant

removed, followed by a wash in 1 mL PBSA at 8,000g for 30 seconds. The cells are then resuspended in a mixture of 50 μL PBSA, 0.25 μL 9E10, and 2.5 μL biotin-(Target), incubated at room temperature for over 15 minutes, and subsequently pelleted. After splitting into two aliquots and pelleting again, the supernatant is discarded. The cells are resuspended in 20 μL of the secondary reagents and incubated in the dark at 4º for over 15 minutes. Following another pelleting and removal of supernatant, the cells are washed with 1 mL of PBSA and then analyzed and sorted using FACS Aria.

2.2.4 Sanger sequencing to determine the DNA sequence of lysozyme binder proteins [104]

In the preparation of a DNA sequencing sample, the following components are combined in a 0.5 mL tube: 900 ng of plasmid DNA, calculated based on 100-200 ng per kbp, and 6.4 pmol of primer, equivalent to 3.2 μL of a 2 μM primer stock solution. The volume is then brought up to 12 μL with ddH2O. Depending on the plasmid type, specific primers are used: pCT-SEQ-R for pCT plasmids and pET-SEQ-F for pET plasmids.

2.3 RESULTS AND DISCUSSION

Three unique DNA sequences of fibronectin type III domain 2 monobody binders that target hen egg white lysozyme were used for homology modeling to create protein models (sequences are provided in Appendix A).[105] SWISS-MODEL, a web-based tool, facilitated the modeling byaligning the target sequences with known protein structures. [106] The algorithm begins with input data of the target protein sequences and searches for evolutionary-related protein structures in its template library. Upon finding suitable templates, the algorithm ranks them based on quality estimates like GMQE (Global Model Quality Estimate), as shown in Figure 2.3. For each sequence, the top two models were chosen based on their sequence similarity and GMQE scores.

Upon the completion of model creation, the selected protein models were then subjected to protein-protein docking studies using ROSETTA, a computational tool renowned for its high-resolution analysis capabilities. The primary target protein for these studies was lysozyme obtained from hen egg white. This enzyme, widely known for its antimicrobial properties and prevalent in various bodily secretions such as saliva and milk, is notable for its ability to enzymatically break down the glycosidic bonds in the peptidoglycan component of bacterial cell walls. The choice of lysozyme as a target protein was influenced by its stability, abundant availability, and inherent antibacterial characteristics, making it an ideal candidate for interaction with the fibronectin binders in our biosensor application.

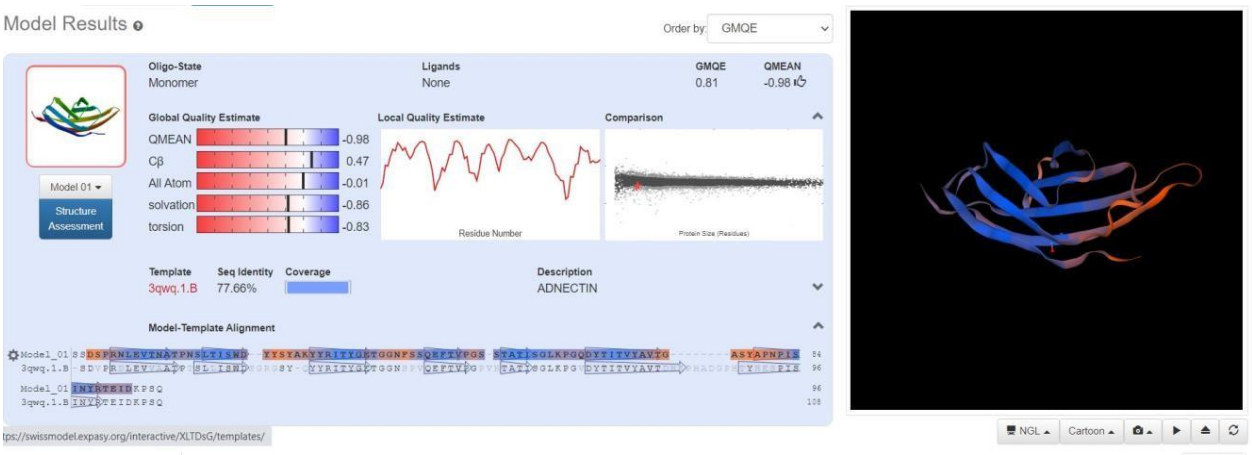

Figure 2.3 Monobody protein model targeting lysozyme made from template 3qwq using SWISS-MODEL.

ROSETTA, accessed via a Python interface, was utilized to simulate these protein-protein interactions. Employing the Metropolis Monte Carlo algorithm, ROSETTA facilitates the analysis by mimicking the complex interplay of local and global interactions that dictate protein structure. The docking process begins with randomly orienting the proteins, followed by a rigid Monte Carlo search involving translational and rotational movements of one protein around the other, known as low-resolution docking. The subsequent addition of explicit sidechains and the use of a rotamer

packing algorithm transition the process into a high-resolution phase. Here, the proteins' free energy minimum is calculated iteratively, with the position of the proteins perturbed slightly before each iteration. The Metropolis acceptance criterion determines whether the new position is accepted or rejected, based on a calculated score function. This docking method's efficiency is further augmented by including variations in sidechain torsion angles, enhancing the prediction accuracy.

Hundreds of fibronectin-lysozyme docked structures, or decoys, were generated for each fibronectin model derived from SWISS-MODEL, using ROSETTA on the High-Performance Computing Cluster (HPCC). The selection of decoys for analysis was based on their energy scores, with preference given to those closest or equal to the median of the population for each fibronectin model. These selected decoys were then visualized using PyMol, enabling the identification of polar bonds between the Fn3 variant and the lysozyme (Figure 2.4). This was followed by assessing the atomic distances between residues on both components of the docked system, specifically focusing on those residues within 5 Å proximity, as they were deemed most likely to be involved in the binding interaction. Further alignment of the amino acid sequences in the docked structures was conducted using multiple alignment tools in Geneious, [107] providing a comprehensive view of the interaction landscape.

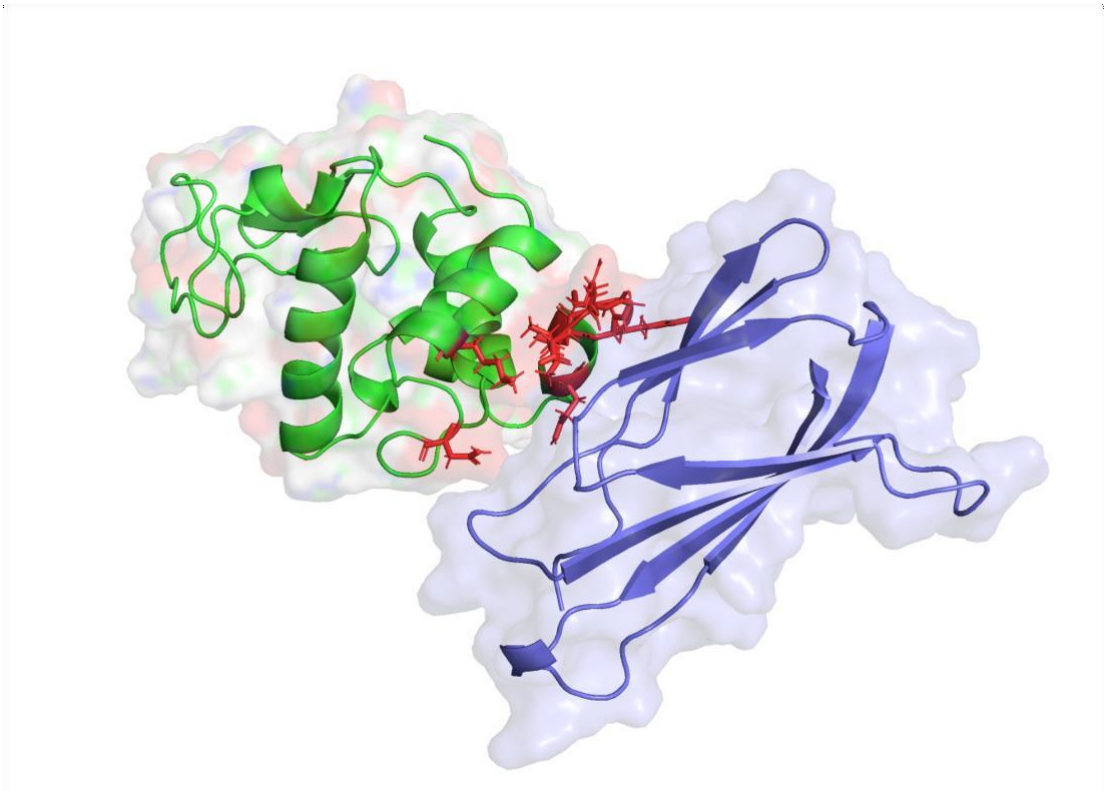

Figure 2.4 Monobody Lysozyme binding decoy predicted by ROSETTA where the active site sequences on lysozyme (green) within 5 A distance of the monobody (purple) are shown in red.

To validate the computational predictions, wet-lab techniques were employed to express the starting sequences of three fibronectin monobody variants. This approach aimed to corroborate the findings obtained from the computational docking studies, ensuring a robust and thorough investigation of the binder-target interactions. G-blocks corresponding to three fibronectin variants were acquired from IDT DNA, along with two types of vectors, pCT and pET, to construct fibronectin plasmids. Appropriate forward and reverse primers for the Polymerase Chain Reaction (PCR) amplification process were designed using online primer designing tool.

For the assembly of the plasmids, PCR was used to amplify both the inserts (g-blocks) and the vectors (pCT & pET). Two different cloning techniques were employed: the Gibson Assembly for

the pCT plasmid and digestion & ligation for the pET vector. Gibson Assembly, an enzymatic reaction in a single tube under isothermal conditions, involves a master mix that creates overhangs, fills gaps, and seals them. The digestion & ligation approach involves using restriction enzymes for cutting and inserting the PCR-amplified Fn3 into the pET vector. The resultant plasmids were verified through Sanger sequencing before being expressed in the yeast cells for flow cytometry experiments and in the T7 cells for protein production.

For the binding check with lysozyme, the pCT plasmids were transformed into yeast cells using yeast surface display. This technique involves expressing recombinant proteins incorporated into the cell walls of yeast cells. The target lysozyme was modified with biotin, and fluorophores Alexa 488 and Alexa 647 were used for flow cytometry studies. The Fn3 gene fragment, tagged with c-Myc and His-tags, allowed binding with Streptavidin (conjugated with A488) to the biotinylated lysozyme and with goat-anti-mouse (conjugated with A647) to the c-Myc tag of Fn3 in yeast cells. Successful binding was indicated by fluorescence in both A488 and A647 during flow cytometry analysis using Accuri. The presence of cells in the double-positive quadrant confirmed strong binding, validating the construction and function of the fibronectin plasmids.

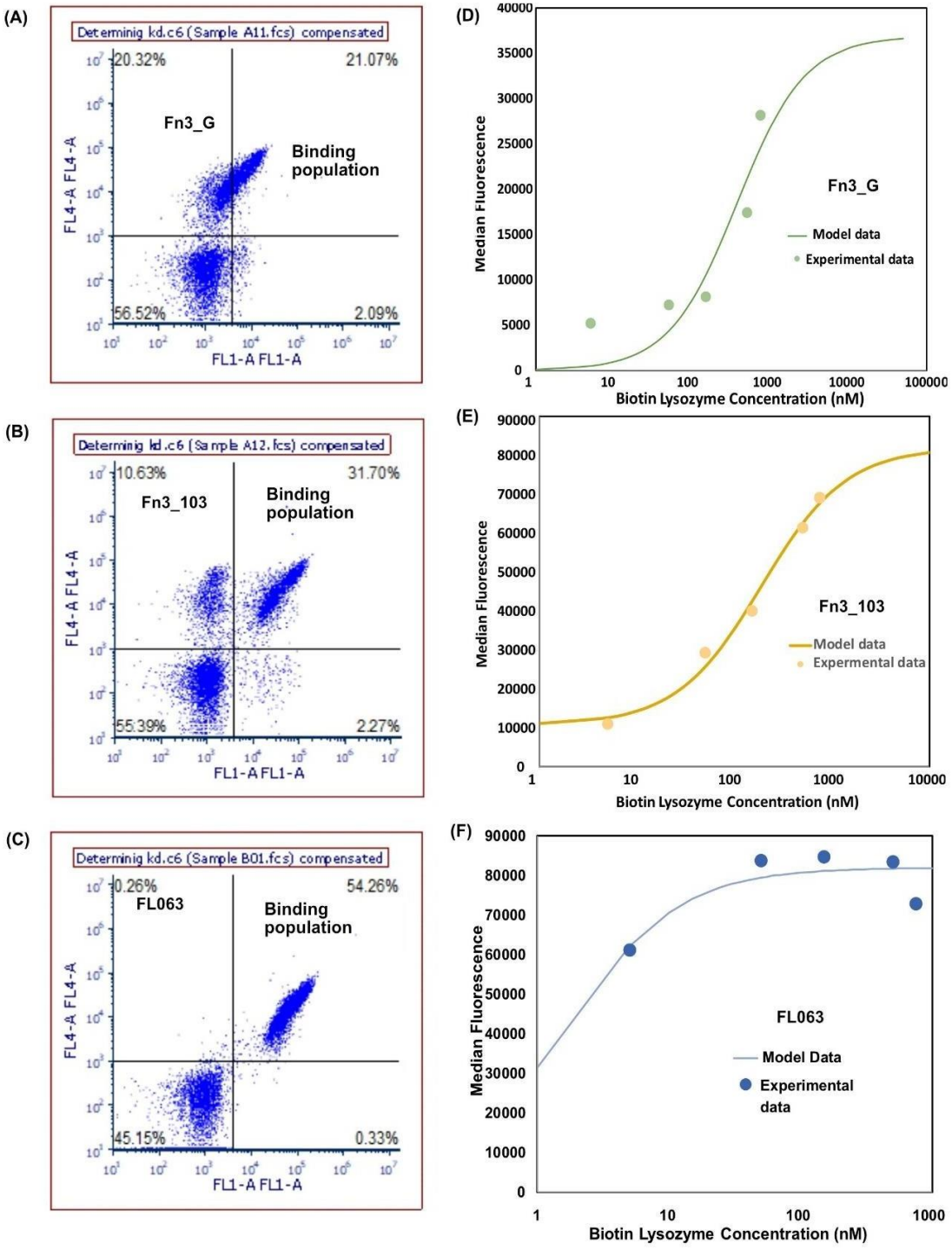

Figure 2.5 Binding check of the three monobody variants Fn3_G, Fn3_103 and FL063 with biotinylated lysozyme (A-C). Concentration dependence studies help in determining dissociation constants (Kd) for each variants using the median fluorescence values (D- F).

The equilibrium dissociation constant (Kd) is determined by fitting the total mean fluorescence (F_{tot}) from the double positive fluorescence percentage of cells against the target concentration ([T]) using the specified equation: [103,108–110]

$$F_{tot} = \frac{F_{min} + (F_{range} \times [T])}{([T] + Kd)} \quad \textbf{Eq. 2.1}$$

The calculation involves minimizing the sum of the squares of the differences between the measured F_{tot} and the F_{tot} calculated from the equation. This minimization is conducted as a function of the three free parameters: K_d, F_{min}, and F_{range}. It is assumed that [T] remains constant, equating to the initial antigen concentration. The equilibrium dissociation constants (Kd values) for the three fibronectin variants, namely G, 103, and FL063, were determined to be 375 nM, 189 nM, and 1.6 nM, respectively, as shown in Figure 2.5. Among these, the variant FL063, exhibiting the strongest binding affinity with a K_d of 1.6 nM, was chosen for subsequent stages of the study. This involved transforming FL063 into a soluble protein form, which was then utilized in electrochemical studies aimed at sensing applications. Detailed protocol of each method and relevant data is provided in the appendix.

2.4 CONCLUSION

The focal point of this chapter is the utilization of both computational and experimental protein engineering techniques to establish a comprehensive protocol for developing monobody variants that bind to clinically relevant targets. These binders are intended for use as biorecognition elements in electrochemical biosensing applications. Initially, the study identified three distinct DNA sequences of fibronectin type III domain 2 monobody, specifically engineered for binding to hen egg white lysozyme, from a curated library. Employing SWISS-MODEL, these selected

binders were accurately structured into protein models. Subsequent protein-protein docking studies using ROSETTA elucidated the detailed interactions between the fibronectin binders and the lysozyme target.[111] This high-resolution computational approach yielded significant insights into the binding dynamics and affinities of the monobodies towards their specific target.

To corroborate these computational insights, a series of wet lab experiments were conducted. This involved amplification of the DNA sequences through Polymerase Chain Reaction (PCR), followed by strategic construction of plasmids. The pCT plasmids were assembled using Gibson Assembly, while the pET vectors underwent a digestion and ligation process. Sanger sequencing played a crucial role in verifying the accuracy of these plasmid constructs. These constructs were then expressed in yeast cells for binding studies and in bacterial cells for protein production. A pivotal aspect of this research was employing yeast surface display to validate the binding efficiency of the engineered monobodies using flow cytometry analysis. This experimental validation not only supported the computational predictions but also demonstrated the functional prowess of the engineered monobodies. Further, the strongest binding variant, FL063, was transformed into a soluble protein form, for its application in electrochemical sensing studies, which is detailed in the next chapter. This integrative approach, merging computational predictions with empirical validations, exemplifies the synergy between different scientific methodologies in advancing biosensor technology.

3. ENGINEERED MONOBODIES ENHANCE ELECTROCHEMICAL DETECTION OF BIOMOLECULES

3.1 INTRODUCTION

Electrochemical biosensors have emerged as exceptionally effective and widely utilized tools for the rapid and specific detection of various analytes, marking their significance in the realms of biomedical research, clinical diagnostics [112,113], and environmental monitoring. These biosensors exploit the specificity of biorecognition elements, including enzymes, antibodies, and oligonucleotides, to accurately identify and quantify target molecules [114,115]. Their efficiency in translating biochemical interactions into readable electrical signals has fostered a transition from central laboratories to point-of-care applications, especially for the detection of small molecules such as glucose and lactate using enzymatic approaches. However, electrochemical biosensors face considerable challenges in detecting larger biomolecules, including nucleic acids and proteins [116,117]. This is due to the non-specific binding of irrelevant molecules and the limited diagnostic enzyme/analyte pairs for many analytes, which calls for more innovation to broaden their use and overcome these challenges [118,119].

To address the challenges associated with the detection of larger biomolecules, the scientific community has turned its attention to innovative biorecognition elements, with monobodies emerging as a promising option [120]. Monobodies are synthetic antibody mimetics that are derived from fibronectin type III domain and are engineered to bind with high specificity and affinity to target proteins. Their small size, stability, and ease of production have made them increasingly popular in various applications ranging from molecular research to therapeutic interventions [121]. Monobodies have been successfully employed in intracellular targeting, modulation of protein functions, and as crystallization chaperones, demonstrating their versatility and effectiveness in

complex biological environments, as shown in figure 3.1 [122]. Given these attributes, there is a growing impetus to integrate monobodies into portable quantitative devices, leveraging their potential to enhance the performance of electrochemical biosensors. In this chapter, we report the development of the first novel electrochemical biosensor using monobody as the biorecognition element to detect lysozyme.

Delving deeper into the characteristics of monobodies, these synthetic constructs showcase distinct binding motifs that contribute to their high specificity and affinity for target proteins [90]. These motifs are constructed through molecular engineering, allowing for the generation of diverse libraries of monobody variants tailored to recognize a wide array of protein conformations and functional states. The modular nature of monobodies, combined with their inherent thermal stability and robustness, makes them particularly advantageous for use in challenging conditions [122,123]. Furthermore, their capacity to maintain functionality across a broad range of temperatures and in the presence of denaturing agents underscores their resilience, a crucial factor for diagnostic tools [124–126]. The ease with which monobodies can be engineered and produced enhances their appeal, facilitating rapid iterations and optimizations to generate variants with improved performance characteristics [121]. By harnessing the specificity and stability of monobodies, it is possible to develop electrochemical biosensors that are not only more sensitive but also more stable, making them well-suited for the detection of large biomolecules in complex biological samples. This advancement could significantly enhance the performance and reliability of portable diagnostic devices, marking a pivotal step forward in electrochemical biosensing technology.

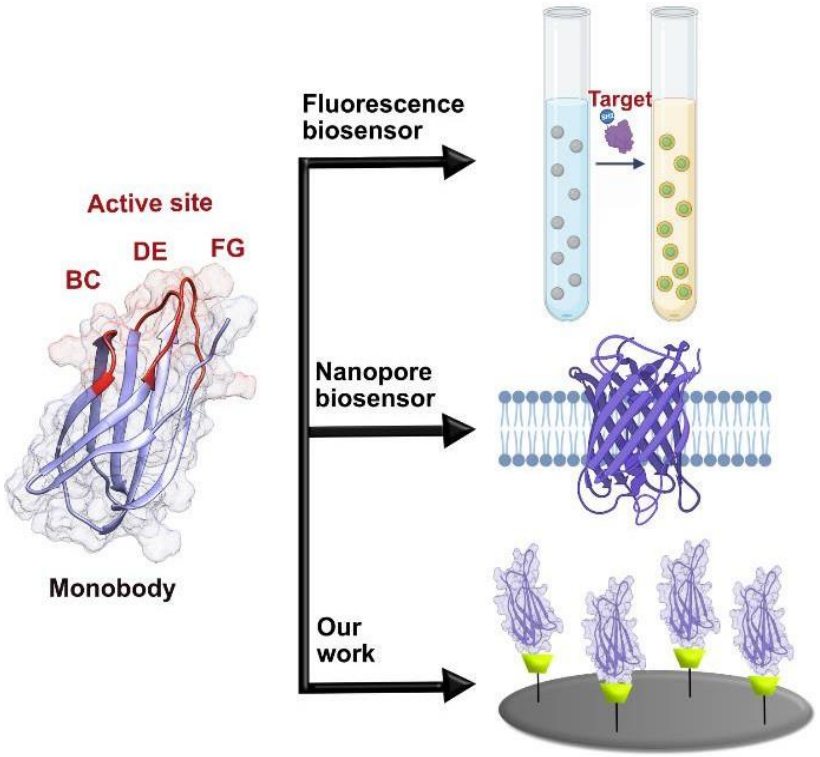

Figure 3.1 Three-dimensional representation of the fibronectin type III (FN3) domain (Protein Data Bank ID: 1TTG), visualized using Chimera.

The β-strands and loop regions, diversified in the combinatorial library, are highlighted in red which is the active site of the monobody. These small synthetic proteins are currently implemented in fluorescence biosensing [126] and nanopore sensors [125] for protein detection. We propose the first-ever monobody-based electrochemical biosensor detecting protein-protein interactions in this chapter.

In this study, we explore a novel electrochemical biosensing method that leverages the unique properties of monobodies for the specific detection of target proteins, such as lysozyme. Our experimental approach involved the modification of a glassy carbon electrode (GCE) surface by covalently attaching monobodies to it. This modification process aimed to create a non-conductive layer on the electrode surface, which is critical for the biosensor's functionality.

The experimental setup begins with the preparation of the GCE surface. We employed cyclic voltammetry to modify the electrode surface with diazonium esters. This initial modification did not create an insulating layer, thus allowing the free movement of reporter molecules, such as ferrocene, within the supporting electrolyte. This step was crucial for establishing a baseline for electrode conductivity and molecule transport. Following this, we immobilized monobodies on the diazonium-ester-modified layer, as shown in Figure 3.2. The introduction of monobodies marked a pivotal change in the electrode's environment. These monobodies acted as a barrier, significantly impeding the transport of ferrocene molecules to the electrode surface. This effect was quantitatively assessed through changes in electrode resistance and peak current. The impact of the monobodies was further amplified upon the introduction of the target analyte, lysozyme. The formation of monobody-lysozyme complexes on the electrode surface further increased the resistance to reporter molecule access. This phenomenon was evidenced by a notable decrease in peak current, as illustrated in Figure 3.3. Our hypothesis was that the monobody-modified GCE would act as a selectively permeable barrier, increasing resistance to nonspecific molecules while allowing for the detection of specific target analytes, such as lysozyme. The results from our experiments support this hypothesis, demonstrating a clear correlation between the presence of lysozyme and changes in the electrochemical properties of the modified electrode. This innovative approach to biosensing utilizes the potential of monobodies in creating highly selective and sensitive biosensors for protein detection.

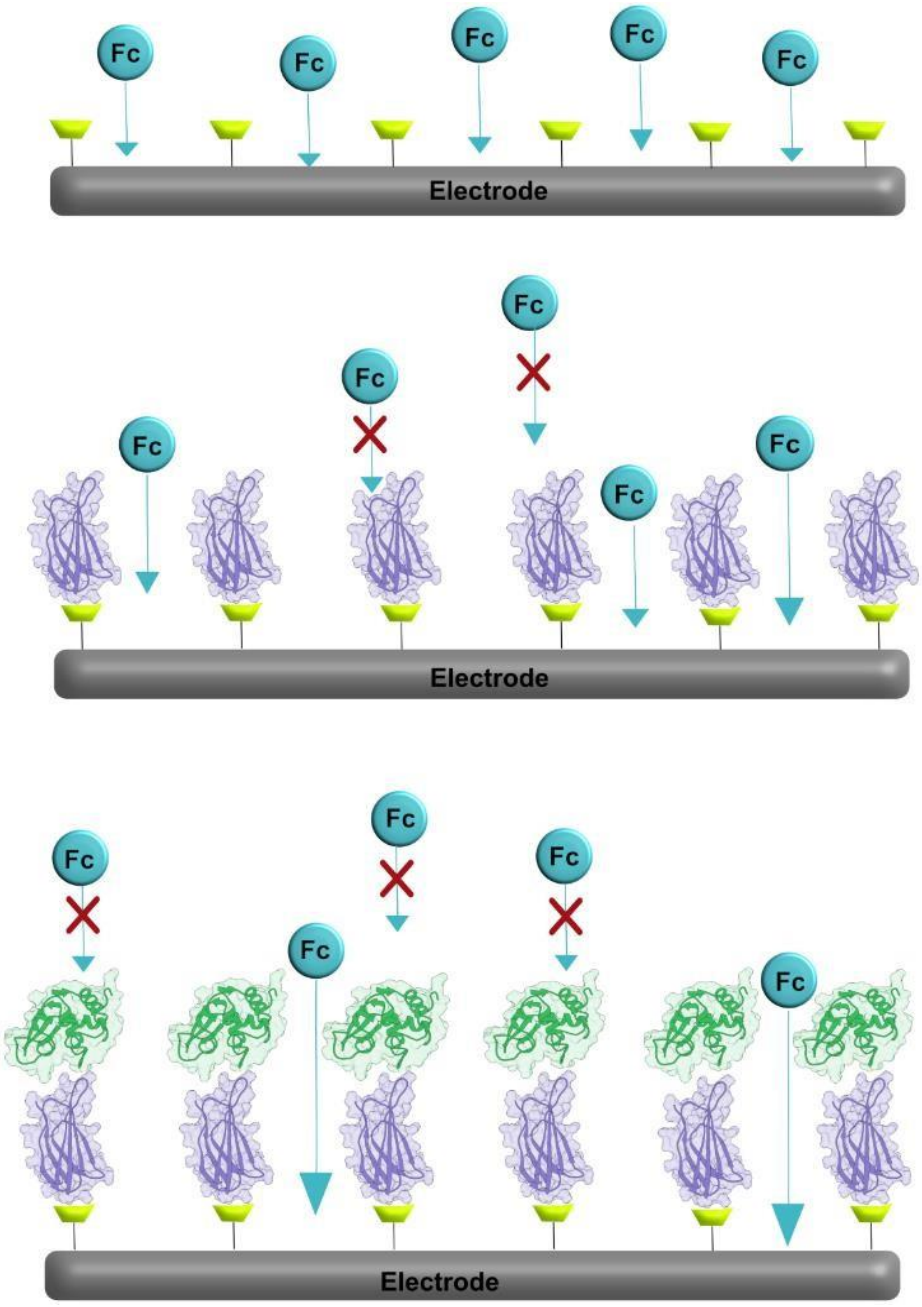

Figure 3.2 Schemati`c representation of the diazonium-modified monobody electrode (1) diazonium ester is grafted on the GCE by cyclic voltammetry in DCM by sweeping from 0 to -0.9V at 100mV/s. The diazonium-ester layer on the electrode is not insulating in nature and, hence provides no resistance in the transport of the ferrocene molecules (blue) (2) The monobody (purple) is immobilized on the grafted diazonium layer by incubating the surface-

Figure 3.2 (cont'd)

modified target for 30 minutes. (3) The monobodies anchored to the electrode surface offer resistance to the ferrocene molecules reaching the electrode surface. When the monobodies further bind to the target lysozyme (green), the ferrocene molecules experience a higher binding resistance to the electrode surface.

3.2 MATERIALS AND METHODS

3.2.1 Chemicals

Reagent-grade chemicals were utilized throughout the study. The PBS buffer, (ferrocenylmethyl)dimethylamine,N-hydroxysuccinimide, and 1-ethyl-3-(3- dimethylaminopropyl) carbodiimide were procured from Sigma Aldrich. Sigma Aldrich and Abcam were the sources for the target protein hen-egg white lysozyme and BSA control, respectively. Electrochemical measurements were performed using the Biologic potentiostat (VSP, 5 channel). An SCE reference electrode and a Pt counter electrode (Bioanalytical Systems, West Lafayette, IN) were used for relative measurements. Glassy carbon electrodes (GCE) with a diameter of 3 mm (CH instruments) were polished with a cloth polishing pad (Buehler, Lake Bluff, IL) and alumina slurry of 1, 0.3, and 0.05 μm sequentially, prior to the measurements.

3.2.2 Protein production

The human fibronectin type-II domain III plasmid FL063 sequence with a cysteine at position 102 was designed using IDTDNA. The pCT and Pet22b plasmids were obtained from IDTDNA and expressed in T7 (E. coli) cells (NEB Cat: C2566H). LB and kanamycin solution were used to cultivate starting cultures of T7 cells, which were grown overnight. These cultures were then transferred to 2 L cell cultures without antibiotics and incubated overnight at room

temperature on an orbital shaker at 250 rpm. The induction with IPTG for 16 hours was revealed to yield the highest protein concentration by SDS-PAGE results. Cell lysis was performed using the French press mechanism, and protein purification was executed using HisPur Cobalt columns in an FPLC. Amicon filters of 10 kDa were utilized for further concentration of the purified proteins. The expression of the desired protein and the yield of production were verified by SDS-PAGE. A Nanodrop was employed for the determination of the protein concentration.

3.2.3 Synthesis of diazonium salt [127]

In a round-bottomed flask, 4-aminobenzoic acid (2.74 g, 20.0 mmol) was dissolved in a solution of fluoroboric acid (48%, 14.6 g, 80 mmol) and water (20 mL). The solution was heated until complete dissolution of the aniline was achieved, followed by cooling in an ice water bath. A solution of sodium nitrite (1.46 g, 21.2 mmol) in water (4 mL) was added dropwise to the cooled solution under stirring. The diazonium product precipitated upon addition of the sodium nitrite solution and subsequent placement in an ice bath. The white solid formed was filtered, washed with cold ether, and dried under vacuum to yield 1.24 g (26%) of the diazonium salt. 1H NMR (400 MHz, DMSO) δ (ppm); 8.42 (2H, d), 8.78 (2H, d), 14 (H, s).

3.2.4 Synthesis of diazonium ester [128]

To a mixture of diazonium salt (100 mg), EDC (115 mg), and NHS (215 mg) in anhydrous CH2Cl2 (12 mL), an ice bath was applied, and the mixture was stirred for 16 hours. The organic layer was subjected to successive washes with 1 M HCl and a saturated aqueous solution of $NaHCO_3$. The aqueous layers combined were dried over $MgSO_4$, and the concentration under vacuum yielded a reddish-orange oily product.

3.2.5 Synthesis of water-soluble (ferrocenylmethyl)trimethylammonium chloride (FcNCl)[129]

A 250 mL Schlenk flask was purged with N_2 gas and kept under an N_2 atmosphere. ((Ferrocenylmethyl)dimethylamine (2 g, 82.3 mmol) and methyl chloride (1 M in tert-butylether, 82.3 mL for 82.3 mmol, 9 mL used) were combined with CH_3CN (5 mL) in the flask.

The reaction mixture was stirred overnight at room temperature. A red-orange precipitate was formed and filtered out. The precipitate and the remaining solution were combined after the addition of 100 mL of ether to the latter. Washing of the combined product was done twice with ether, and it was subsequently dried under vacuum. The hygroscopic product was stored in a dry desiccator, with the yield being approximately 95% (23.0 g). The 1H NMR spectrum (300 MHz, in D_2O) exhibited characteristic peaks: δ (in ppm), 2.91 (s, 9 H), 4.24(s, 5 H), 4.35 (s, 2H), 4.39 (s, 2H), 4.47 (d, 2H).

3.2.6 Surface modification of the electrode [130]

A 4 mM solution of diazonium ester in anhydrous CH2Cl2 was prepared. Grafting of the ester onto the GCE was conducted by applying a potential from 0V to -0.9V against a Pt-wire counter electrode and Ag/AgNO3 reference electrode in DCM. Post grafting, the modified electrode was incubated with a 10-micromolar solution of the binding protein FL063 in PBS buffer (pH 7) for 30 minutes.

3.2.7 Electrochemical methods

The electrochemical studies were carried out in triplicates using identical electrodes. Biologic VPS 5 Channel potentiostat was utilized for square wave experiments. These experiments were performed in a 100 mM phosphate buffer, the pH of which was adjusted to 7.4 at room temperature. Square wave voltammetry was executed with a frequency of 10 milliseconds, employing a Pt-wire

counter electrode and SCE reference electrode, for all measurements on 3 mm glassy carbon electrodes purchased from CH Instruments (part number CHI104).

3.3 RESULTS AND DISCUSSIONS

Initially, the electrode is covalently functionalized with diazonium-NHS ester. This functionalization facilitates the attachment of monobodies to the electrode surface. The diazonium ester molecule covalently attaches to the free primary amine group of the monobody (FL063), thus anchoring the protein on the surface of the glassy carbon electrode (GCE). The square wave voltammetry measurements for a monobody-modified GCE show a characteristic decrease in the peak currents when compared to a bare GCE. Electrodes modified by only the NHS ester do not show significant difference (about 2 µA) in peak current in comparison to a bare GCE in ferrocene solution (Figure 3.3). This indicates that the reduced peak is due to the deposition of the binding protein on the surface alone. On incubating the electrodes further in the target lysozyme solution, the peak current decreased further. To further test the binding specificity of the FL063-modified GCE, the electrodes were incubated with a 10 µM solution of BSA in PBS, as shown in Figure 3.4. No change in peak currents was observed for the BSA control. Furthermore, the binding protein-modified electrode was incubated with the lysozyme solution ranging in concentration from 1 µM to 50 µM (Figure 3.5), and square wave measurements were taken to determine the concentration dependence.

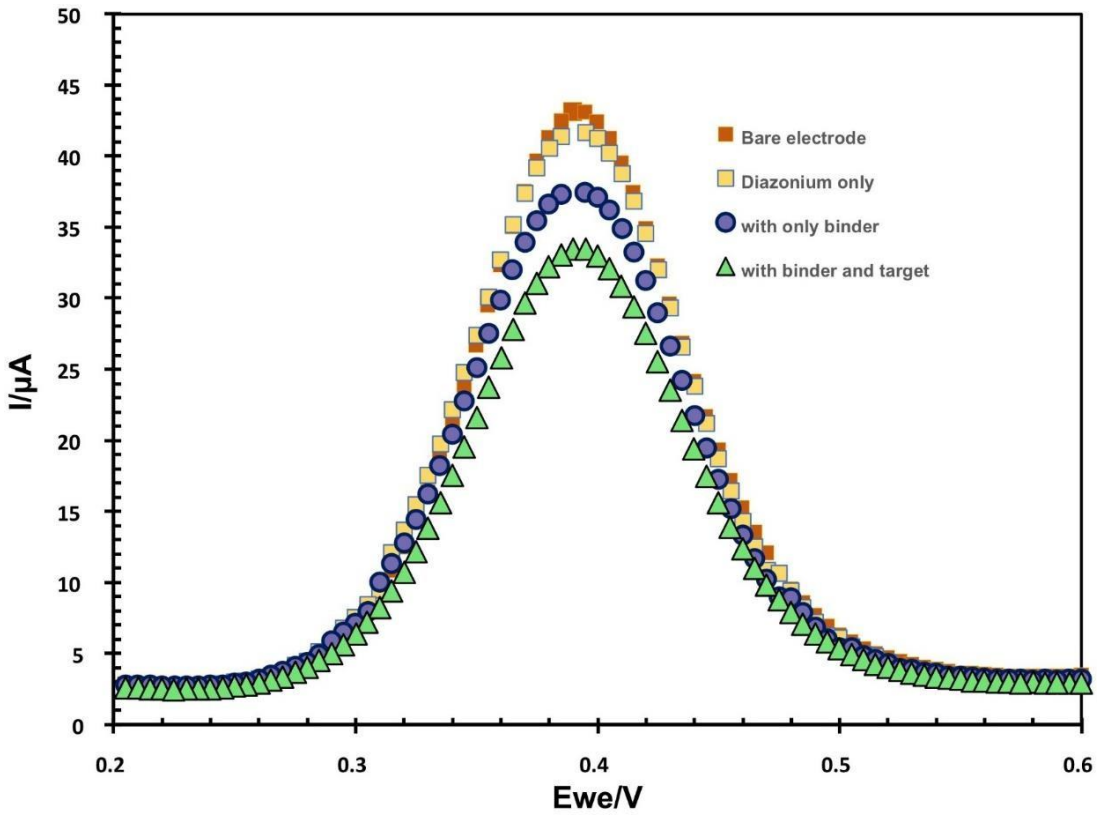

Figure 3.3 Squarewave voltammogram showing electrode modification with diazonium grafting. The diazonium layer itself does not change the peak current, only the insulating layer of immobilized monobodies help in creating a non-conductive layer, thereby decreasing the peak current signal. The measurements were taken using a 3 mm glassy carbon working electrode, Pt-wire counter electrode, SCE reference electrode, and 100 mM phosphate buffer at pH 7 and 25 °C.

To quantify the range of analyte concentrations for which biosensor response changes linearly and understand the resolution of the biosensor, knowing the working, as well as the linear range of the sensor, is crucial. With increasing concentrations of target lysozyme, the difference between the peak currents of only the binder-modified electrode and the lysozyme-binder-modified (Figure

3.4 , part A) electrode increased till it reached a saturation point. Similar concentration studies were conducted for BSA control, which showed no change in the difference in the peak currents of the

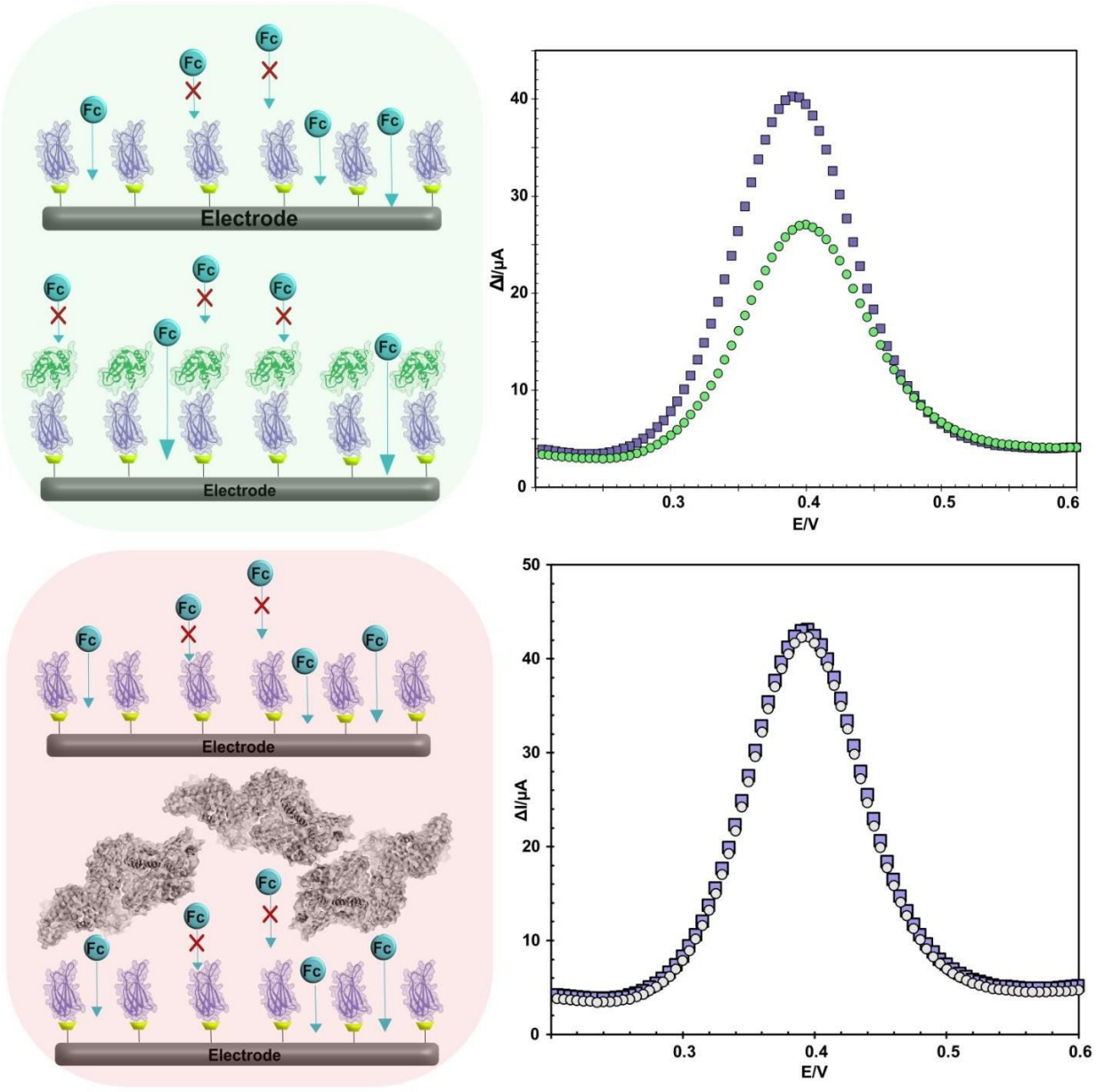

Figure 3.4 Square wave voltammetry measurements of GCEs modified with (A) FL063 (purple), FL063-Lysozyme (green), and (B) FL063-BSA (grey) control in 1mM ferrocene at a frequency of 10ms. Experiments were performed using a 3 mm glassy carbon working

Figure 3.4 (cont'd)

electrode, Pt-wire counter electrode, SCE reference electrode, and 100 mM phosphate buffer at pH 7 and 25 °C.

binder-modified electrode vs the binder-modified electrodes subjected to the albumin solution. The detection limit (LOD) for the monobody-modified electrochemical biosensor has been determined to be 0.9 µM, with the quantification limit (LOQ) established at 2.7 µM. These parameters were derived utilizing the standard deviation method, where the LOD was calculated by tripling the standard deviation of the blank readings and dividing it by the slope of the calibration curve within the linear range. Similarly, the LOQ was ascertained by multiplying the standard deviation of the blank by ten and dividing by the same slope [131]. The calibration curve, delineated in Figure 3.6, demonstrates a robust linear relationship between the variations in peak current and the concentrations of lysozyme across a range spanning from 0.1 µM to 1 µM, with a correlation coefficient (R^2) of 0.97.

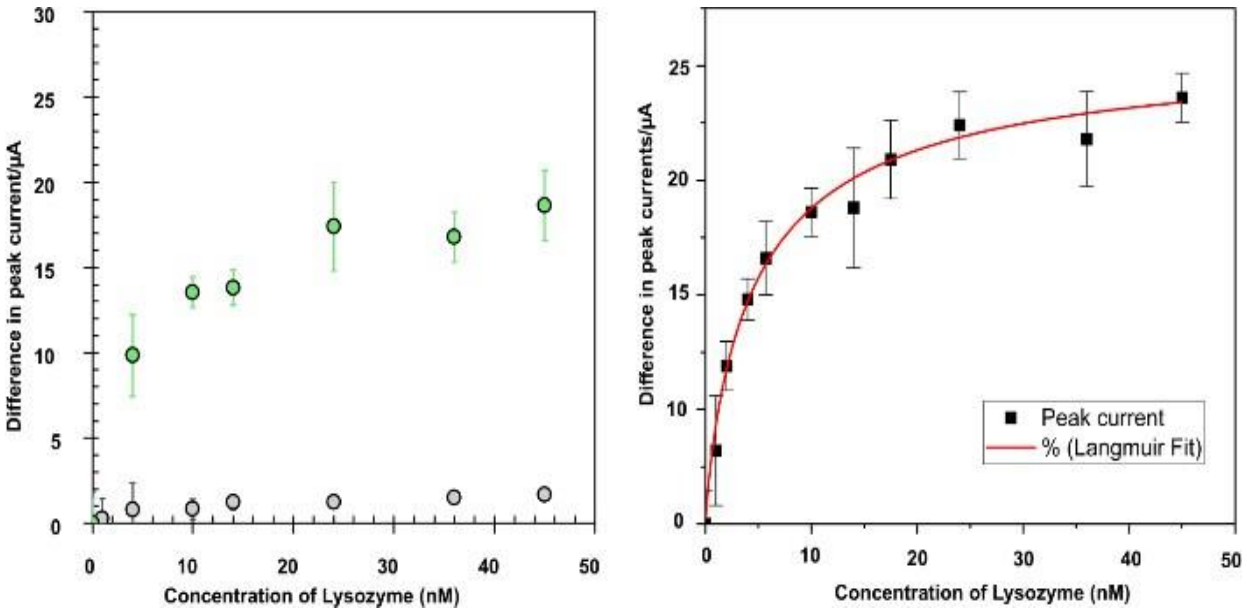

Figure 3.5 Concentration studies of GCEs modified with (A) FL063-Lysozyme (green), and FL063-BSA (grey) were done by measuring peak currents using square wave voltammetry

Figure 3.5 (cont'd)

control in 1 mM ferrocene at a frequency of 10 ms. The modified electrodes were incubated in the target solution of lysozyme with concentrations ranging from 1 to 50 µM. Experiments were performed using a 3 mm glassy carbon working electrode, Pt-wire counter electrode, SCE reference electrode, and 50 mM phosphate buffer at pH 7 and 25 °C. Error bars represent one standard deviation from the mean, *n*= 3. (B) The signaling peak current values with increasing concentrations of target lysozyme in phosphate buffer was fitted with the Langmuir adsorption isotherm model. The red curve shows the fit and the black square markers represent the actual peak current values. The fit successfully converged after 400 iterations.

The diazonium molecules are electrochemically grafted on the surface of the GCE (Figure B.1.). These diazonium-grafted electrodes are then incubated in the monobody solution to create a stable linkage. The monobodies then adhere to the surface of the electrode in a uniform manner and create a monolayer. This is in line with the Langmuir adsorption isotherm, which predicts that molecules will form a monolayer on the adsorption surface[132,133]. The adsorption isotherm also assumes that all adsorption sites are equivalent. On a GCE surface, this would mean that each site where a diazonium molecule grafted monobody can attach is equivalent in terms of its ability to bind the complex. This is a simplification, as the surface might have imperfections or varying functional groups, but for the model, we assume uniformity. Furthermore, it is assumed that each adsorption site can only be occupied by one molecule. In this case, it means that once a monobody has attached to a diazonium-grafted site on the GCE, no other molecules can bind to that exact site. This ensures that a monolayer is formed, rather than a multilayer, governed by the equation [134,135]:

$$q_e = \frac{q_m K C^X}{(1 + K C^X)} \qquad \textbf{Eq.3.3.1}$$

Where *qe* is the equilibrium adsorbent-phase concentration of adsorbate (mg L^{-1}), C is the concentration of adsorbate (mg L^{-1}), q_m is the maximal adsorption (mg g^{-1}), K is the constant related to the free adsorption energy and the reciprocal of the concentration at which half saturation of the adsorbent is reached, and X is a parameter that indicates the level of concentration dependence. When X<1, the adsorbate-adsorbent system shows less dependence on concentration, while when X>1, the system experiences higher dependence on concentration. The adsorption isotherm assumes that all adsorption sites are equivalent where q_e is the equilibrium adsorbent-phase concentration of adsorbate (mg L^{-1}), C is the concentration of adsorbate (mg L^{-1}), q_m is the maximal adsorption (mg g^{-1}), K is the constant related to the free adsorption energy and the reciprocal of the concentration at which half saturation of the adsorbent is reached, and *X* is a parameter that indicates the level of concentration dependence. For $X < 1$, the adsorbate-adsorbent system shows less dependence on concentration, while when $X > 1$, the system experiences higher dependence on concentration.

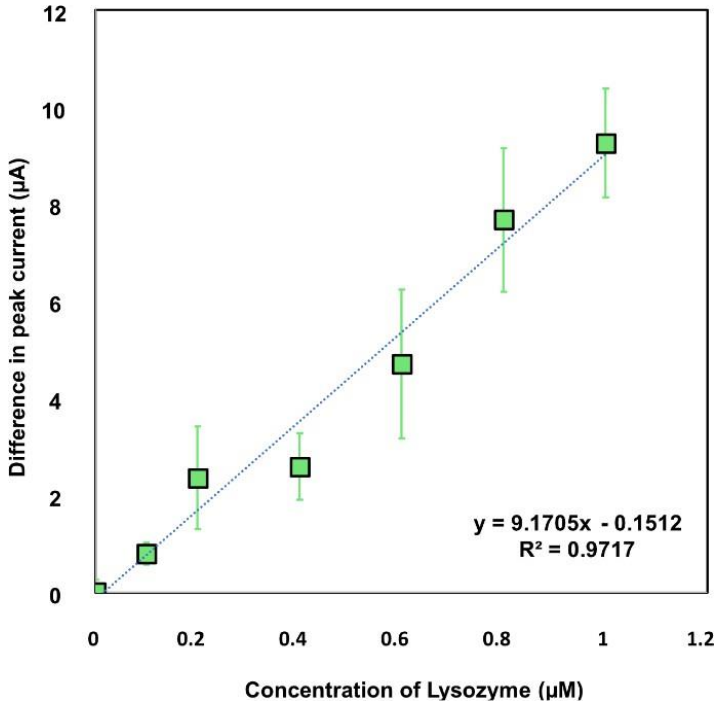

Figure 3.6 The linear range of target lysozyme detection in phosphate buffer was seen between 0.2 µM to 1 µM. Using the standard deviation rule, the limit of detection has been calculated as 0.904 µM. The measurements were taken using a 3 mm glassy carbon working electrode, Pt-wire counter electrode, SCE reference electrode, and 100 mM phosphate buffer at pH 7 and 25 °C. Mean values are plotted where each error bar represents one standard deviation, n=3.

The difference in the peak currents when plotted with increasing concentrations of the target lysozyme in phosphate buffer (as shown in Figure 3.5 (part B)) fits the Langmuir adsorption isotherm model, where the calculated monolayer adsorption capacity matches with the experimentally determined saturation peak current value of 21 µA. The parameter X can be plausibly compared to surface heterogeneity factor [135,136]. A heterogeneous surface might demonstrate a weaker concentration dependency, as areas of high energy on the surface tend to be covered first, even at low concentrations of solute. Hence, a heterogeneous surface (meaning n<1)

tends to align with a system showing reduced dependence on solute concentration (indicating X<1). [137] The Langmuir adsorption coefficient determined from the isotherm model is 260nM with the concentration-dependent factor, X value as 0.86.

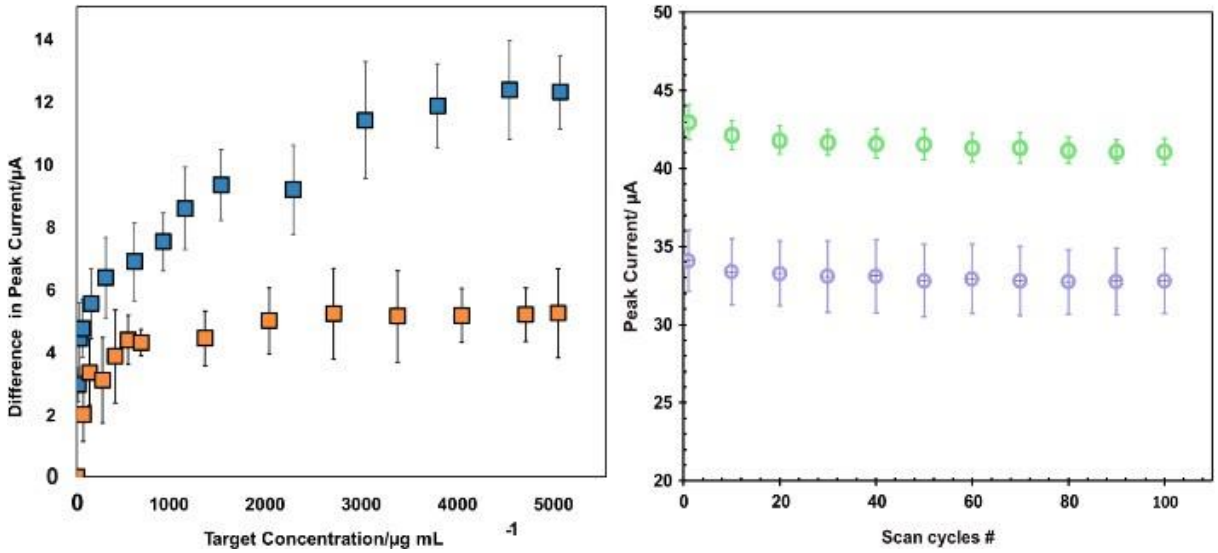

Figure 3.7 (A) Concentration dependence study of GCEs modified with monobody-lysozyme in PB in 30% canine serum (blue), and BSA control in 30% canine serum (orange). All experiments were performed using a 3 mm glassy carbon working electrode, Pt-wire counter electrode, and SCE reference electrode. Error bars represent one standard deviation from the mean, *n*= 3. (B) Electrical stability of the biosensor was studied by continuously applying 100 scans of square wave current (frequency 10ms) in 0.1M PB at room temperature for 90 minutes. No change in current is seen in the monobody immobilized GCE in the presence (green) and absence (purple) of the target lysozyme. Error bars represent one standard deviation from the mean, *n*= 3.

Bioelectrodes modified with monobodies were subjected to evaluation in 30% canine serum. [138]Incremental concentrations of target lysozyme were introduced into the serum matrix, and the monobody-augmented electrodes were maintained under stirring conditions for a duration of 15

minutes prior to electrochemical analysis. The square wave voltammetry experiments were conducted in a 1mM Ferrocene solution in 0.1M phosphate buffer (pH 7), using a platinum wire counter electrode and SCE as the reference electrode. An analogous decrement in peak current was observed during the detection of lysozyme in serum. During lysozyme detection in serum, a comparable decrease in peak current was noted. As demonstrated in Figure 3.7 (A), there is a notable rise followed by a stabilization in the peak current differential between electrodes modified solely with binder and those with lysozyme-bound binder in canine serum (illustrated in blue). Conversely, the bovine serum albumin (BSA) negative control (represented in orange) exhibited only a marginal fluctuation in peak currents, suggestive of minimal nonspecific adsorption to the electrode surface. This minor deviation was deemed inconsequential in the context of lysozyme interaction. The nonspecific adsorption observed upon the addition of BSA to the canine serum may be ascribed to non-target interactions, potentially with proteins inherently present in the serum, as the clinical history of the donor canines was not established. This interaction could account for the observed alterations in peak currents for the BSA control assays.

Literature shows that electrochemical biosensors comprised of larger biorecognition elements exhibit 6% signal loss after 50 scans of alternating current voltammetry, whereas sensors using monothiols lose ~25% of their signal.[118] In order to test the electrical stability of our sensor, we subjected it to continuous 100 scans of square wave current Vs SCE in 0.1M PB at room temperature. Figure 3.6 (B) shows that even after 100 scans there was no significant signal loss. The monobody-modified electrode in the absence of target lysozyme was also subjected to a continuous 100 scans of square wave current (purple) and showed no change in signal. This provides evidence of the high electrical stability exhibited by our model monobody-based electrochemical biosensor.

3.4 CONCLUSION

In this chapter, a novel strategy was developed for the determination of lysozyme using a monobody-modified electrochemical biosensor that has demonstrated a unique and sensitive detection capability. The covalent attachment of diazonium-ester to a monobody and its subsequent uniform adherence to a glassy carbon electrode surface has been systematically characterized, showing significant promise for lysozyme quantification. This biosensor exhibits a high degree of specificity, negligible nonspecific adsorption in complex matrices such as canine serum, and outstanding electrical stability, with no significant signal loss observed after extensive electrochemical scanning. With a detectable range from 0.1 µM to 1 µM and LOD and LOQ values of 1.31 ng/µL and 4.35 ng/µL, respectively, the biosensor's performance is underpinned by a robust calibration curve. The findings suggest the monobody-based biosensing platform holds considerable potential as an alternative method for the accurate and reliable detection of biomolecules, warranting further exploration and validation for clinical and analytical applications.

4. MULTIPLEXING AND USING TANDEM MONOBODY BINDERS ENHANCE SENSITIVITY AND VERSATILITY OF THE BIOSENSOR

4.1 INTRODUCTION

An advanced electrochemical biosensor employing monobody binders was developed, utilizing synthetic small proteins extracted from the fibronectin type III domain. Due to the inherent inability of monobodies to generate a signal upon binding to target proteins, they were functionalized via NHS-EDC chemistry. [139] Subsequently, these functionalized monobodies were immobilized onto the electrode surface through electrochemical grafting. As elucidated in Chapter 3, this immobilization resulted in the formation of a non-conductive monobody layer on the electrode surface, which effectively obstructed the access of reporter molecules to the electrode. The introduction of the target protein, lysozyme, further amplified this resistance, leading to an increase in electrical impedance and a consequent decrease in peak current. As the binder-target complex adds further insulation on the electrode surface, there is an automatic increase in resistance for the redox probe to reach the surface of the electrode, resulting in a biosensor that is highly specific to its target, Comprehensive evaluations of the biosensor have demonstrated minimal non-specific interactions and exceptional electrical stability. Moreover, the biosensor has proven to be effective in the detection of target molecules even in complex physiological mediums, such as serum, highlighting its potential for broad application in biomedical diagnostics and research. While lysozyme is an exemplary model biomarker, it is not sufficient as a standalone diagnostic indicator for specific diseases. This situation necessitates the development of a biosensor that is not only highly modular but also capable of being engineered with ease to identify a variety of clinically relevant targets. The simultaneous detection of multiple relevant targets in real-time is essential to enhance the biosensor's versatility and provide a more definitive diagnosis

of diseases. An effective strategy to achieve such a biosensor is through the multiplexing of the one-on-one model monobody biosensor previously developed. [140]

As elaborated in Chapters 2 and 3, monobodies stand out as ideal biorecognition elements due to their high stability, robustness, and most importantly, modularity to bind to biomarkers of interest. We hypothesize that engineering multiple monobody binders, each binding to different clinically relevant targets can result in the creation of individually addressable bio-electrodes. These electrodes would collectively function as an array of sensors. This approach is expected to generate different signals for each target, thereby offering a more comprehensive overview for disease detection. In this chapter, we will discuss our work on finding monobody binders for targets such as different types of immunoglobulins[141] and human transferrin[142,143] to create an array of individually addressable bio-electrodes.

While our biosensor demonstrated remarkable specificity for lysozyme, there is potential for enhancing its sensitivity. As noted in Chapter 3, the observed variation in peak currents between target-bound and unbound monobodies lies in the lower microampere range. Although this difference is statistically significant, a larger change in the signaling peak current would result in increased sensor sensitivity. In our sensor design, where the electrochemically active reporter molecule is in the supporting electrolyte, eliminating redox activity completely is challenging even when the electrode surface is covered with the binder-target complex. This limitation restricts the difference between the signal and the blank, impacting sensitivity. To address this challenge, we can utilize the high modularity of monobodies to create non-competitive tandem binders. These monobody binders would attach to the same target, forming a binder-target sandwich complex. We propose that engineering monobodies that non-competitively binds to the same target, would not only retain high specificity, as discussed in Chapter 3, but also exhibit enhanced sensitivity.

In this proposed sensor design, two monobody binders would be connected by a flexible linker to form a binder 1-linker-binder 2 complex. The N-terminus of binder 1 would be anchored to the electrode's surface, while binder 2 would be covalently functionalized with a reporter probe. These binders, joined by a flexible polypeptide linker, would keep binder 2 sufficiently distant from the electrode in the absence of the target, preventing any signal generation. However, upon encountering the target biomarker, the engineered monobodies, designed to bind non-competitively, would form a binder-target-binder sandwich. This configuration would bring the reporter molecule closer to the electrode surface, thereby creating an ON signal. This innovative design could significantly improve the sensor's ability to detect the presence of a biomarker, offering a more distinct and sensitive response. In this chapter, we will outline the progress achieved in enhancing the current biosensor's capabilities, focusing on two primary areas: expanding the target range through multiplexing and developing an innovative tandem binding sensor that offers increased sensitivity.

4.2 MATERIALS AND METHODS

4.2.1 Chemicals

Reagent-grade chemicals were utilized throughout the study. The PBS buffer, (ferrocenylmethyl)dimethylamine, N-hydroxysuccinimide, and 1-ethyl-3-(3- dimethylaminopropyl) carbodiimide were procured from Sigma Aldrich. Sigma Aldrich and Abcam were the sources for the target protein hen-egg white lysozyme and BSA control, respectively. Electrochemical measurements were performed using the Biologic potentiostat (VSP, 5 channel). An SCE reference electrode and a Pt counter electrode (Bioanalytical Systems, West Lafayette, IN) were used for relative measurements. Glassy carbon electrodes (GCE) with a diameter of 3 mm (CH instruments) were polished with a cloth polishing

pad (Buehler, Lake Bluff, IL) and alumina slurry of 1, 0.3, and 0.05 μm sequentially, prior to the measurements.

4.2.2 High-efficiency bacterial transformation

For the NEB5α *E. coli* Transformation, a water bath is prepared at 42˚C, and wet ice is also prepared for the NEB5α cells to thaw in a vial for 5-10 minutes. Between 0.5-5 μL of plasmid, typically 2.5 μL, is pipetted directly into the NEB5α cells, followed by gentle tapping to mix. The mixture is incubated on wet ice for 30 minutes. The vial is then subjected to heat shock by placing it in the 42˚C water bath for exactly 30 seconds and placed on wet ice for 5 minutes. Subsequently, 950 μL of SOB (or SOC) is added to the vial. This vial is then shaken at an angle of 250 rpm at 37˚C for 1-2 hours. 200 μL of the mixture is spread on an LB agar plate, which is then incubated overnight, at 37˚C.

4.2.3 Plasmid preparation from bacterial cells

E. coli cell cultures ranging from 3.0-7.5 mL of bacteria are pelleted either by spinning the entire tube at 3,200g for 10 minutes in a large centrifuge, or by using 1.5 mL aliquots in 2 mL vials at 12,000g for 1 minute in a microcentrifuge. The supernatant is then discarded, including any residual liquid. Pelleted cells are resuspended in 250 μL of resuspension buffer MX1, and pipetted until the pellet is fully resuspended. This is followed by the addition of 250 μL of lysis buffer MX2 to the vial, and mixed until the solution becomes viscous and clear. After adding 350 μL of neutralizing buffer MX3 to the vial, the mixture is centrifuged at 12,000g for 10 minutes.

The supernatant is applied to an Epoch column placed in a collection tube, ensuring it is poured away from the pellet. The column is then centrifuged at 8,000g for 60 seconds, and the flowthrough is discarded as biohazardous waste. This is followed by adding 500 μL of wash buffer to the column, centrifuging at 8,000g for 30 seconds, and discarding the flowthrough. Another 500 μL

of wash buffer WS (that comes with the miniprep kit) is added, and the column is centrifuged again at 8,000g for 60 seconds, with the flowthrough discarded as hazardous waste. An additional centrifugation step at 12,000g for 60 seconds is performed to remove residual waste. The Epoch column is then placed in a 1.5 mL vial, and 30-75 µL of elution buffer EB is added to the center of the column and incubated for at least 1 minute. The column is then centrifuged at 12,000g for 60 seconds. The DNA collected in the vial is stored at -20˚C. This amount of elution buffer determines the DNA concentration and yield, with 30 µL yielding a higher concentration suitable for sequencing and transformation, and 75 µL providing a higher total yield suitable for DNA prep for library synthesis.

4.2.4 Yeast surface display to check binding using flow cytometry

Fluorophore solutions are prepared by combining 198 µL of PBSA with 1.86 µL of streptavidin-Alexa488 (2 mg/mL) to achieve a concentration of 333 nM. Secondary reagents are prepared by mixing 36 µL PBSA with 2 µL streptavidin-Alexa488 (333 nM) and 0.5 µL GαM-A647. Yeast cells containing the plasmid are prepared by pelleting a 10x diversity sample at 1000g for 1 minute and removing the supernatant. The yeast cells are then washed with 1 mL PBSA at 8,000g for 30 seconds and resuspended in a mixture of 50 µL PBSA, 0.25 µL 9E10 (0.5 mg/mL), and 2.5µL biotin-(Target). This mixture is incubated at room temperature for over 15 minutes, then pelleted. After splitting into two aliquots and pelleting again, the supernatant is removed. The cells are then resuspended in 20 µL of secondary reagents and incubated at 4º in the dark for over 15 minutes. Following another pelleting and removal of the supernatant, the yeast cells are washed with 1 mL of PBSA at 8,000g for 30 seconds and are ready to be analyzed using BD-Accuri.

4.2.5 Protein production in bacteria

The human fibronectin type-II domain III plasmid FL063 sequence with a cysteine at position 102 was designed using IDTDNA. The pCT and Pet22b plasmids were obtained from IDTDNA and expressed in T7 (E. coli) cells (NEB Cat: C2566H). LB and kanamycin solution were used to cultivate starting cultures of T7 cells, which were grown overnight. These cultures were then transferred to 2 L cell cultures without antibiotics and incubated overnight at room temperature on an orbital shaker at 250 rpm. The induction with IPTG for 16 hours was revealed to yield the highest protein concentration by SDS-PAGE results. Cell lysis was performed using the French press mechanism, and protein purification was executed using HisPur Cobalt columns in an FPLC. Amicon filters of 10 kDa were utilized for further concentration of the purified proteins. The expression of the desired protein and the yield of production were verified by SDS-PAGE. A Nanodrop was employed for the determination of the protein concentration.

4.2.6 Synthesis of diazonium salt [127]

In a round-bottomed flask, 4-aminobenzoic acid (2.74 g, 20.0 mmol) was dissolved in a solution of fluoroboric acid (48%, 14.6 g, 80 mmol) and water (20 mL). The solution was heated until complete dissolution of the aniline was achieved, followed by cooling in an ice water bath. A solution of sodium nitrite (1.46 g, 21.2 mmol) in water (4 mL) was added dropwise to the cooled solution under stirring. The diazonium product precipitated upon addition of the sodium nitrite solution and subsequent placement in an ice bath. The white solid formed was filtered, washed with cold ether, and dried under vacuum to yield 1.24 g (26%) of the diazonium salt. 1H NMR (400 MHz, DMSO) δ (ppm); 8.42 (2H, d), 8.78 (2H, d), 14 (H, s).

4.2.7 Synthesis of diazonium ester [128]

To a mixture of diazonium salt (100 mg), EDC (115 mg), and NHS (215 mg) in anhydrous CH_2Cl_2 (12 mL), an ice bath was applied, and the mixture was stirred for 16 hours. The organic layer was subjected to successive washes with 1 M HCl and a saturated aqueous solution of $NaHCO_3$. The aqueous layers combined were dried over $MgSO_4$, and the concentration under vacuum yielded a reddish-orange oily product.

4.2.8 Synthesis of 6-Aminohexyl Ferrocene [144,145]

1.25 g (3.60 mmol) of (6-Bromohexyl) ferrocene was dissolved in 50 ml of dimethylformamide. To this solution, 0.26 g (4.00 mmol) of sodium azide was added, and the mixture was stirred at room temperature for 12 hours. The reaction was then quenched with 100 ml of H2O. The solution underwent extraction thrice using 50 ml of ethyl acetate each time. The organic layer was washed with brine, dried over anhydrous Na2SO4, filtered, and concentrated under reduced pressure. Purification was carried out using silica gel chromatography. The yield of 6-Azidohexyl ferrocene was 92.4%. The product's 1H NMR ($CDCl_3$) and MS (EI) results were as follows: d 1.32-1.62 (m, 8H, CH2), 2.32 (t, J = 7.6 Hz, 2H), 3.26 (t, J = 6.9 Hz, 2H, CH2), 4.09 (s, 4H, Fc), 4.13 (s, 5H, Fc); M+ calculated for C16H21FeN3: 311.11 m/z, found: 311.0 m/z.

For the synthesis of 6-Aminohexyl ferrocene, 1.00 g (3.20 mmol) of 6-Azidohexyl ferrocene was dissolved in 50 ml of dry diethyl ether. Separately, 0.18 g (4.8 mmol) of LiAlH4 was suspended in 30 ml of dry diethyl ether. The 6-azidohexyl ferrocene solution was then added dropwise under N2 to the LiAlH4 suspension over 2 hours and quenched with 20 ml of 1mM aqueous NaOH. The mixture was extracted three times with 50 ml of ethyl acetate, and the organic layer was dried over anhydrous Na2SO4, filtered, and concentrated under reduced pressure. The yield was 80.0%. The 1H NMR (CDCl3) and MS (EI) results for the product were: d 1.08-

1.53(m, 10H, CH2 and NH2), 2.33 (t, J = 7.6 Hz, 2H, CH2), 2.68 (t, J = 6.8 Hz, 2H, CH2), 4.04 (4H, s), 4.08 (5H, s); M+ calculated for C16H23FeN: 285.12 m/z, found: 285.1 m/z.

4.2.9 Surface modification of the electrode

A 4 mM solution of diazonium ester in anhydrous CH2Cl2 was prepared. Grafting of the ester onto the GCE was conducted by applying a potential from 0V to -0.9V against a Pt-wire counter electrode and Ag/AgNO3 reference electrode in DCM. Post grafting, the modified electrode was incubated with a 10-micromolar solution of the binding protein FL063 in PBS buffer (pH 7) for 30 minutes.

4.3 RESULTS AND DISCUSSION

4.3.1 Multiplexing the Current Biosensor

As discussed in chapters 2 and 3, we determined monobody binding sequences that have a strong affinity to lysozyme. To create a more versatile biosensing platform, we aimed to generate monobody sequences that target additional biomarkers. Immunoglobulins and human transferrin protein were our next targets of interest for multiplexing the one-on-one lysozyme biosensor.

Immunoglobulins are glycoproteins synthesized by plasma cells. These plasma cells originate from B cells that have been activated by specific immunogens, like bacterial proteins. B cells, upon encountering an immunogen, receive a signal through their B-cell receptors (BCR) on the surface. This interaction initiates a cascade of events leading to the activation of transcription factors and subsequent antibody synthesis, with each B cell clone producing a specific immunoglobulin for the activating immunogen.

Immunoglobulin G (IgG) stands out as a major component of human serum, comprising 10-20% of plasma protein. It possesses two identical antigen-binding sites, each formed by two light (L) chains and two heavy (H) chains connected by disulfide bonds. IgG production is primarily

during the secondary immune response. It activates the classical pathway of the complement system and offers substantial protection. Alterations in antigen-specific IgG, its subclasses (IgG1-4), and the overall N-glycosylation pattern of IgG are commonly seen in infectious and inflammatory diseases. By analyzing the N-glycosylation patterns of IgG in patients with diseases and comparing them with healthy individuals, insights into the immune status of the host can be obtained. Additionally, monitoring changes in a patient's IgG N-glycosylation from the time of diagnosis and throughout the course of treatment provides valuable information about the patient's immune response. [141]

The other biomarker of interest for generating monobodies is the human transferrin protein which plays a critical role in iron metabolism. These blood plasma glycoproteins are primarily responsible for the delivery and transport of ferric ions. Due to their high affinity for ferric iron, transferrins bind to almost all the plasma iron, thus maintaining very low levels of free iron in the body. This binding is essential for various physiological processes, as iron is a vital element for numerous metabolic pathways. The maintenance of iron homeostasis is crucial, as any imbalance, whether an excess or a deficiency, can be harmful. The functions of transferrins extend beyond simple iron transport. One of their key roles is making free Fe3+, which is insoluble at neutral pH, and soluble once bound to transferrin. This solubility is vital for the efficient delivery and transfer of iron to various biological tissues. It includes the movement of iron between sites of absorption, utilization, and storage, such as the liver, spleen, and bone marrow. In doing so, transferrins act as a significant ferric pool within the body, marking them as essential biochemical markers for the body's iron status.[143] Furthermore, transferrins contribute to the prevention of reactive oxygen species formation. By chelating free toxic iron, transferrins act as protective scavengers, mitigating potential damage from these harmful ions. Their role

extends to the immune system as well; by binding to iron, transferrins impede bacterial survival, thus being an integral part of the innate immune defense. Additionally, during inflammation, the level of transferrins in the body decreases, making them a marker for inflammatory conditions. This characteristic of transferrins underscores their significance in both the physiological and pathological aspects of human health.

The development of potent monobody binding sequences targeting two distinct immunoglobulins - goat IgG, rabbit IgG, and the human transferrin protein - began with the transformation of the binder DNA into bacteria. Initially, the monobody binder libraries existed as zymoprep DNA, extracted directly from yeast cells. Due to the relatively low concentration of this zymoprep DNA, direct transformation into yeast cells for flow cytometry experiments risked insufficient signal detection. To address this, the zymoprep DNA was transformed into NEB5alpha high-efficiency E. coli cells, as depicted in Figure C.1.

Subsequently, the bacterial plasmid from each binding library was isolated using the miniprep method. Nanodrop assessments of these plasmids indicated high concentrations and purity levels, evidenced in Figure C.2. Before proceeding with yeast surface display using these DNA samples, it was essential to ascertain their quality and usability. A commonly used metric for DNA purity is the absorbance ratio at 260 and 280 nm, with a ratio around 1.8 generally accepted as indicative of "pure" DNA.[146] Ratios that significantly fall to 1.6 or below suggests potential contamination with proteins, phenol, or other substances that absorb strongly at or near 280 nm. In this case, the high absorbance values observed in the A260/280 and A260/230 measurements confirmed the high purity of the miniprep DNA, thus validating its suitability for subsequent yeast surface display experiments.

The yeast cells containing the Fn3 monobody libraries were targeted towards respective populations of biotinylated targets. In the flow cytometry experiments, the primary fluorophores used were streptavidin-conjugated Alexa 488 and goat anti-mouse conjugated Alexa 647. The presence of the monobody gene segment in the yeast cells, functionalized with a c-myc tag, facilitated interaction with goat anti-mouse Alexa 647. Concurrently, since the monobody was engineered to bind to its specific target, the biotin attached to the target engaged with the streptavidin linked to Alexa 488. In the absence of a target, the only fluorescence detection

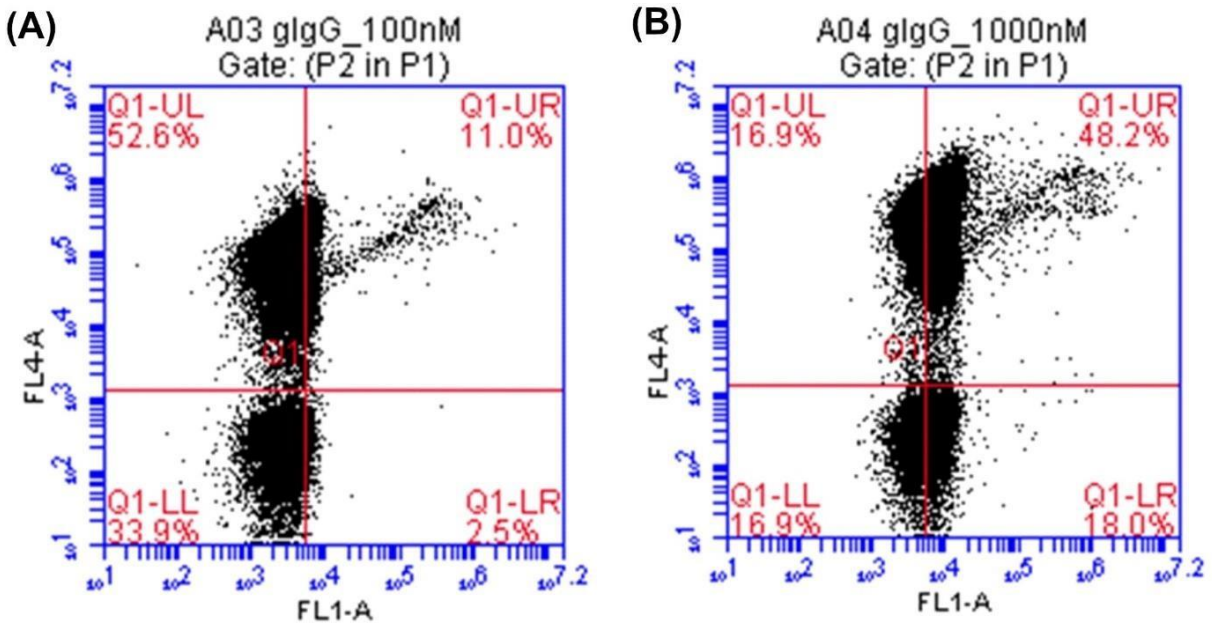

Figure 4.1 Flow cytometry data showing binding populations of monobody in the upper right quadrant (double positive) of the plots for 1000 nM (A) and 1 µM (B) biotinylated goat IgG.

originated from the interaction between the c-myc tag of the monobody within the yeast cells and the goat anti-mouse Alexa 647. However, when a biotinylated target was present and bound to the yeast cells with the monobody binders, the biotin-streptavidin chemistry activated Alexa 488 fluorescence alongside the already active Alexa 647. This process resulted in a double-positive

signal, indicating successful target binding. In Figure 4.1, it is seen that 11% of the yeast cells exhibited a double-positive signal (visible in the top right quadrant) upon incubation with Goat IgG. Notably, as the concentration of the target increased from 100 nM to 1 μM, there was an increase in the cell population binding to the target, reaching 48.2%. However, the flow cytometry analysis of yeast cells containing the monobody library designed to bind to transferrin showed no binding signal, as depicted in part B. This lack of signal could be attributed to several factors: the initial low concentration of the yeast cell culture, insufficient induction time in SG media, or the potential presence of a very small percentage of binders within the library. To further investigate this, the transferrin binder library could be exposed to escalating concentrations of the target. This approach would help in determining the binding coefficient (as discussed in chapter 3).

Gaining insight into the binding kinetics of the libraries for goat IgG and human transferrin is crucial for isolating the strongest binders using BD Aria. Following the cell sorting, the DNA of the strongest binders can be sequenced. Subsequently, this sequenced DNA can be cultivated in bacterial cells to produce soluble proteins. After extraction and purification of these proteins, they can be functionalized using NHS ester. This step is key for immobilizing them on the electrode surface through diazonium grafting. This would lead to the formation of individually addressable electrodes, each modified with monobody binders that are specifically designed to target different biomarkers concurrently in a solution.

4.3.2 Tandem Binder Biosensing

While remarkable specificity for lysozyme has been demonstrated by our biosensor, the potential for enhancing its sensitivity is acknowledged. As noted in Chapter 3, the variation in peak currents between target-bound and unbound monobodies, which falls in the lower microampere range, suggests that a greater change in signaling peak current could lead to increased sensor

sensitivity. In the sensor design, where the electrochemically active reporter molecule is present in the supporting electrolyte, the complete elimination of redox activity is challenging, even when the electrode surface is covered with the binder-target complex. This situation impacts the differentiation between signal and blank, affecting sensitivity.

To address this challenge, the development of an ON-OFF sensor, rather than a current gradient sensor, could be considered. This approach would involve utilizing the modularity of monobodies to create non-competitive tandem binders. One binder would be anchored to the surface of the electrode and the other binder would be functionalized with the redox probe instead of dissolving it in the supporting electrolyte.

As discussed in chapter 2, a series of protein models targeting hen egg white lysozyme were generated using SWISS-MODEL from three distinct DNA sequences of fibronectin type III domain 2 monobody binders. Subsequent protein-protein docking studies, focusing on the interaction between the monobody binders and lysozyme, were performed using the ROSETTA computational tool. 1200 docked structures, known as decoys, were generated, out of which 15 were selected based on their energy scores. The selected decoys were visualized using PyMol to identify the key binding interactions. Two docked structures were superimposed to determine if the fibronectin variants bind non-competitively. In this process, the target lysozyme was held fixed while the two PDB files were superimposed. The residues on the active sites of the fibronectin variants and the lysozyme were then examined to ascertain whether the bindings occurred in different regions (as shown in Figure 4.2). Further alignment of these docked structures was conducted using multiple alignment tools in Geneious software. To validate the computational predictions, the starting sequences of three non-competitive Fn3 variants were chosen for expression using wet-lab techniques.

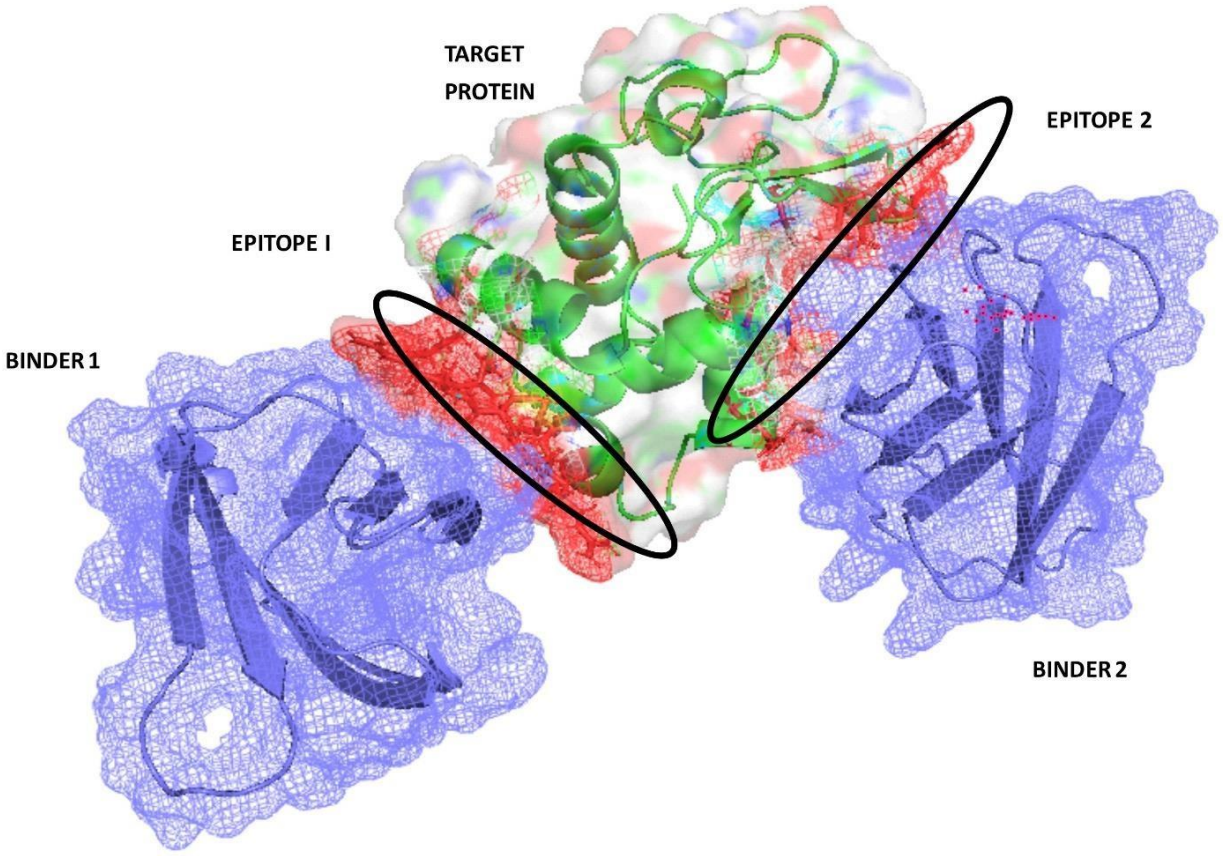

Figure 4.2 ROSETTA predictions show non-competitive tandem monobody binders with cooperative binding sites that target different domains (epitopes) on the surface of lysozyme.

Despite predictions from ROSETTA, non-competitive binding was not observed in flow cytometry experiments using Fn3_G and Fn3_103 sequences with the purified FL063 protein. Consequently, a different lysozyme-binding monobody library DNA was expressed in yeast cells to identify sequences that non-competitively bind to the soluble FL063 protein. Figure 4.3 displays the non-competitive binder population using the BD Aria flow cytometry cell sorter. In this experiment, yeast cells containing the monobody library were incubated with a mixture of 500 µM biotinylated lysozyme pre-bound to FL063. The biotinylated lysozyme and FL063 were collectively termed B1, while the yeast cells with the monobody library 0.4f were designated B2.

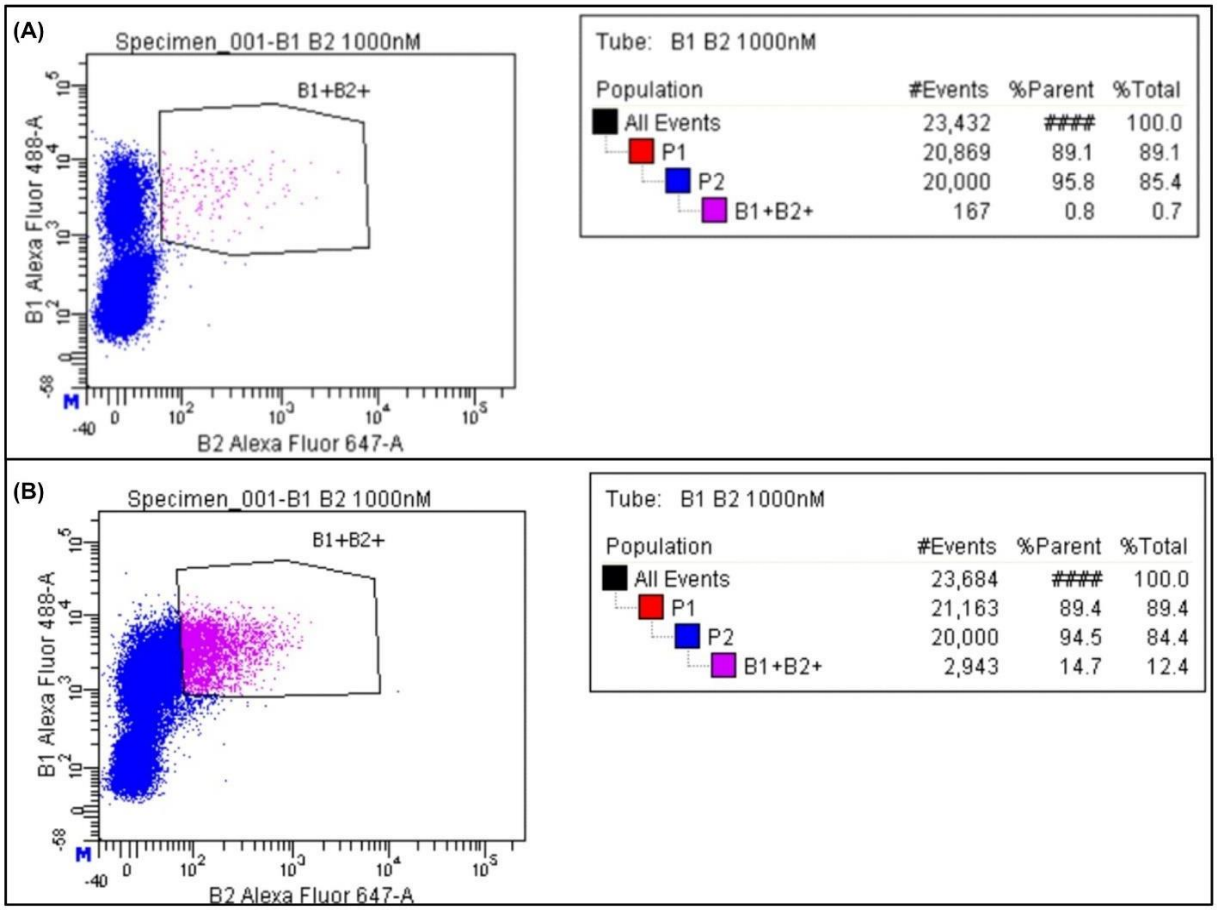

Figure 4.3 Flow-assisted cell sorting data shows an increase in the non-competitive binding population of the cells expressing lysozyme binding monobodies from 0.8% in round 1 (A) to 14.7 % in round 2(B).

As shown in part A of Figure 4.3, a 0.8% double positive signal was observed, indicating that while one binding site (epitope) of the lysozyme was engaged by FL063, the yeast cells with the binder library were still able to bind to another epitope, demonstrating non-competitive binding. These cells were then cultivated in appropriate media for a second round of sorting to isolate stronger binders. As depicted in part B of Figure 4.3, the double positive fluorescence signal increased from 0.8% to 14.7% following this second round of sorting. The yeast cells were then harvested, and their DNA was extracted for sequencing to determine the diversity of monobody

sequences present in the non-competitive binder library. Identifying one or two unique sequences from this process would allow for their expression in bacterial cells to produce soluble proteins. These proteins can then be utilized in electrochemical studies, further advancing the research.

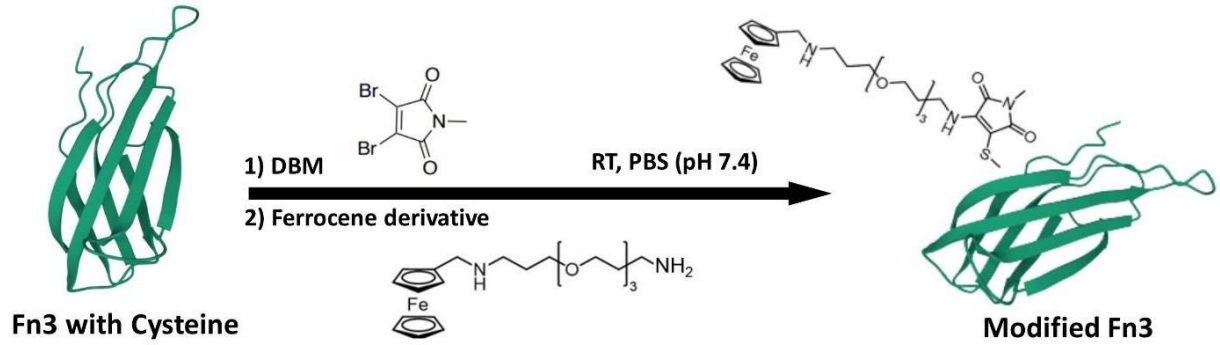

Figure 4.4 Reaction scheme of modifying monobody with ferrocene derivative using maleimide chemistry.

Enhancing the sensitivity of the tandem binding sensor involved a significant modification where one of the binder proteins was tagged with a redox probe, rather than having it dissolved in the supporting electrolyte. For this purpose, maleimide chemistry was employed for the site-selective modification, enabling the covalent attachment of the protein to ferrocene. [144,147] Maleimides are favored in conjugation chemistry for their efficient reaction kinetics with thiols.[148] Given that the soluble protein FL063 has been engineered to include a cysteine residue at position 103, it is anticipated that this modification would facilitate thiol conjugation with dibromo maleimide, as illustrated in the reaction scheme (Figure 4.4). The interaction of the maleimide-modified protein with ferrocene, which contains a primary amine, is expected to result in secondary conjugation, forming a protein-maleimide-ferrocene complex.

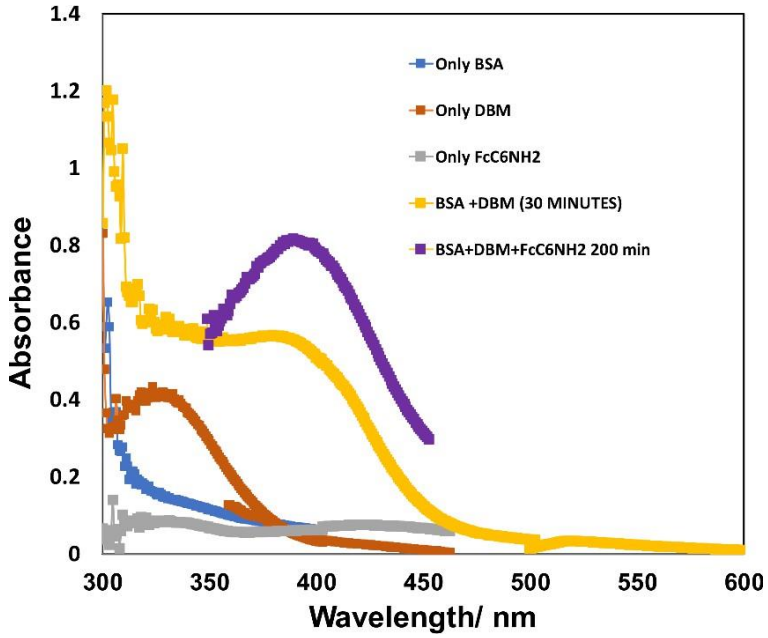

Figure 4.5 Absorbance data showing BSA conjugation with ferrocene derivative using dibromomaleimide. The process of thiol-amine bioconjugation on WT-HSA was examined through UV/visible spectroscopy, tracking the absorbance of the produced bromothiomaleimide at 375 nm. Following the completion of this reaction, ferrocene was introduced to the conjugation mix, with its progress observed at an absorbance of 415 nm.

The feasibility of the conjugation strategy was initially tested using Bovine Serum Albumin (BSA), chosen for its inherent cysteine at position 55 (Figure C.5). The successful conjugation of BSA with maleimide and subsequently with ferrocene was confirmed through absorbance data, demonstrating the practicality and effectiveness of this approach, as shown in Figure 4.5. Encouraged by these results, the next step involves applying this modification strategy to the monobody, FL063. The goal is to covalently attach it to a redox probe, thereby enhancing the sensor's performance by creating a more effective pathway for electron transfer. This modification is expected to significantly improve the sensor sensitivity by ensuring that the redox probe is in close proximity to the target site, facilitating rapid and accurate detection of the analyte. This

approach not only aims to enhance the sensor's performance but also highlights the potential for innovative modifications in biosensor technology, paving the way for more sophisticated and sensitive detection methods.

4.4 CONCLUSION

This chapter elaborates on the modifications made to the current biosensor in two key areas: multiplexing for broader target detection and the development of a novel tandem binding sensor with increased sensitivity. Initial efforts focused on identifying monobody binding sequences with strong affinity to lysozyme, expanding later to target additional biomarkers such as immunoglobulins and human transferrin protein. Subsequent steps involved expressing the DNA sequences targeting IgG and transferrin into soluble proteins. These proteins will be then immobilized on the surface of a glassy carbon electrode using NHS-modified diazonium grafting. By integrating these proteins with the lysozyme-targeting monobody, the goal is to create a biosensor with a multi-individually addressable bio-electrode panel capable of targeting multiple biomarkers concurrently within the same solution.

Enhancing the biosensor's sensitivity involved two critical strategies: developing a tandem binder system and removing the necessity to dissolve the redox molecule in the supporting electrolyte. Through flow cytometry-assisted cell sorting, we identified monobody binders that target lysozyme non-competitively, in relation to the already identified purified binder protein (FL063). The forthcoming experiments aim to analyze these tandem binders' sequences for subsequent protein expression. Additionally, we investigated maleimide conjugation chemistry for attaching a redox probe to a protein. In this context, we successfully achieved the conjugation of Bovine Serum Albumin (BSA), which has a cysteine residue at position 55, with ferrocene via thiol-amine-maleimide conjugation.

This approach will next be applied to the FL063 protein, engineered with a cysteine residue at position 103.[149,150] The subsequent phase involves designing polypeptide linkers to construct a fusion protein interface, laying the groundwork for a state-of- the-art tandem binding biosensor with enhanced sensitivity, a process that will be elaborated in the last chapter.

5. CONCLUSIONS & FUTURE WORK

5.1 CONTROLLED DIAZONIUM GRAFTING TO ENSURE MONOLAYER FORMATION

Diazonium chemistry is a widely explored method for the covalent modification of carbon surfaces by creating a robust C–C bond.[151] The application of diazonium chemistry for carbon electrode modification was initially introduced in 1992.[152,153] Its popularity in research, especially for sensing applications, stems from the simplicity of the process, its quick execution time (ranging from seconds to minutes), the versatility of the terminal functionality produced, and the strength of the bond formed. This method has been particularly adopted for linking biosensor recognition elements to the surface of screen-printed carbon electrodes. [154]The typical use of diazonium coupling agents involves the electrochemical reduction of diazonium salt molecules. This reduction produces reactive radicals that can attach to carbon structures, including the electrochemical signal transducing screen-printed graphene working electrode, in a process known as electrografting. In the biosensor that has been created, a diazonium ester has been synthesized and electrochemically grafted onto a Glassy Carbon Electrode (GCE) to assist in anchoring the monobodies to the electrode surface.

Though diazonium electrografting is extremely advantageous for its rapid processing time, the high reactivity of the aryl radicals during this short timeframe can lead the carbon atoms in positions 3 and 5 (with respect to the amine group) to react with the grafted molecules. This can result in the uncontrolled formation of dendritic structures.[155] A significant challenge in developing diazonium films is preventing the formation of multilayers or avoiding the polymerization process (for example, the creation of dendritic structures as molecules continuously attach to one another) while functionalizing the surface of carbon electrodes with diazonium.

Achieving true monolayer coverage with the diazonium coupling agent could optimize the charge transfer between the transducer surface and the recognition domain, thereby improving the performance of the sensor. To study the structure of the film grafted on the electrode surface and determine the layer thickness, XPS [153]can be used for further characterization. In efforts to address side reactions and prevent the formation of multilayers during the growth of diazonium films, five key strategies can be considered for future implementation. Firstly, the electrical charge consumed during the reaction could be controlled.[156] Secondly, the introduction of steric hindrance to impede radical attack can be achieved by employing reagents with substituents located at the 3 and 5 positions on the aryl ring. [157]Thirdly, instead of aiming for controlled monolayer grafting, a strategy involving the controlled degradation of deposited multilayers may be adopted.[158] Fourthly, the utilization of radical scavengers could be explored to inhibit the radical attack on molecules that have already been grafted, without interfering with the process of monolayer grafting.[159–161] Lastly, the application of ionic liquids may be utilized to improve molecular diffusion throughout the electrografting medium.[160]

5.2 Linker design to create tandem binding fusion proteins

As outlined in Chapter 4, for the development of an ON-OFF biosensor with enhanced sensitivity, non-competitive monobody binders to the target lysozyme have been developed, and a strategy has been formulated to modify one of the binders with a redox probe using maleimide chemistry. However, the integration of a linker is identified as a critical component in the creation of this tandem fusion protein. The function of the linker is to maintain a specified distance between the two binding proteins in the absence of the target, ensuring the redox probe remains distant from the electrode surface, thereby keeping the sensor in the OFF state. Upon

target binding, the flexibility of the linker facilitates the closeness of the two binders, forming a sandwich complex which, in turn, brings the redox probe into contact with the electrode surface, generating an ON signal. The linker's main attributes should include flexibility, inertness to avoid interference with the biorecognition process, and chemical-thermal stability.[162]

For creating these types of fusion proteins, flexible linkers are usually the top choice. [163]These linkers are often made up of small, either non-polar (such as Gly) or polar (such as Ser or Thr) amino acids, as recommended by Argos. The small size of these amino acids affords the linkers flexibility and permits the mobility of the attached functional domains. The presence of Ser or Thr is known to enhance the stability of the linker in aqueous solutions by engaging in hydrogen bonding with water molecules, thus minimizing undesirable interactions with the protein components. Linkers that are frequently used for their flexibility are characterized by sequences that predominantly contain Gly and Ser residues, known as “GS” linkers. A commonly employed flexible linker sequence is $(Gly\text{-}Gly\text{-}Gly\text{-}Gly\text{-}Ser)_n$. Through modulation of the repeat unit "n," the length of the GS linker can be adjusted, allowing for optimal spacing between functional domains or preserving required interactions between domains. A library of linkers, ranging in length from 40 to 120 amino acids, can be designed, featuring alternating or repeating segments of residues inspired by naturally available linkers such as (GGGGG)n, (EAAK)n, (APSP)n, etc. This library can then undergo testing for flexibility and inertness using yeast surface display. Screened linkers will subsequently be examined for their stability and their ability to limit interaction between the redox probe and the electrode in the absence of the target.[164]

In this proposed sensor design, two monobody binders would be connected by a flexible linker to form a binder 1-linker-binder 2 complex, as shown in Figure 5.1. The N-terminus of binder 1 would be anchored to the electrode's surface, while binder 2 would be covalently functionalized with a reporter probe. These binders, joined by a flexible polypeptide linker, would keep binder 2 sufficiently distant from the electrode in the absence of the target, preventing any signal generation. However, upon encountering the target biomarker, the engineered monobodies, designed to bind non-competitively, would form a binder-target-binder sandwich. This configuration would bring the reporter molecule closer to the electrode surface, thereby creating an ON signal. This innovative design could significantly improve the sensor's ability to detect the presence of a biomarker, offering a more distinct and sensitive response. In this chapter, we will outline the progress achieved in enhancing the current biosensor's capabilities, focusing on two primary areas: expanding the target range through multiplexing and developing an innovative tandem binding sensor that offers increased sensitivity.

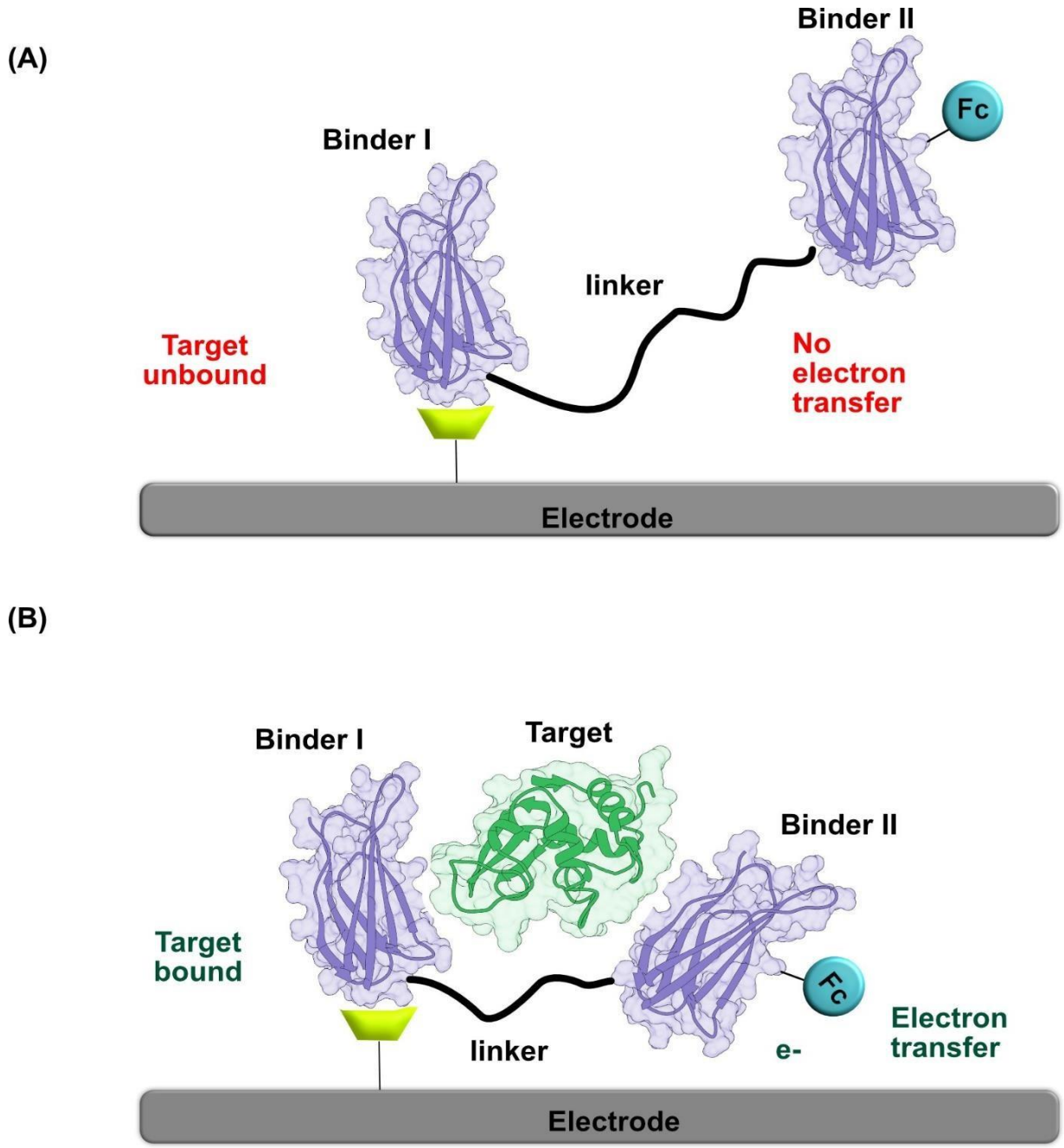

Figure 5.1 Schematic showing tandem binder monobody sensor. (A) In the absence of a target, the linker keeps the binders at a distance such that there is no electron transfer due to the redox probe, hence an OFF state, whereas (B) in the presence of a target, the linker helps in bringing the binders closer to form a sandwich complex with the target, facilitating the electron transfer due to the Fc probe, creating an ON state of the sensor.

5.3 VERSATILITY EXPANSION OF THE BIORECOGNITION ELEMENT

In the scope of the research conducted for this dissertation, monobodies have been primarily utilized as biorecognition elements. However, the incorporation of other small synthetic binding proteins, such as affibodies and DARPins, alongside monobodies, presents an intriguing opportunity. Due to their comparable sizes, the immobilization of these proteins on the electrode surface could be achieved through the same diazonium grafting process. It would be of particular interest to examine how the varying sizes of the target molecules to which they bind affect the signal generated. Furthermore, the miniaturization of individually addressable electrodes into microelectrodes for the development of a lab-on-chip interface will necessitate enhancing spatial resolution as a critical priority. This development would represent a significant advancement towards the creation of a composite sensing interface, characterized by an ensemble of synthetic small binding proteins serving as the biorecognition element.

BIBLIOGRAPHY

(1) Thévenot, D. R.; Toth, K.; Durst, R. A.; Wilson, G. S.; Thévenot, D. R. *Electrochemical Biosensors: Recommended Definitions and Classification*; 2001; Vol. 16. www.elsevier.com/locate/bios.

(2) Clark, L. C.; Lyons, C. ELECTRODE SYSTEMS FOR CONTINUOUS MONITORING IN CARDIOVASCULAR SURGERY. *Ann N Y Acad Sci* **1962**, *102* (1), 29–45. https://doi.org/10.1111/j.1749-6632.1962.tb13623.x.

(3) Pohanka, M. Glucose Electrochemical Biosensors: The Past and Current Trends. *Int J Electrochem Sci* **2021**, *16* (7), 1–12. https://doi.org/10.20964/2021.07.52.

(4) Rahi, A.; Sattarahmady, N.; Heli, H. Label-Free Electrochemical Aptasensing of the Human Prostate-Specific Antigen Using Gold Nanospears. *Talanta* **2016**, *156–157*, 218–224. https://doi.org/10.1016/j.talanta.2016.05.029.

(5) Shu, H.; Wen, W.; Xiong, H.; Zhang, X.; Wang, S. Novel Electrochemical Aptamer Biosensor Based on Gold Nanoparticles Signal Amplification for the Detection of Carcinoembryonic Antigen. *Electrochem commun* **2013**, *37*, 15–19. https://doi.org/10.1016/j.elecom.2013.09.018.

(6) Felix, F. S.; Angnes, L. Electrochemical Immunosensors – A Powerful Tool for Analytical Applications. *Biosensors and Bioelectronics*. Elsevier Ltd April 15, 2018, pp 470–478. https://doi.org/10.1016/j.bios.2017.11.029.

(7) Shu, H.; Wen, W.; Xiong, H.; Zhang, X.; Wang, S. Novel Electrochemical Aptamer Biosensor Based on Gold Nanoparticles Signal Amplification for the Detection of Carcinoembryonic Antigen. *Electrochem commun* **2013**, *37*, 15–19. https://doi.org/10.1016/j.elecom.2013.09.018.

(8) Felix, F. S.; Angnes, L. Electrochemical Immunosensors – A Powerful Tool for Analytical Applications. *Biosensors and Bioelectronics*. Elsevier Ltd April 15, 2018, pp 470–478. https://doi.org/10.1016/j.bios.2017.11.029.

(9) Jin, H.; Gui, R.; Yu, J.; Lv, W.; Wang, Z. Fabrication Strategies, Sensing Modes and Analytical Applications of Ratiometric Electrochemical Biosensors. *Biosensors and Bioelectronics*. Elsevier Ltd May 15, 2017, pp 523–537. https://doi.org/10.1016/j.bios.2017.01.011.

(10) Jin, H.; Gui, R.; Yu, J.; Lv, W.; Wang, Z. Fabrication Strategies, Sensing Modes and Analytical Applications of Ratiometric Electrochemical Biosensors. *Biosensors and Bioelectronics*. Elsevier Ltd May 15, 2017, pp 523–537. https://doi.org/10.1016/j.bios.2017.01.011.

(11) Yang, H. Enzyme-Based Ultrasensitive Electrochemical Biosensors. *Current Opinion in Chemical Biology*. August 2012, pp 422–428. https://doi.org/10.1016/j.cbpa.2012.03.015.

(12) Rocchitta, G.; Spanu, A.; Babudieri, S.; Latte, G.; Madeddu, G.; Galleri, G.; Nuvoli, S.; Bagella, P.; Demartis, M. I.; Fiore, V.; Manetti, R.; Serra, P. A. Enzyme Biosensors for Biomedical Applications: Strategies for Safeguarding Analytical Performances in Biological Fluids. *Sensors (Switzerland)*. MDPI AG June 1, 2016. https://doi.org/10.3390/s16060780.

(13) Kilic, N. M.; Singh, S.; Keles, G.; Cinti, S.; Kurbanoglu, S.; Odaci, D. Novel Approaches to Enzyme-Based Electrochemical Nanobiosensors. *Biosensors*. Multidisciplinary Digital Publishing Institute (MDPI) June 1, 2023. https://doi.org/10.3390/bios13060622.

(14) Kucherenko, I. S.; Soldatkin, O. O.; Dzyadevych, S. V.; Soldatkin, A. P. Electrochemical Biosensors Based on Multienzyme Systems: Main Groups, Advantages and Limitations – A Review. *Analytica Chimica Acta*. Elsevier B.V. May 15, 2020, pp 114–131. https://doi.org/10.1016/j.aca.2020.03.034.

(15) Altun, A.; Apetrei, R.-M.; Camurlu, P. Reagentless Amperometric Glucose Biosensors: Ferrocene-Tethering and Copolymerization. *J Electrochem Soc* **2020**, *167* (10), 107507. https://doi.org/10.1149/1945-7111/ab9c81.

(16) Kilic, N. M.; Singh, S.; Keles, G.; Cinti, S.; Kurbanoglu, S.; Odaci, D. Novel Approaches to Enzyme-Based Electrochemical Nanobiosensors. *Biosensors*. Multidisciplinary Digital Publishing Institute (MDPI) June 1, 2023. https://doi.org/10.3390/bios13060622.

(17) Sauer, M. J.; Foulke~, J. A.; O'neill Maff, P. M. *A COMPARISON OF ALKALINE PHOSPHATASE, Q-GALACTOSIDASE, PENICILLINASE AND PEROXIDASE USED AS LABELS FOR PROGESTERONE DETERMINATION IN MILK BY HETEROLOGOUS MICROTITRE PLATE ENZYMEIMMUNOASSAY*; 1989; Vol. 33.

(18) Yang, H. Enzyme-Based Ultrasensitive Electrochemical Biosensors. *Current Opinion in Chemical Biology*. August 2012, pp 422–428. https://doi.org/10.1016/j.cbpa.2012.03.015.

(19) Johnson, K. A.; Goody, R. S. The Original Michaelis Constant: Translation of the 1913 Michaelis-Menten Paper. *Biochemistry* **2011**, *50* (39), 8264–8269. https://doi.org/10.1021/bi201284u.

(20) Johnson, K. A.; Goody, R. S. The Original Michaelis Constant: Translation of the 1913 Michaelis-Menten Paper. *Biochemistry* **2011**, *50* (39), 8264–8269. https://doi.org/10.1021/bi201284u.

(21) Navaee, A.; Salimi, A. Enzyme-Based Electrochemical Biosensors. In *Electrochemical Biosensors*; Elsevier, 2019; pp 167–211. https://doi.org/10.1016/B978-0-12-816491-4.00007-3.

(22) Kucherenko, I. S.; Soldatkin, O. O.; Dzyadevych, S. V.; Soldatkin, A. P. Electrochemical Biosensors Based on Multienzyme Systems: Main Groups, Advantages and Limitations – A Review. *Analytica Chimica Acta*. Elsevier B.V. May 15, 2020, pp 114–131. https://doi.org/10.1016/j.aca.2020.03.034.

(23) Cadoux, C.; Milton, R. D. Recent Enzymatic Electrochemistry for Reductive Reactions. *ChemElectroChem*. Wiley-VCH Verlag May 4, 2020, pp 1974–1986. https://doi.org/10.1002/celc.202000282.

(24) Sheikholeslam, M.; Nanda, P.; Sanati, A.; Pritzker, M.; Chen, P. Direct Electrochemistry of Hemoglobin/Peptide-Carbon Nanotube Modified Electrode for Hydrogen Peroxide Biosensing. *Mater Lett* **2023**, *335*. https://doi.org/10.1016/j.matlet.2022.133799.

(25) Yan, X.; Tang, J.; Tanner, D.; Ulstrup, J.; Xiao, X. Direct Electrochemical Enzyme Electron Transfer on Electrodes Modified by Self-Assembled Molecular Monolayers. *Catalysts*. MDPI December 1, 2020, pp 1–26. https://doi.org/10.3390/catal10121458.

(26) Thévenot, D. R.; Toth, K.; Durst, R. A.; Wilson, G. S.; Thévenot, D. R. *Electrochemical Biosensors: Recommended Definitions and Classification*; 2001; Vol. 16. www.elsevier.com/locate/bios.

(27) Pohanka, M. Glucose Electrochemical Biosensors: The Past and Current Trends. *Int J Electrochem Sci* **2021**, *16* (7), 1–12. https://doi.org/10.20964/2021.07.52.

(28) Ito, Y.; Okuda-Shimazaki, J.; Tsugawa, W.; Loew, N.; Shitanda, I.; Lin, C. E.; La Belle, J.; Sode, K. Third Generation Impedimetric Sensor Employing Direct Electron Transfer Type Glucose Dehydrogenase. *Biosens Bioelectron* **2019**, *129*, 189–197. https://doi.org/10.1016/j.bios.2019.01.018.

(29) Khor, S. M.; Choi, J.; Won, P.; Ko, S. H. Challenges and Strategies in Developing an Enzymatic Wearable Sweat Glucose Biosensor as a Practical Point-Of-Care Monitoring Tool for Type II Diabetes. *Nanomaterials*. MDPI January 1, 2022. https://doi.org/10.3390/nano12020221.

(30) Khor, S. M.; Choi, J.; Won, P.; Ko, S. H. Challenges and Strategies in Developing an Enzymatic Wearable Sweat Glucose Biosensor as a Practical Point-Of-Care Monitoring Tool for Type II Diabetes. *Nanomaterials*. MDPI January 1, 2022. https://doi.org/10.3390/nano12020221.

(31) Clark, L. C.; Lyons, C. *ELECTRODE SYSTEMS FOR CONTINUOUS MONITORING IN CARDIOVASCULAR SURGERY*.

(32) Lin, M. J.; Wu, C. C.; Chang, K. S. Effect of Poly-l-Lysine Polycation on the Glucose Oxidase/Ferricyanide Composite-Based Second-Generation Blood Glucose Sensors. *Sensors (Switzerland)* **2019**, *19* (6). https://doi.org/10.3390/s19061448.

(33) Dayakar, T.; Rao, K. V.; Bikshalu, K.; Malapati, V.; Sadasivuni, K. K. Non-Enzymatic Sensing of Glucose Using Screen-Printed Electrode Modified with Novel Synthesized CeO2@CuO Core Shell Nanostructure. *Biosens Bioelectron* **2018**, *111*, 166–173. https://doi.org/10.1016/j.bios.2018.03.063.

(34) Zhao, L.; Li, L.; Zhao, Y.; Zhu, C.; Yang, R.; Fang, M.; Luan, Y. Aptamer-Based Point-of-Care-Testing for Small Molecule Targets: From Aptamers to Aptasensors, Devices and Applications. *TrAC - Trends in Analytical Chemistry*. Elsevier B.V. December 1, 2023. https://doi.org/10.1016/j.trac.2023.117408.

(35) Tuerk, C.; Gold, L. *Systematic Evolution of Ligands by Exponential Enrichment: RNA Ligands to Bacteriophage T4 DNA Polymerase Downloaded From*. http://science.sciencemag.org/.

(36) Shadman, S. M.; Daneshi, M.; Shafiei, F.; Azimimehr, M.; Khorasgani, M. R.; Sadeghian, M.; Motaghi, H.; Mehrgardi, M. A. Aptamer-Based Electrochemical Biosensors. In *Electrochemical Biosensors*; Elsevier, 2019; pp 213–251. https://doi.org/10.1016/B978-0-12-816491-4.00008-5.

(37) He, L.; Huang, R.; Xiao, P.; Liu, Y.; Jin, L.; Liu, H.; Li, S.; Deng, Y.; Chen, Z.; Li, Z.; He,N. Current Signal Amplification Strategies in Aptamer-Based Electrochemical Biosensor: A Review. *Chinese Chemical Letters* **2021**, *32* (5), 1593–1602. https://doi.org/10.1016/j.cclet.2020.12.054.

(38) Zhang, S.; Hu, X.; Yang, X.; Sun, Q.; Xu, X.; Liu, X.; Shen, G.; Lu, J.; Shen, G.; Yu, R. Background Eliminated Signal-on Electrochemical Aptasensing Platform for Highly Sensitive Detection of Protein. *Biosens Bioelectron* **2015**, *66*, 363–369. https://doi.org/10.1016/j.bios.2014.11.044.

(39) Negahdary, M. Aptamers in Nanostructure-Based Electrochemical Biosensors for Cardiac Biomarkers and Cancer Biomarkers: A Review. *Biosensors and Bioelectronics*. Elsevier Ltd March 15, 2020. https://doi.org/10.1016/j.bios.2020.112018.

(40) Bai, L.; Yan, B.; Chai, Y.; Yuan, R.; Yuan, Y.; Xie, S.; Jiang, L.; He, Y. An Electrochemical Aptasensor for Thrombin Detection Based on Direct Electrochemistry of Glucose Oxidase Using a Functionalized Graphene Hybrid for Amplification. *Analyst* **2013**, *138* (21), 6595–6599. https://doi.org/10.1039/c3an00983a.

(41) Bao, T.; Wen, W.; Zhang, X.; Wang, S. An Exonuclease-Assisted Amplification Electrochemical Aptasensor of Thrombin Coupling "Signal on/off" Strategy. *Anal Chim Acta* **2015**, *860*, 70–76. https://doi.org/10.1016/j.aca.2014.12.027.

(42) Li, Y.; Wang, Q.; Zhang, Y.; Deng, D.; He, H.; Luo, L.; Wang, Z. A Label-Free Electrochemical Aptasensor Based on Graphene Oxide/Double-Stranded DNA Nanocomposite. *Colloids Surf B Biointerfaces* **2016**, *145*, 160–166. https://doi.org/10.1016/j.colsurfb.2016.04.048.

(43) Wang, L.; Ma, R.; Jiang, L.; Jia, L.; Jia, W.; Wang, H. A Novel "Signal-on/off" Sensing Platform for Selective Detection of Thrombin Based on Target-Induced Ratiometric Electrochemical Biosensing and Bio-Bar-Coded Nanoprobe Amplification Strategy. *Biosens Bioelectron* **2017**, *92*, 390–395. https://doi.org/10.1016/j.bios.2016.10.089.

(44) Heydari-Bafrooei, E.; Amini, M.; Ardakani, M. H. An Electrochemical Aptasensor Based on TiO2/MWCNT and a Novel Synthesized Schiff Base Nanocomposite for the Ultrasensitive Detection of Thrombin. *Biosens Bioelectron* **2016**, *85*, 828–836. https://doi.org/10.1016/j.bios.2016.06.012.

(45) Zheng, Y.; Yuan, Y.; Chai, Y.; Yuan, R. A Label-Free Electrochemical Aptasensor Based on the Catalysis of Manganese Porphyrins for Detection of Thrombin. *Biosens Bioelectron* **2015**, *66*, 585–589. https://doi.org/10.1016/j.bios.2014.12.022.

(46) Wang, L.; Ma, R.; Jiang, L.; Jia, L.; Jia, W.; Wang, H. A Novel "Signal-on/off" Sensing Platform for Selective Detection of Thrombin Based on Target-Induced Ratiometric Electrochemical Biosensing and Bio-Bar-Coded Nanoprobe Amplification Strategy. *Biosens Bioelectron* **2017**, *92*, 390–395. https://doi.org/10.1016/j.bios.2016.10.089.

(47) Jarczewska, M.; Rębiś, J.; Górski, Ł.; Malinowska, E. Development of DNA Aptamer-Based Sensor for Electrochemical Detection of C-Reactive Protein. *Talanta* **2018**, *189*, 45–54. https://doi.org/10.1016/j.talanta.2018.06.035.

(48) Erdem, A.; Congur, G. Dendrimer Enriched Single-Use Aptasensor for Impedimetric Detection of Activated Protein C. *Colloids Surf B Biointerfaces* **2014**, *117*, 338–345. https://doi.org/10.1016/j.colsurfb.2014.03.003.

(49) Fu, X. M.; Liu, Z. J.; Cai, S. X.; Zhao, Y. P.; Wu, D. Z.; Li, C. Y.; Chen, J. H.Electrochemical Aptasensor for the Detection of Vascular Endothelial Growth Factor (VEGF) Based on DNA-Templated Ag/Pt Bimetallic Nanoclusters. *Chinese Chemical Letters* **2016**, *27* (6), 920–926. https://doi.org/10.1016/j.cclet.2016.04.014.

(50) Da, H.; Liu, H.; Zheng, Y.; Yuan, R.; Chai, Y. A Highly Sensitive VEGF165 Photoelectrochemical Biosensor Fabricated by Assembly of Aptamer Bridged DNA Networks. *Biosens Bioelectron* **2018**, *101*,213–218. https://doi.org/10.1016/j.bios.2017.10.032.

(51) He, L.; Zhang, S.; Ji, H.; Wang, M.; Peng, D.; Yan, F.; Fang, S.; Zhang, H.; Jia, C.; Zhang,Z. Protein-Templated Cobaltous Phosphate Nanocomposites for the Highly Sensitive and Selective Detection of Platelet-Derived Growth Factor-BB. *Biosens Bioelectron* **2016**, *79*, 553–560. https://doi.org/10.1016/j.bios.2015.12.095.

(52) Zhang, J.; Yuan, Y.; biXie, S.; Chai, Y.; Yuan, R. Amplified Amperometric Aptasensor for Selective Detection of Protein Using Catalase-Functional DNA-PtNPs Dendrimer as a Synergetic Signal Amplification Label. *Biosens Bioelectron* **2014**, *60*, 224–230. https://doi.org/10.1016/j.bios.2014.04.024.

(53) Liu, Y. M.; Zhou, M.; Liu, Y. Y.; Shi, G. F.; Zhang, J. J.; Cao, J. T.; Huang, K. J.; Chen, Y.H. Fabrication of Electrochemiluminescence Aptasensor Based on in Situ Growth of Gold Nanoparticles on Layered Molybdenum Disulfide for Sensitive Detection of Platelet-Derived Growth Factor-BB. *RSC Adv* **2014**, *4* (44), 22888–22893. https://doi.org/10.1039/c4ra02162b.

(54) Florea, A.; Taleat, Z.; Cristea, C.; Mazloum-Ardakani, M.; Săndulescu, R. Label Free MUC1 Aptasensors Based on Electrodeposition of Gold Nanoparticles on Screen Printed Electrodes. *Electrochem commun* **2013**, *33*,127–130. https://doi.org/10.1016/j.elecom.2013.05.008.

(55) Ma, F.; Ho, C.; Cheng, A. K. H.; Yu, H. Z. Immobilization of Redox-Labeled Hairpin DNA Aptamers on Gold: Electrochemical Quantitation of Epithelial Tumor Marker Mucin 1. *Electrochim Acta* **2013**, *110*, 139–145. https://doi.org/10.1016/j.electacta.2013.02.088.

(56) Nawaz, M. A. H.; Rauf, S.; Catanante, G.; Nawaz, M. H.; Nunes, G.; Marty, J. L.; Hayat, A. One Step Assembly of Thin Films of Carbon Nanotubes on Screen Printed Interface for Electrochemical Aptasensing of Breast Cancer Biomarker. *Sensors (Switzerland)* **2016**, *16* (10). https://doi.org/10.3390/s16101651.

(57) Jolly, P.; Zhurauski, P.; Hammond, J. L.; Miodek, A.; Liébana, S.; Bertok, T.; Tkáč, J.; Estrela, P. Self-Assembled Gold Nanoparticles for Impedimetric and Amperometric Detection of a Prostate Cancer Biomarker. *Sens Actuators B Chem* **2017**, *251*, 637–643. https://doi.org/10.1016/j.snb.2017.05.040.

(58) Rahi, A.; Sattarahmady, N.; Heli, H. Label-Free Electrochemical Aptasensing of the Human Prostate-Specific Antigen Using Gold Nanospears. *Talanta* **2016**, *156–157*, 218–224. https://doi.org/10.1016/j.talanta.2016.05.029.

(59) Chen, Z.; Guo, J.; Li, J.; Guo, L. Tetrahexahedral Au Nanocrystals/Aptamer Based Ultrasensitive Electrochemical Biosensor. *RSC Adv* **2013**, *3* (34), 14385–14389. https://doi.org/10.1039/c3ra41065j.

(60) Ocaña, C.; Hayat, A.; Mishra, R. K.; Vasilescu, A.; del Valle, M.; Marty, J. L. Label Free Aptasensor for Lysozyme Detection: A Comparison of the Analytical Performance of Two Aptamers. *Bioelectrochemistry* **2015**, *105*,72–77. https://doi.org/10.1016/j.bioelechem.2015.05.009.

(61) Ocaña, C.; Hayat, A.; Mishra, R. K.; Vasilescu, A.; del Valle, M.; Marty, J. L. Label Free Aptasensor for Lysozyme Detection: A Comparison of the Analytical Performance of Two Aptamers. *Bioelectrochemistry* **2015**, *105*,72–77. https://doi.org/10.1016/j.bioelechem.2015.05.009.

(62) Chen, Z.; Guo, J. A Reagentless Signal-off Architecture for Electrochemical Aptasensor for the Detection of Lysozyme. *Electrochim Acta* **2013**, *111*, 916–920. https://doi.org/10.1016/j.electacta.2013.08.116.

(63) Jarczewska, M.; Rębiś, J.; Górski, Ł.; Malinowska, E. Development of DNA Aptamer-Based Sensor for Electrochemical Detection of C-Reactive Protein. *Talanta* **2018**, *189*, 45–54. https://doi.org/10.1016/j.talanta.2018.06.035.

(64) Villalonga, A.; Pérez-Calabuig, A. M.; Villalonga, R. Electrochemical Biosensors Based on Nucleic Acid Aptamers. *Analytical and Bioanalytical Chemistry*. Springer January 1, 2020, pp 55–72. https://doi.org/10.1007/s00216-019-02226-x.

(65) Negahdary, M. Aptamers in Nanostructure-Based Electrochemical Biosensors for Cardiac Biomarkers and Cancer Biomarkers: A Review. *Biosensors and Bioelectronics*. Elsevier Ltd March 15, 2020. https://doi.org/10.1016/j.bios.2020.112018.

(66) Chen, Z.; Guo, J.; Li, J.; Guo, L. Tetrahexahedral Au Nanocrystals/Aptamer Based Ultrasensitive Electrochemical Biosensor. *RSC Adv* **2013**, *3* (34), 14385–14389. https://doi.org/10.1039/c3ra41065j.

(67) Zhang, S.; Hu, X.; Yang, X.; Sun, Q.; Xu, X.; Liu, X.; Shen, G.; Lu, J.; Shen, G.; Yu, R. Background Eliminated Signal-on Electrochemical Aptasensing Platform for Highly Sensitive Detection of Protein. *Biosens Bioelectron* **2015**, *66*, 363–369. https://doi.org/10.1016/j.bios.2014.11.044.

(68) Zhu, Y.; Mandal, K.; Hernandez, A. L.; Kawakita, S.; Huang, W.; Bandaru, P.; Ahadian, S.; Kim, H. J.; Jucaud, V.; Dokmeci, M. R.; Khademhosseini, A. State of the Art in Integrated Biosensors for Organ-on-a-Chip Applications. *Current Opinion in Biomedical Engineering*. Elsevier B.V. September 1,2021. https://doi.org/10.1016/j.cobme.2021.100309.

(69) Mirceski, V.; Gulaboski, R. RECENT ACHIEVEMENTS IN SQUARE-WAVE VOLTAMMETRY (A REVIEW). *Macedonian Journal of Chemistry and Chemical Engineering* **2014**, *33* (1), 1–12.

(70) Archer, M. D. *Electrochemistry, Past and Present*; UTC, 2024; Vol. 33. https://pubs.acs.org/sharingguidelines.

(71) Magar, H. S.; Hassan, R. Y. A.; Mulchandani, A. Electrochemical Impedance Spectroscopy (Eis): Principles, Construction, and Biosensing Applications. *Sensors*. MDPI October 1, 2021. https://doi.org/10.3390/s21196578.

(72) Evans, T. I.; White, R. E.; Ying, R. Y.; Ng, P. K.; Mao, Z. *Modification of the Cottrell Equation to Account for Electrode Growth; Application to Diffusion Data in the Ag-Au System You May Also like A Thermal Analysis of a Spirally Wound Battery Using a Simple Mathematical Model Electrodeposition of CopperNickel Alloys from Citrate Solutions on a Rotating Disk Electrode: II. Mathematical Modeling*.

(73) Yu, P.; Zhou, J.; Wu, L.; Xiong, E.; Zhang, X.; Chen, J. A Ratiometric Electrochemical Aptasensor for Sensitive Detection of Protein Based on Aptamer-Target-Aptamer Sandwich

Structure. *Journal of Electroanalytical Chemistry* **2014**, *732*, 61–65. https://doi.org/10.1016/j.jelechem.2014.08.034.

(74) Magar, H. S.; Hassan, R. Y. A.; Mulchandani, A. Electrochemical Impedance Spectroscopy (Eis): Principles, Construction, and Biosensing Applications. *Sensors*. MDPI October 1, 2021. https://doi.org/10.3390/s21196578.

(75) Wadhera, T.; Kakkar, D.; Wadhwa, G.; Raj, B. Recent Advances and Progress in Development of the Field Effect Transistor Biosensor: A Review. *Journal of Electronic Materials*. Springer New York LLC December 1, 2019, pp 7635–7646. https://doi.org/10.1007/s11664-019-07705-6.

(76) Wadhera, T.; Kakkar, D.; Wadhwa, G.; Raj, B. Recent Advances and Progress in Development of the Field Effect Transistor Biosensor: A Review. *Journal of Electronic Materials*. Springer New York LLC December 1, 2019, pp 7635–7646. https://doi.org/10.1007/s11664-019-07705-6.

(77) Zhu, Y.; Mandal, K.; Hernandez, A. L.; Kawakita, S.; Huang, W.; Bandaru, P.; Ahadian, S.; Kim, H. J.; Jucaud, V.; Dokmeci, M. R.; Khademhosseini, A. State of the Art in Integrated Biosensors for Organ-on-a-Chip Applications. *Current Opinion in Biomedical Engineering*. Elsevier B.V. September 1,2021. https://doi.org/10.1016/j.cobme.2021.100309.

(78) Sha, F.; Salzman, G.; Gupta, A.; Koide, S. Monobodies and Other Synthetic Binding Proteins for Expanding Protein Science. *Protein Science*. Blackwell Publishing Ltd May 1, 2017, pp 910–924. https://doi.org/10.1002/pro.3148.

(79) DiRusso, C. J.; Dashtiahangar, M.; Gilmore, T. D. Scaffold Proteins as Dynamic Integrators of Biological Processes. *Journal of Biological Chemistry*. American Society for Biochemistry and Molecular Biology Inc. December 1, 2022. https://doi.org/10.1016/j.jbc.2022.102628.

(80) Bruce, V. J.; Ta, A. N.; McNaughton, B. R. Minimalist Antibodies and Mimetics: An Update and Recent Applications. *ChemBioChem*. Wiley-VCH Verlag October 17, 2016, pp 1892–1899. https://doi.org/10.1002/cbic.201600303.

(81) Shaw, A. S.; Filbert, E. L. Scaffold Proteins and Immune-Cell Signalling. *Nature Reviews Immunology*. January 2009, pp 47–56. https://doi.org/10.1038/nri2473.

(82) Tolmachev, V.; Orlova, A. Affibody Molecules as Targeting Vectors for PET Imaging. *Cancers*. MDPI AG March 1, 2020. https://doi.org/10.3390/cancers12030651.

(83) Plückthun, A. Designed Ankyrin Repeat Proteins (DARPins): Binding Proteins for Research, Diagnostics, and Therapy. *Annual Review of Pharmacology and Toxicology*. Annual Reviews Inc. January 6, 2015, pp 489–511. https://doi.org/10.1146/annurev-pharmtox-010611-134654.

(84) Wang, X.; Li, F.; Qiu, W.; Xu, B.; Li, Y.; Lian, X.; Yu, H.; Zhang, Z.; Wang, J.; Li, Z.; Xue, W.; Zhu, F. SYNBIP: Synthetic Binding Proteins for Research, Diagnosis and Therapy. *Nucleic Acids Res* **2022**, *50* (D1), D560–D570. https://doi.org/10.1093/nar/gkab926.

(85) Dikic, I.; Wakatsuki, S.; Walters, K. J. Ubiquitin-Binding Domains from Structures to Functions. *Nature Reviews Molecular Cell Biology*. October 2009, pp 659–671. https://doi.org/10.1038/nrm2767.

(86) Koide, A.; Bailey, C. W.; Huang, X.; Koide, S. *The Fibronectin Type III Domain as a Scaffold for Novel Binding Proteins*.

(87) Baron, M.; Main, A. L.; Driscoll, P. C.; Mardon, H. J.; Boyd, J.; Campbell, I. D. *NMR Assignment and Secondary Structure of the Cell Adhesion Type III Module of Fibronectin1'*; Shechter, Y, 1990; Vol. 41. https://pubs.acs.org/sharingguidelines.

(88) Chandler, P. G.; Buckle, A. M. Development and Differentiation in Monobodies Based on the Fibronectin Type 3 Domain. *Cells*. NLM (Medline) March 4, 2020. https://doi.org/10.3390/cells9030610.

(89) Koide, A.; Wojcik, J.; Gilbreth, R. N.; Hoey, R. J.; Koide, S. Teaching an Old Scaffold New Tricks: Monobodies Constructed Using Alternative Surfaces of the FN3 Scaffold. *J Mol Biol* **2012**, *415* (2), 393–405. https://doi.org/10.1016/j.jmb.2011.12.019.

(90) Woldring, D. R.; Holec, P. V.; Zhou, H.; Hackel, B. J. High-Throughput Ligand Discovery Reveals a Sitewise Gradient of Diversity in Broadly Evolved Hydrophilic Fibronectin Domains. *PLoS One* **2015**, *10* (9). https://doi.org/10.1371/journal.pone.0138956.

(91) Hackel, B. J.; Kapila, A.; Dane Wittrup, K. Picomolar Affinity Fibronectin Domains Engineered Utilizing Loop Length Diversity, Recursive Mutagenesis, and Loop Shuffling. *J Mol Biol* **2008**, *381* (5), 1238–1252. https://doi.org/10.1016/j.jmb.2008.06.051.

(92) Rosano, G. L.; Morales, E. S.; Ceccarelli, E. A. New Tools for Recombinant Protein Production in Escherichia Coli: A 5-Year Update. *Protein Science*. Blackwell Publishing Ltd August 1, 2019, pp 1412–1422. https://doi.org/10.1002/pro.3668.

(93) Bertoni, M.; Kiefer, F.; Biasini, M.; Bordoli, L.; Schwede, T. Modeling Protein Quaternary Structure of Homo- and Hetero-Oligomers beyond Binary Interactions by Homology. *Sci Rep* **2017**, *7* (1). https://doi.org/10.1038/s41598-017-09654-8.

(94) Schwede, T.; Kopp, J.; Guex, N.; Peitsch, M. C. SWISS-MODEL: An Automated Protein Homology-Modeling Server. *Nucleic Acids Res* **2003**, *31* (13), 3381–3385. https://doi.org/10.1093/nar/gkg520.

(95) Waterhouse, A.; Bertoni, M.; Bienert, S.; Studer, G.; Tauriello, G.; Gumienny, R.; Heer, F. T.; De Beer, T. A. P.; Rempfer, C.; Bordoli, L.; Lepore, R.; Schwede, T. SWISS-MODEL:

Homology Modelling of Protein Structures and Complexes. *Nucleic Acids Res* **2018**, *46* (W1), W296–W303. https://doi.org/10.1093/nar/gky427.

(96) Biasini, M.; Bienert, S.; Waterhouse, A.; Arnold, K.; Studer, G.; Schmidt, T.; Kiefer, F.; Cassarino, T. G.; Bertoni, M.; Bordoli, L.; Schwede, T. SWISS-MODEL: Modelling Protein Tertiary and Quaternary Structure Using Evolutionary Information. *Nucleic Acids Res* **2014**, *42* (W1). https://doi.org/10.1093/nar/gku340.

(97) Remmert, M.; Biegert, A.; Hauser, A.; Söding, J. HHblits: Lightning-Fast Iterative Protein Sequence Searching by HMM-HMM Alignment. *Nat Methods* **2012**, *9* (2), 173–175. https://doi.org/10.1038/nmeth.1818.

(98) Jumper, J.; Evans, R.; Pritzel, A.; Green, T.; Figurnov, M.; Ronneberger, O.; Tunyasuvunakool, K.; Bates, R.; Žídek, A.; Potapenko, A.; Bridgland, A.; Meyer, C.; Kohl, S. A. A.; Ballard, A. J.; Cowie, A.; Romera-Paredes, B.; Nikolov, S.; Jain, R.; Adler, J.; Back, T.; Petersen, S.; Reiman, D.; Clancy, E.; Zielinski, M.; Steinegger, M.; Pacholska, M.; Berghammer, T.; Bodenstein, S.; Silver, D.; Vinyals, O.; Senior, A. W.; Kavukcuoglu, K.; Kohli, P.; Hassabis, D. Highly Accurate Protein Structure Prediction with AlphaFold. *Nature* **2021**, *596* (7873), 583–589. https://doi.org/10.1038/s41586-021-03819-2.

(99) Weitzner, B. D.; Jeliazkov, J. R.; Lyskov, S.; Marze, N.; Kuroda, D.; Frick, R.; Adolf-Bryfogle, J.; Biswas, N.; Dunbrack, R. L.; Gray, J. J. Modeling and Docking of Antibody Structures with Rosetta. *Nat Protoc* **2017**, *12* (2), 401–416. https://doi.org/10.1038/nprot.2016.180.

(100) Combs, S. A.; Deluca, S. L.; Deluca, S. H.; Lemmon, G. H.; Nannemann, D. P.; Nguyen, E. D.; Willis, J. R.; Sheehan, J. H.; Meiler, J. Small-Molecule Ligand Docking into Comparative Models with Rosetta. *Nat Protoc* **2013**, *8* (7), 1277–1298. https://doi.org/10.1038/nprot.2013.074.

(101) Biasini, M.; Schmidt, T.; Bienert, S.; Mariani, V.; Studer, G.; Haas, J.; Johner, N.; Schenk, A. D.; Philippsen, A.; Schwede, T. OpenStructure: An Integrated Software Framework for Computational Structural Biology. *Acta Crystallogr D Biol Crystallogr* **2013**, *69* (5), 701–709. https://doi.org/10.1107/S0907444913007051.

(102) Chaudhury, S.; Berrondo, M.; Weitzner, B. D.; Muthu, P.; Bergman, H.; Gray, J. J. Benchmarking and Analysis of Protein Docking Performance in Rosetta v3.2. *PLoS One* **2011**, *6* (8). https://doi.org/10.1371/journal.pone.0022477.

(103) Teymennet-Ramírez, K. V.; Martínez-Morales, F.; Trejo-Hernández, M. R. Yeast Surface Display System: Strategies for Improvement and Biotechnological Applications. *Frontiers in Bioengineering and Biotechnology*. Frontiers Media S.A. January 10, 2022. https://doi.org/10.3389/fbioe.2021.794742.

(104) Crossley, B. M.; Bai, J.; Glaser, A.; Maes, R.; Porter, E.; Killian, M. L.; Clement, T.; Toohey-Kurth, K. Guidelines for Sanger Sequencing and Molecular Assay Monitoring.

Journal of Veterinary Diagnostic Investigation **2020**, *32* (6), 767–775. https://doi.org/10.1177/1040638720905833.

(105) Woldring, D. R.; Holec, P. V.; Zhou, H.; Hackel, B. J. High-Throughput Ligand Discovery Reveals a Sitewise Gradient of Diversity in Broadly Evolved Hydrophilic Fibronectin Domains. *PLoS One* **2015**, *10* (9). https://doi.org/10.1371/journal.pone.0138956.

(106) Muhammed, M. T.; Aki-Yalcin, E. Homology Modeling in Drug Discovery: Overview, Current Applications, and Future Perspectives. *Chemical Biology and Drug Design*. Blackwell Publishing Ltd January 1, 2019, pp 12–20. https://doi.org/10.1111/cbdd.13388.

(107) Kearse, M.; Moir, R.; Wilson, A.; Stones-Havas, S.; Cheung, M.; Sturrock, S.; Buxton, S.; Cooper, A.; Markowitz, S.; Duran, C.; Thierer, T.; Ashton, B.; Meintjes, P.; Drummond, A. Geneious Basic: An Integrated and Extendable Desktop Software Platform for the Organization and Analysis of Sequence Data. *Bioinformatics* **2012**, *28* (12), 1647–1649. https://doi.org/10.1093/bioinformatics/bts199.

(108) Medina-Cucurella, A. V.; Whitehead, T. A. Characterizing Protein-Protein Interactions Using Deep Sequencing Coupled to Yeast Surface Display. In *Methods in Molecular Biology*; Humana Press Inc., 2018; Vol. 1764, pp 101–121. https://doi.org/10.1007/978-1-4939-7759-8_7.

(109) Kajiwara, K.; Aoki, W.; Koike, N.; Ueda, M. Development of a Yeast Cell Surface Display Method Using the SpyTag/SpyCatcher System. *Sci Rep* **2021**, *11* (1). https://doi.org/10.1038/s41598-021-90593-w.

(110) Chao, G.; Lau, W. L.; Hackel, B. J.; Sazinsky, S. L.; Lippow, S. M.; Wittrup, K. D. Isolating and Engineering Human Antibodies Using Yeast Surface Display. *Nat Protoc* **2006**, *1* (2), 755–768. https://doi.org/10.1038/nprot.2006.94.

(111) *Workshop #7: Docking*. http://haddock.chem.uu.nl.

(112) Newman, J. D.; Turner, A. P. F. Home Blood Glucose Biosensors: A Commercial Perspective. *Biosensors and Bioelectronics*. Elsevier Ltd June 15, 2005, pp 2435–2453. https://doi.org/10.1016/j.bios.2004.11.012.

(113) Li, H.; Dauphin-Ducharme, P.; Ortega, G.; Plaxco, K. W. Calibration-Free Electrochemical Biosensors Supporting Accurate Molecular Measurements Directly in Undiluted Whole Blood. *J Am Chem Soc* **2017**, *139* (32), 11207–11213. https://doi.org/10.1021/jacs.7b05412.

(114) Grabowska, I.; Sharma, N.; Vasilescu, A.; Iancu, M.; Badea, G.; Boukherroub, R.; Ogale, S.; Szunerits, S. Electrochemical Aptamer-Based Biosensors for the Detection of Cardiac Biomarkers. *ACS Omega* **2018**, *3* (9), 12010–12018. https://doi.org/10.1021/acsomega.8b01558.

(115) Keefe, A. D.; Pai, S.; Ellington, A. Aptamers as Therapeutics. *Nature Reviews Drug Discovery*. July 2010, pp 537–550. https://doi.org/10.1038/nrd3141.

(116) Zhou, W.; Huang, P.-J. J.; Ding, J.; Liu, J. *Aptamer-Based Biosensors for Biomedical Diagnostics.*

(117) Liu, J.; Cao, Z.; Lu, Y. Functional Nucleic Acid Sensors. *Chem Rev* **2009**, *109* (5), 1948–1998. https://doi.org/10.1021/cr030183i.

(118) Shaver, A.; Arroyo-Currás, N. The Challenge of Long-Term Stability for Nucleic Acid-Based Electrochemical Sensors. *Current Opinion in Electrochemistry*. Elsevier B.V. April 1, 2022. https://doi.org/10.1016/j.coelec.2021.100902.

(119) Feng, D.; Shaikh, A. S.; Wang, F. Recent Advance in Tumor-Associated Carbohydrate Antigens (TACAs)-Based Antitumor Vaccines. *ACS Chemical Biology*. American Chemical Society April 15, 2016, pp850–863. https://doi.org/10.1021/acschembio.6b00084.

(120) Wang, X.; Li, F.; Qiu, W.; Xu, B.; Li, Y.; Lian, X.; Yu, H.; Zhang, Z.; Wang, J.; Li, Z.; Xue, W.; Zhu, F. SYNBIP: Synthetic Binding Proteins for Research, Diagnosis and Therapy. *Nucleic Acids Res* **2022**, *50* (D1), D560–D570. https://doi.org/10.1093/nar/gkab926.

(121) Sha, F.; Salzman, G.; Gupta, A.; Koide, S. Monobodies and Other Synthetic Binding Proteins for Expanding Protein Science. *Protein Science*. Blackwell Publishing Ltd May 1, 2017, pp 910–924. https://doi.org/10.1002/pro.3148.

(122) Akkapeddi, P.; Teng, K. W.; Koide, S. Monobodies as Tool Biologics for Accelerating Target Validation and Druggable Site Discovery. *RSC Medicinal Chemistry*. Royal Society of Chemistry November 1, 2021, pp 1839–1853. https://doi.org/10.1039/d1md00188d.

(123) Carrasco-López, C.; Zhao, E. M.; Gil, A. A.; Alam, N.; Toettcher, J. E.; Avalos, J. L. Development of Light-Responsive Protein Binding in the Monobody Non-Immunoglobulin Scaffold. *Nat Commun* **2020**, *11* (1). https://doi.org/10.1038/s41467-020-17837-7.

(124) Limsakul, P.; Peng, Q.; Wu, Y.; Allen, M. E.; Liang, J.; Remacle, A. G.; Lopez, T.; Ge, X.; Kay, B. K.; Zhao, H.; Strongin, A. Y.; Yang, X. L.; Lu, S.; Wang, Y. Directed Evolution to Engineer Monobody for FRET Biosensor Assembly and Imaging at Live-Cell Surface. *Cell Chem Biol* **2018**, *25* (4), 370-379.e4. https://doi.org/10.1016/j.chembiol.2018.01.002.

(125) Ahmad, M.; Ha, J. H.; Mayse, L. A.; Presti, M. F.; Wolfe, A. J.; Moody, K. J.; Loh, S. N.; Movileanu, L. A Generalizable Nanopore Sensor for Highly Specific Protein Detection at Single-Molecule Precision. *Nat Commun* **2023**, *14* (1). https://doi.org/10.1038/s41467-023-36944-9.

(126) Sekhon, H.; Ha, J.-H.; Presti, M. F.; Procopio, S. B.; Mirsky, P. O.; John, A. M.; Loh, S. N. Adaptable, Turn-On Monobody (ATOM) Fluorescent Biosensors for Multiplexed Detection in Cells. https://doi.org/10.1101/2023.03.28.534597.

(127) McNab, H.; Monahan, L. C. 3-Hydroxypyrroles and 1h-Pyrrol-3(2H)-Ones. Part 8. Reactions of 1-Isopropyl-2,2-Dimethyl-1H-Pyrrol-3(2H)-One with Electrophiles. *J Chem Soc Perkin 1* **1989**, No. 3, 419–424. https://doi.org/10.1039/P19890000419.

(128) Polsky, R.; Harper, J. C.; Wheeler, D. R.; Dirk, S. M.; Arango, D. C.; Brozik, S. M. Electrically Addressable Diazonium-Functionalized Antibodies for Multianalyte Electrochemical Sensor Applications. *Biosens Bioelectron* **2008**, *23* (6), 757–764. https://doi.org/10.1016/j.bios.2007.08.013.

(129) Hu, B.; Debruler, C.; Rhodes, Z.; Liu, T. L. Long-Cycling Aqueous Organic Redox Flow Battery (AORFB) toward Sustainable and Safe Energy Storage. *J Am Chem Soc* **2017**, *139* (3), 1207–1214. https://doi.org/10.1021/jacs.6b10984.

(130) Polsky, R.; Harper, J. C.; Dirk, S. M.; Arango, D. C.; Wheeler, D. R.; Brozik, S. M. Diazonium-Functionalized Horseradish Peroxidase Immobilized via Addressable Electrodeposition: Direct Electron Transfer and Electrochemical Detection. *Langmuir* **2007**, *23* (2), 364–366. https://doi.org/10.1021/la062916a.

(131) Wilkirson, E. C.; Singampalli, K. L.; Li, J.; Dixit, D. D.; Jiang, X.; Gonzalez, D. H.; Lillehoj, P. B. Affinity-Based Electrochemical Sensors for Biomolecular Detection in Whole Blood. *Analytical and Bioanalytical Chemistry*. Springer Science and Business Media Deutschland GmbH July 1, 2023, pp 3983–4002. https://doi.org/10.1007/s00216-023-04627-5.

(132) Azizian, S.; Eris, S. Adsorption Isotherms and Kinetics. In *Interface Science and Technology*; Elsevier B.V., 2021; Vol. 33, pp 445–509. https://doi.org/10.1016/B978-0-12-818805-7.00011-4.

(133) Ratkowsky, D. A.; Ratkowsky, D. A.; Mcmeekin, T. A. *Principles of Nonlinear Regression Modeling*; 1993; Vol. 12.

(134) Mohammadi, M.; Ameri Shahrabi, M. J.; Sedighi, M. Comparative Study of Linearized and Non-Linearized Modified Langmuir Isotherm Models on Adsorption of Asphaltene onto Mineral Surfaces. *Surface Engineering and Applied Electrochemistry* **2012**, *48* (3), 234–243. https://doi.org/10.3103/S1068375512030088.

(135) Sohn, S.; Kim, D. Modification of Langmuir Isotherm in Solution Systems - Definition and Utilization of Concentration Dependent Factor. *Chemosphere* **2005**, *58* (1), 115–123. https://doi.org/10.1016/j.chemosphere.2004.08.091.

(136) Sips, R. On the Structure of a Catalyst Surface. *J Chem Phys* **1948**, *16* (5), 490–495. https://doi.org/10.1063/1.1746922. Zito, P. F.; Caravella, A.; Brunetti, A.; Drioli, E.;

Barbieri, G. Estimation of Langmuir and Sips Models Adsorption Parameters for NaX and NaY FAU Zeolites. *J Chem Eng Data* **2015**, *60* (10), 2858–2868. https://doi.org/10.1021/acs.jced.5b00215.

(137) Battaglia, F.; Baldoneschi, V.; Meucci, V.; Intorre, L.; Minunni, M.; Scarano, S. Detection of Canine and Equine Procalcitonin for Sepsis Diagnosis in Veterinary Clinic by the Development of Novel MIP-Based SPR Biosensors. *Talanta* **2021**, *230*. https://doi.org/10.1016/j.talanta.2021.122347.

(138) Shepherd, D. V.; Shepherd, J. H.; Ghose, S.; Kew, S. J.; Cameron, R. E.; Best, S. M. The Process of EDC-NHS Cross-Linking of Reconstituted Collagen Fibres Increases Collagen Fibrillar Order and Alignment. *APL Mater* **2015**, *3* (1). https://doi.org/10.1063/1.4900887.

(139) Glatz, R. T.; Ates, H. C.; Mohsenin, H.; Weber, W.; Dincer, C. Designing Electrochemical Microfluidic Multiplexed Biosensors for On-Site Applications. *Anal Bioanal Chem* **2022**, *414* (22), 6531–6540. https://doi.org/10.1007/s00216-022-04210-4.

(140) Reddy, M. M.; Wilson, R.; Wilson, J.; Connell, S.; Gocke, A.; Hynan, L.; German, D.; Kodadek, T. Identification of Candidate IgG Biomarkers for Alzheimer's Disease via Combinatorial Library Screening. *Cell* **2011**, *144* (1), 132–142. https://doi.org/10.1016/j.cell.2010.11.054.

(141) Winter, W. E.; Bazydlo, L. A. L.; Harris, N. S. The Molecular Biology of Human Iron Metabolism. *Lab Medicine* **2014**, *45* (2),92–102. https://doi.org/10.1309/LMF28S2GIMXNWHMM.

(142) Elsayed, M. E.; Sharif, M. U.; Stack, A. G. Transferrin Saturation: A Body Iron Biomarker. In *Advances in Clinical Chemistry*; Academic Press Inc., 2016; Vol. 75, pp 71–97. https://doi.org/10.1016/bs.acc.2016.03.002.

(143) Wall, A.; Wills, A. G.; Forte, N.; Bahou, C.; Bonin, L.; Nicholls, K.; Ma, M. T.; Chudasama, V.; Baker, J. R. One-Pot Thiol-Amine Bioconjugation to Maleimides: Simultaneous Stabilisation and Dual Functionalisation. *Chem Sci* **2020**, *11* (42), 11455–11460. https://doi.org/10.1039/d0sc05128d.

(144) Lee, Y.; Morales, G. M.; Yu, L. Self-Assembled Monolayers of Isocyanides on Nickel Electrodes. *Angewandte Chemie - International Edition* **2005**, *44* (27), 4228–4231. https://doi.org/10.1002/anie.200500942.

(145) Lucena-Aguilar, G.; Sánchez-López, A. M.; Barberán-Aceituno, C.; Carrillo-Ávila, J. A.; López-Guerrero, J. A.; Aguilar-Quesada, R. DNA Source Selection for Downstream Applications Based on DNA Quality Indicators Analysis. In *Biopreservation and Biobanking*; Mary Ann Liebert Inc., 2016; Vol. 14, pp 264–270. https://doi.org/10.1089/bio.2015.0064.

(146) Lee, Y.; Morales, G. M.; Yu, L. Self-Assembled Monolayers of Isocyanides on Nickel Electrodes. *Angewandte Chemie - International Edition* **2005**, *44* (27), 4228–4231. https://doi.org/10.1002/anie.200500942.

(147) Menanteau, T.; Dias, M.; Levillain, E.; Downard, A. J.; Breton, T. Electrografting via Diazonium Chemistry: The Key Role of the Aryl Substituent in the Layer Growth Mechanism. *Journal of Physical Chemistry C* **2016**, *120* (8), 4423–4429. https://doi.org/10.1021/acs.jpcc.5b12565.

(148) Wall, A.; Wills, A. G.; Forte, N.; Bahou, C.; Bonin, L.; Nicholls, K.; Ma, M. T.; Chudasama, V.; Baker, J. R. One-Pot Thiol-Amine Bioconjugation to Maleimides: Simultaneous Stabilisation and Dual Functionalisation. *Chem Sci* **2020**, *11* (42), 11455–11460. https://doi.org/10.1039/d0sc05128d.

(149) Smith, M. E. B.; Schumacher, F. F.; Ryan, C. P.; Tedaldi, L. M.; Papaioannou, D.; Waksman, G.; Caddick, S.; Baker, J. R. Protein Modification, Bioconjugation, and Disulfide Bridging Using Bromomaleimides. *J Am Chem Soc* **2010**, *132* (6), 1960–1965. https://doi.org/10.1021/ja908610s.

(150) Harris, T. G. A. A.; Heidary, N.; Kozuch, J.; Frielingsdorf, S.; Lenz, O.; Mroginski, M. A.; Hildebrandt, P.; Zebger, I.; Fischer, A. In Situ Spectroelectrochemical Studies into the Formation and Stability of Robust Diazonium-Derived Interfaces on Gold Electrodes for the Immobilization of an Oxygen-Tolerant Hydrogenase. *ACS Appl Mater Interfaces* **2018**, *10* (27), 23380–23391. https://doi.org/10.1021/acsami.8b02273.

(151) Tahara, K.; Kubo, Y.; Lindner, B.; Hashimoto, S.; Hirose, S.; Brown, A.; Hirsch, B.; Daukiya, L.; De Feyter, S.; Tobe, Y. Steric and Electronic Effects of Electrochemically Generated Aryl Radicals on Grafting of the Graphite Surface. *Langmuir* **2019**, *35* (6), 2089–2098. https://doi.org/10.1021/acs.langmuir.8b03339.

(152) Drevet, R.; Dragoé, D.; Barthés-Labrousse, M. G.; Chaussé, A.; Andrieux, M. XPS-Nanocharacterization of Organic Layers Electrochemically Grafted on the Surface of SnO 2 Thin Films to Produce a New Hybrid Material Coating. *Appl Surf Sci* **2016**, *384*, 442–448. https://doi.org/10.1016/j.apsusc.2016.05.064.

(153) Nielsen, L. T.; Vase, K. H.; Dong, M.; Besenbacher, F.; Pedersen, S. U.; Daasbjerg, K. Electrochemical Approach for Constructing a Monolayer of Thiophenolates from Grafted Multilayers of Diaryl Disulfides. *J Am Chem Soc* **2007**, *129* (7), 1888–1889. https://doi.org/10.1021/ja0682430.

(154) Nielsen, L. T.; Vase, K. H.; Dong, M.; Besenbacher, F.; Pedersen, S. U.; Daasbjerg, K. Electrochemical Approach for Constructing a Monolayer of Thiophenolates from Grafted Multilayers of Diaryl Disulfides. *J Am Chem Soc* **2007**, *129* (7), 1888–1889. https://doi.org/10.1021/ja0682430.

(155) Gillan, L.; Teerinen, T.; Johansson, L. S.; Smolander, M. Controlled Diazonium Electrodeposition towards a Biosensor for C-Reactive Protein. *Sensors International* **2021**, *2*. https://doi.org/10.1016/j.sintl.2020.100060.

(156) Menanteau, T.; Levillain, E.; Breton, T. Electrografting via Diazonium Chemistry: From Multilayer to Monolayer Using Radical Scavenger. *Chemistry of Materials* **2013**, *25* (14), 2905–2909. https://doi.org/10.1021/cm401512c.

(157) Greenwood, J.; Phan, T. H.; Fujita, Y.; Li, Z.; Ivasenko, O.; Vanderlinden, W.; Van Gorp, H.; Frederickx, W.; Lu, G.; Tahara, K.; Tobe, Y.; Uji-I, H.; Mertens, S. F. L.; De Feyter, S. Covalent Modification of Graphene and Graphite Using Diazonium Chemistry: Tunable Grafting and Nanomanipulation. *ACS Nano* **2015**, *9* (5), 5520–5535. https://doi.org/10.1021/acsnano.5b01580.

(158) Combellas, C.; Kanoufi, F.; Pinson, J.; Podvorica, F. I. Sterically Hindered Diazonium Salts for the Grafting of a Monolayer on Metals. *J Am Chem Soc* **2008**, *130* (27), 8576–8577. https://doi.org/10.1021/ja8018912.

(159) Fontaine, O.; Ghilane, J.; Martin, P.; Lacroix, J. C.; Randriamahazaka, H. Ionic Liquid Viscosity Effects on the Functionalization of Electrode Material through the Electroreduction of Diazonium. *Langmuir* **2010**, *26* (23), 18542–18549. https://doi.org/10.1021/la103000u.

(160) Mattiuzzi, A.; Lenne, Q.; Carvalho Padilha, J.; Troian-Gautier, L.; Leroux, Y. R.; Jabin, I.; Lagrost, C. Strategies for the Formation of Monolayers From Diazonium Salts: Unconventional Grafting Media, Unconventional Building Blocks. *Frontiers in Chemistry*. Frontiers Media S.A. July 14, 2020. https://doi.org/10.3389/fchem.2020.00559.

(161) Van Rosmalen, M.; Krom, M.; Merkx, M. Tuning the Flexibility of Glycine-Serine Linkers to Allow Rational Design of Multidomain Proteins. *Biochemistry* **2017**, *56* (50), 6565–6574. https://doi.org/10.1021/acs.biochem.7b00902.

(162) Chen, X.; Zaro, J. L.; Shen, W. C. Fusion Protein Linkers: Property, Design and Functionality. *Advanced Drug Delivery Reviews*. October 15, 2013, pp 1357–1369. https://doi.org/10.1016/j.addr.2012.09.039.

(163) Van Rosmalen, M.; Krom, M.; Merkx, M. Tuning the Flexibility of Glycine-Serine Linkers to Allow Rational Design of Multidomain Proteins. *Biochemistry* **2017**, *56* (50), 6565–6574. https://doi.org/10.1021/acs.biochem.7b00902.

APPENDIX A: (CHAPTER 2)

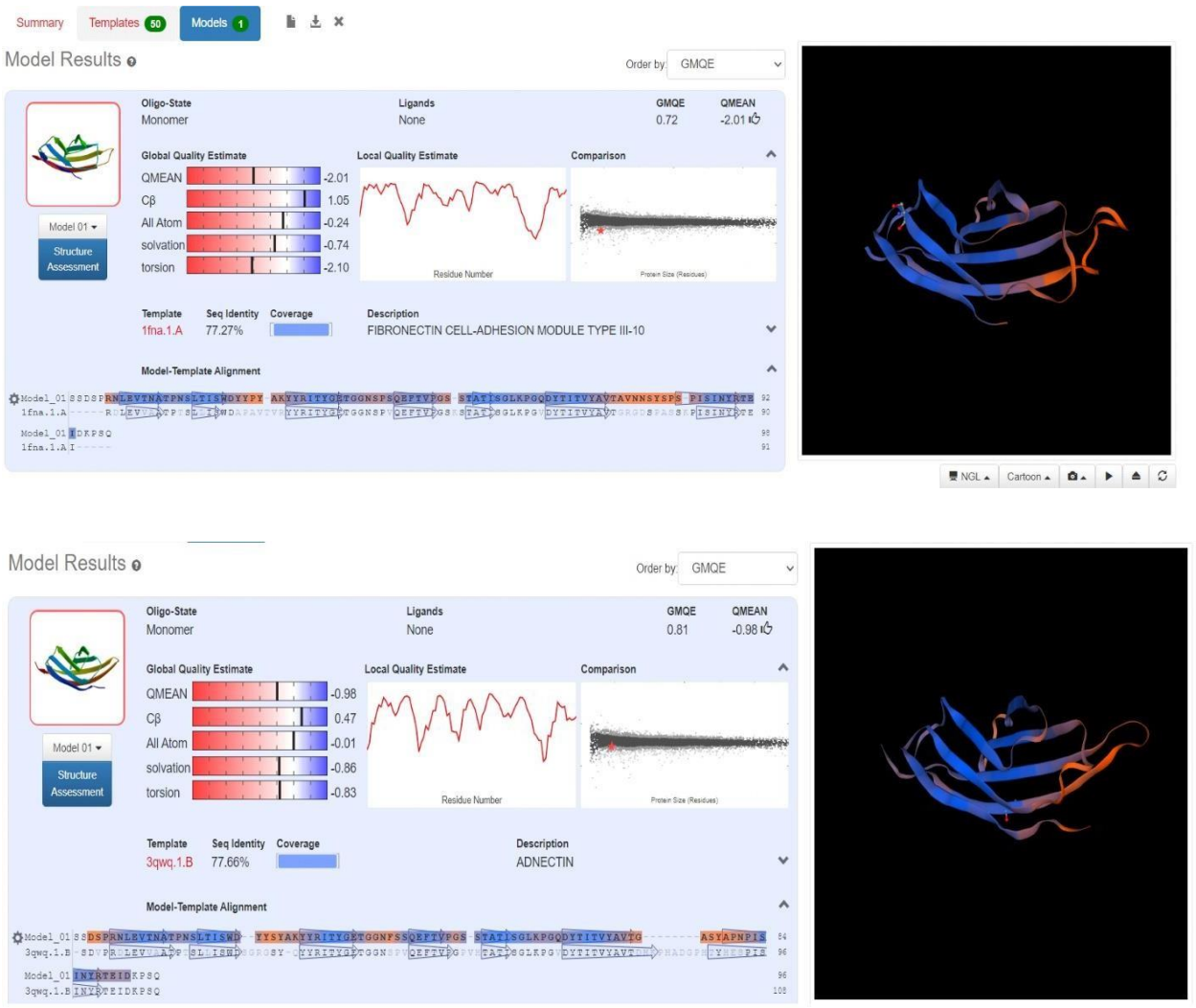

Figure A.1 3D monobody protein models targeting lysozyme made from templates 1fna and 3qwq using SWISS-MODEL.

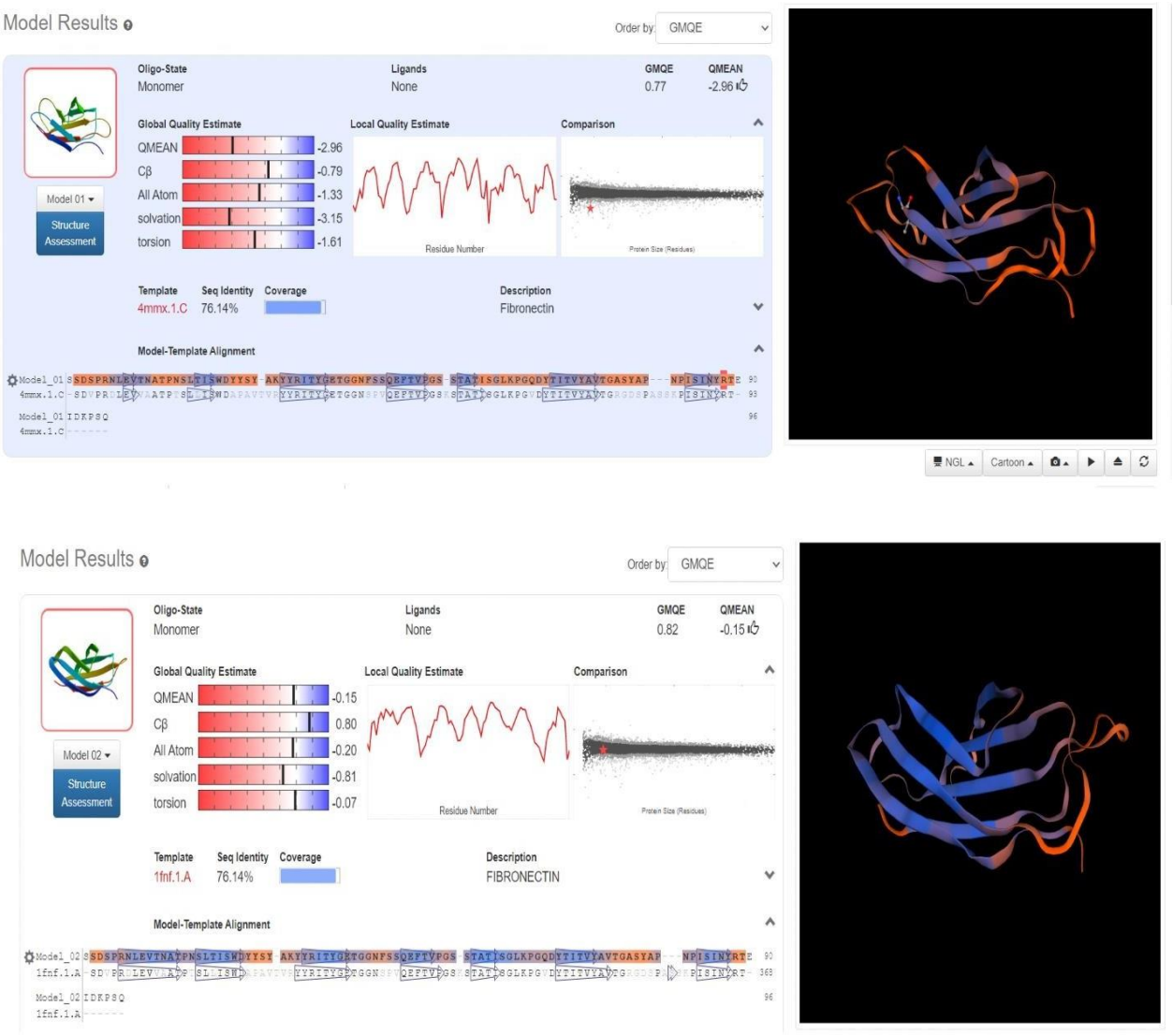

Figure A.2 3D monobody protein models targeting lysozyme made from templates 4mmx and 1fnf using SWISS-MODEL.

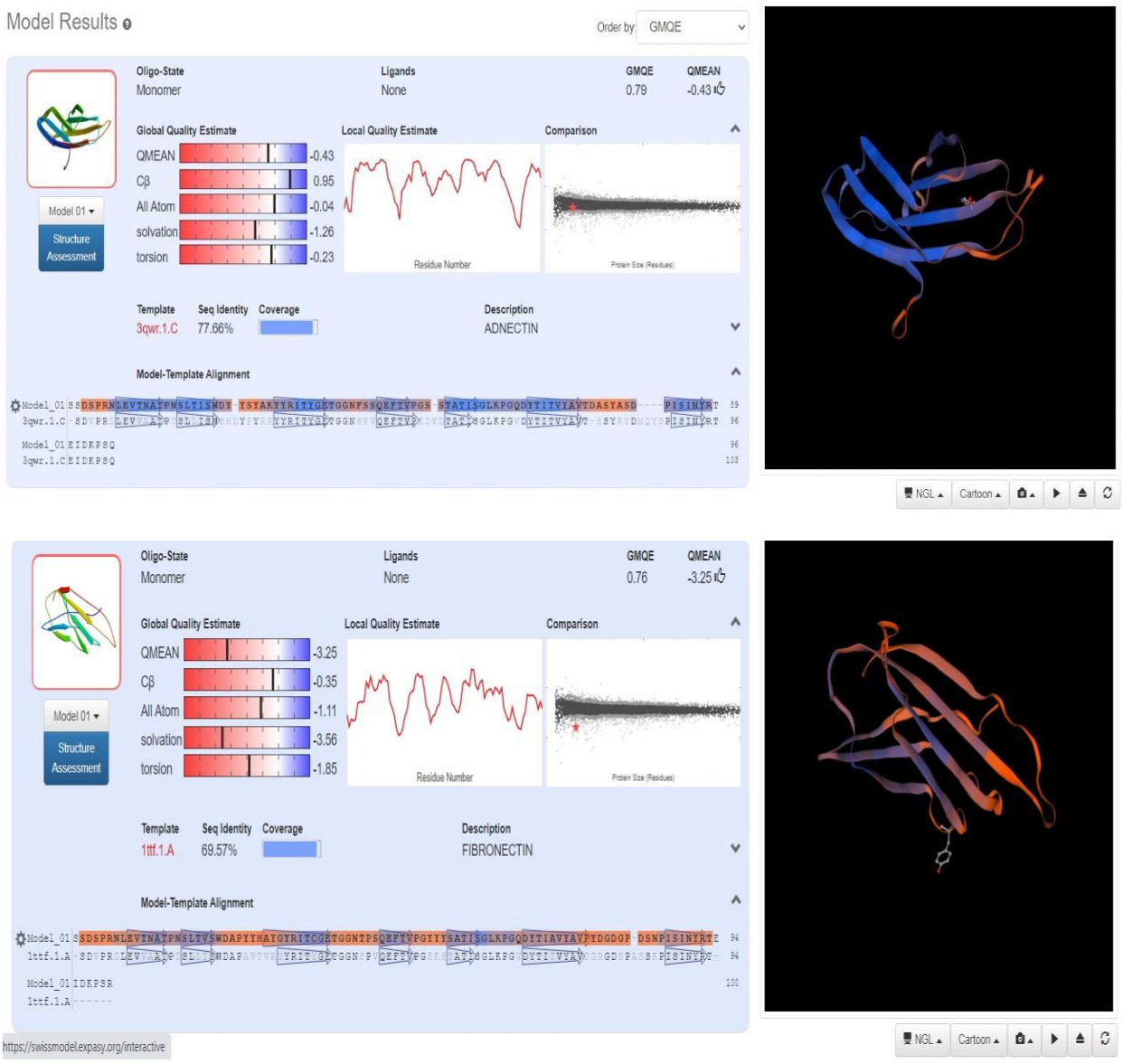

Figure A.3 3D monobody protein models targeting lysozyme made from templates 3qwr and 1ttf using SWISS-MODEL.

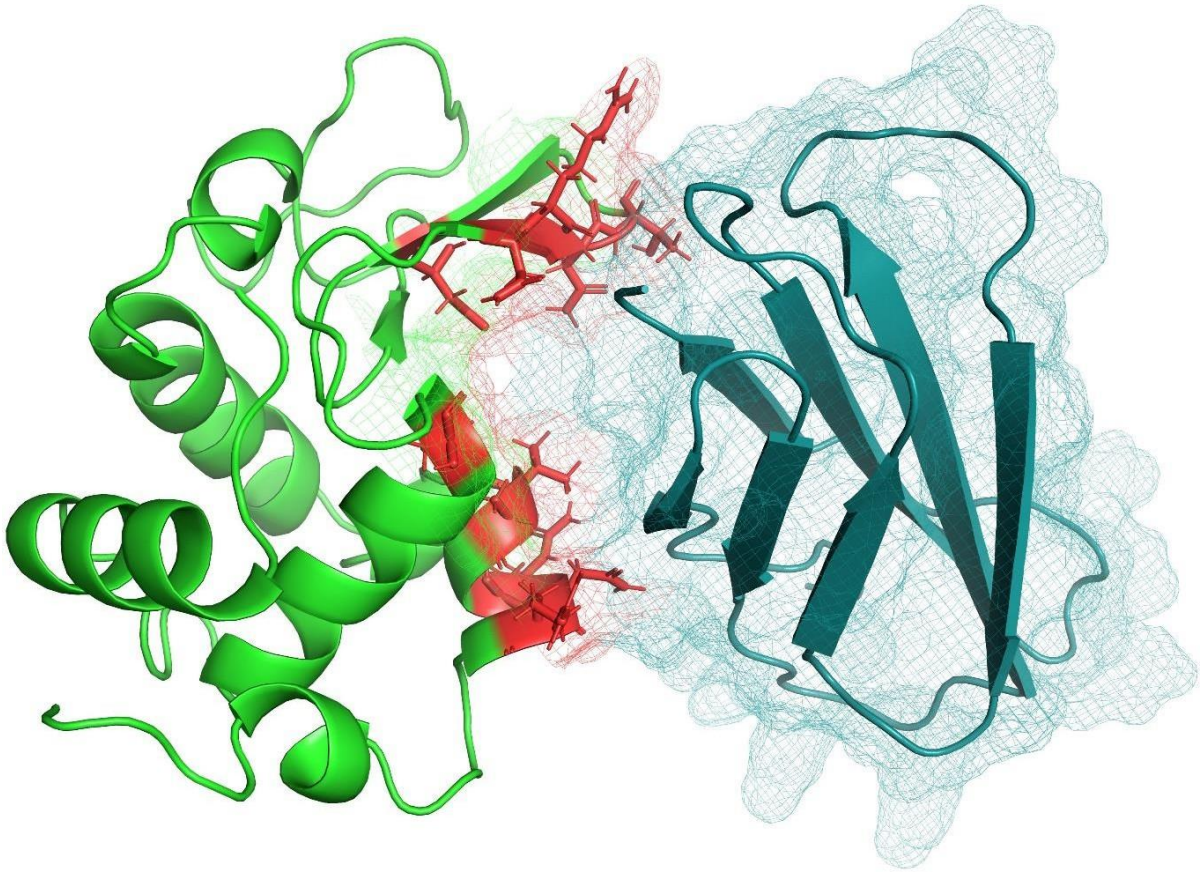

Figure A.4 Monobody Lysozyme decoy predicted by ROSETTA where the active sites on lysozyme (light green) that are within 5 A distance of the binder are shown in red.

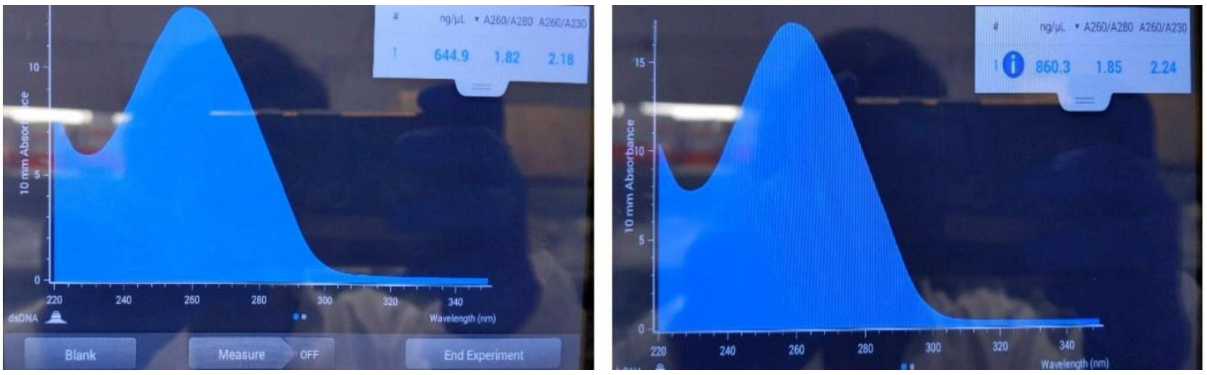

Figure A.5 Amplified DNA of Fn3_G (left) and Fn3_103 (right) showing high purity.

Primers used for amplification:

bcHPamp5: CTGGAGGTTACCAACGCAACTC (Tm 57.6)

fgHPamp3: CTGAGACGGTTTGTCGATTTCGGTGCGATAATT (Tm 64.1)

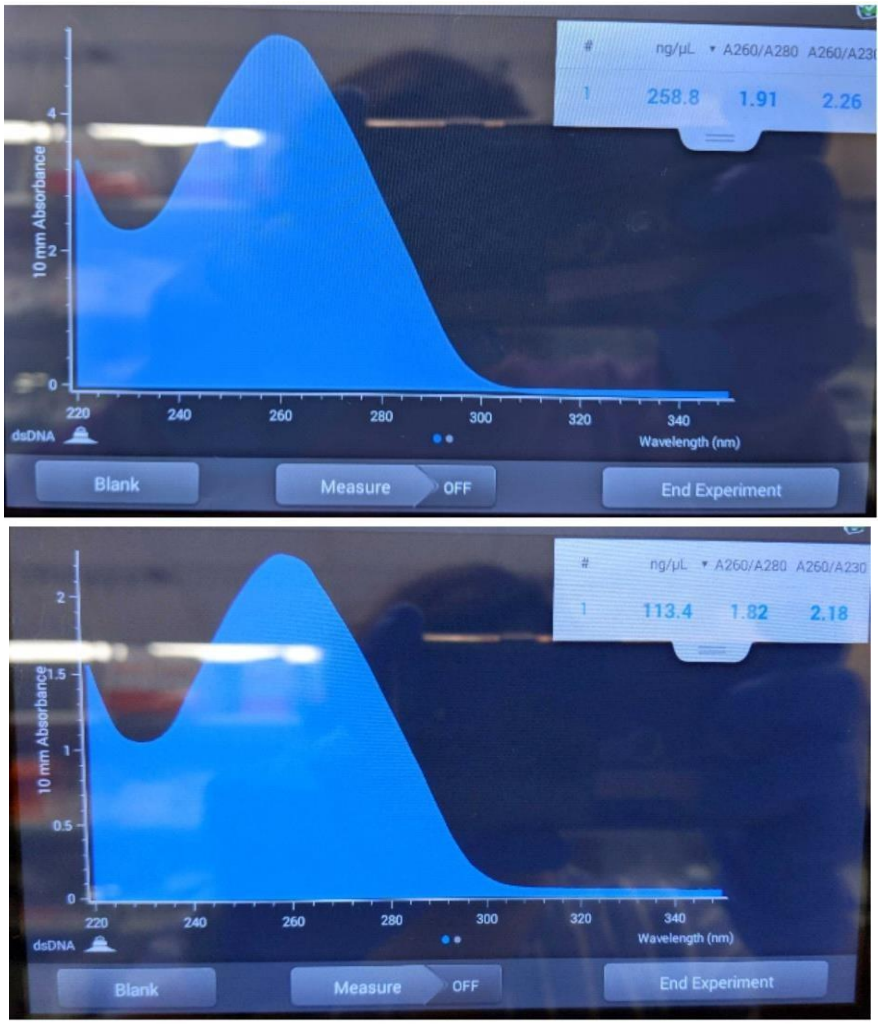

Figure A.6 Amplified DNA of pCT vector (top) and pET vector (bottom) showing high purity.

Primers (pCT):

fgHPamp3_fwd: AATTATCGCACCGAAATCGACAAACCGTCTCAG (Tm 64.1)

bcHPamp5_rev: GAGTTGCGTTGGTAACCTCCAG (Tm 57.6)

Primers used (pET)

XhoI half of forward primer: TCGAGCACCACCACCAC MscI half of reverse primer:

CCATCGCCGGCTGG Forward Primer Fn3+Pet22b:

CGAAATCGACAAACCGTCTCAG CTCGAGCACCACCACCAC

Reverse Primer Fn3 +pet22b: CGCGGAGAGTCGGAGGA GG CCATCGCCGGCTGGG

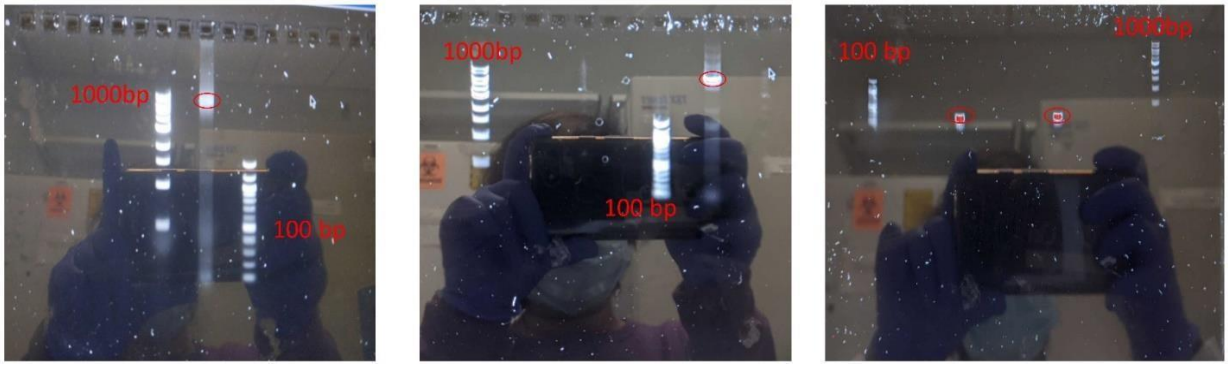

Figure A.7 Gel electrophoresis showing DNA band of pET 22b vector (left), pCTvector (middle), and monobody Fn3_G and Fn3_103 (right).

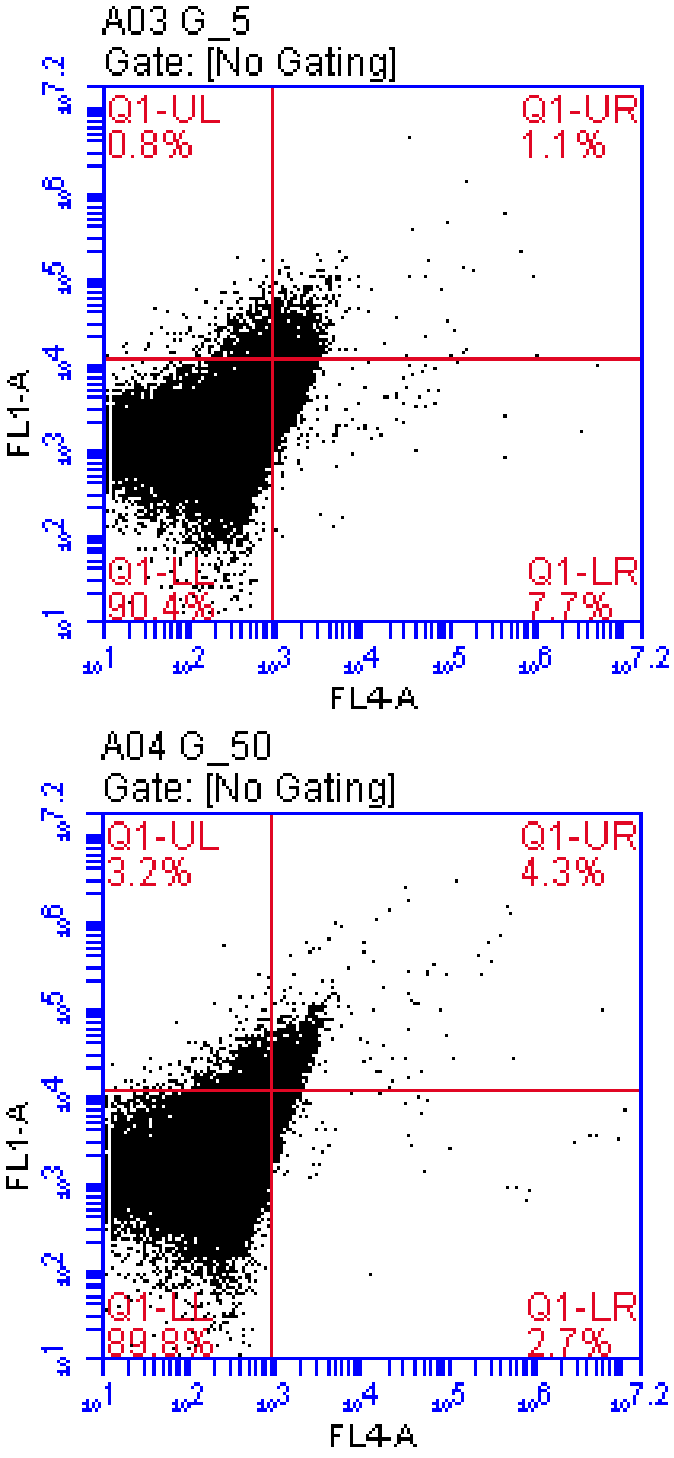

Figure A.8 Flow cytometry data showing binding populations of Fn3_G in the upper right quadrant (double positive) of the plots for 5nM(top) and 50nM (bottom) biotinylated lysozyme.

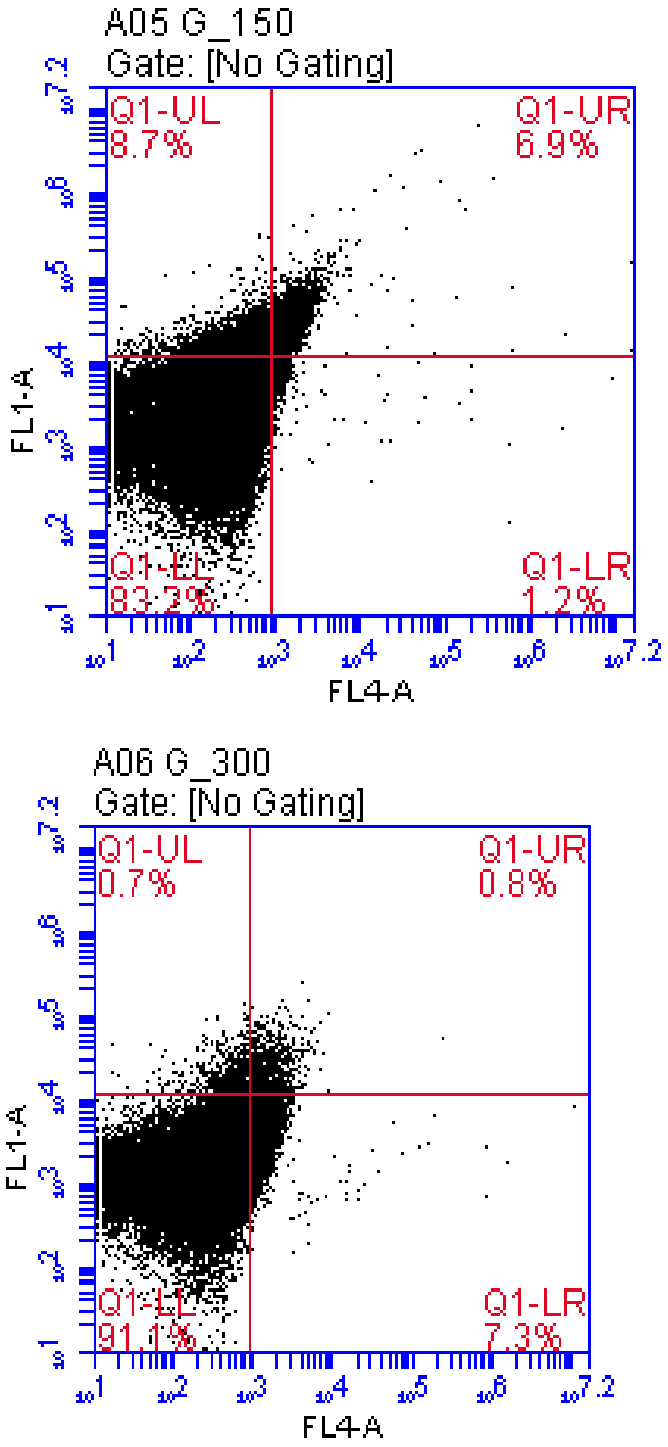

Figure A.9 Flow cytometry data showing binding populations of Fn3_G in the upper right quadrant (double positive) of the plots for 150nM(top) and 300nM (bottom) biotinylated lysozyme.

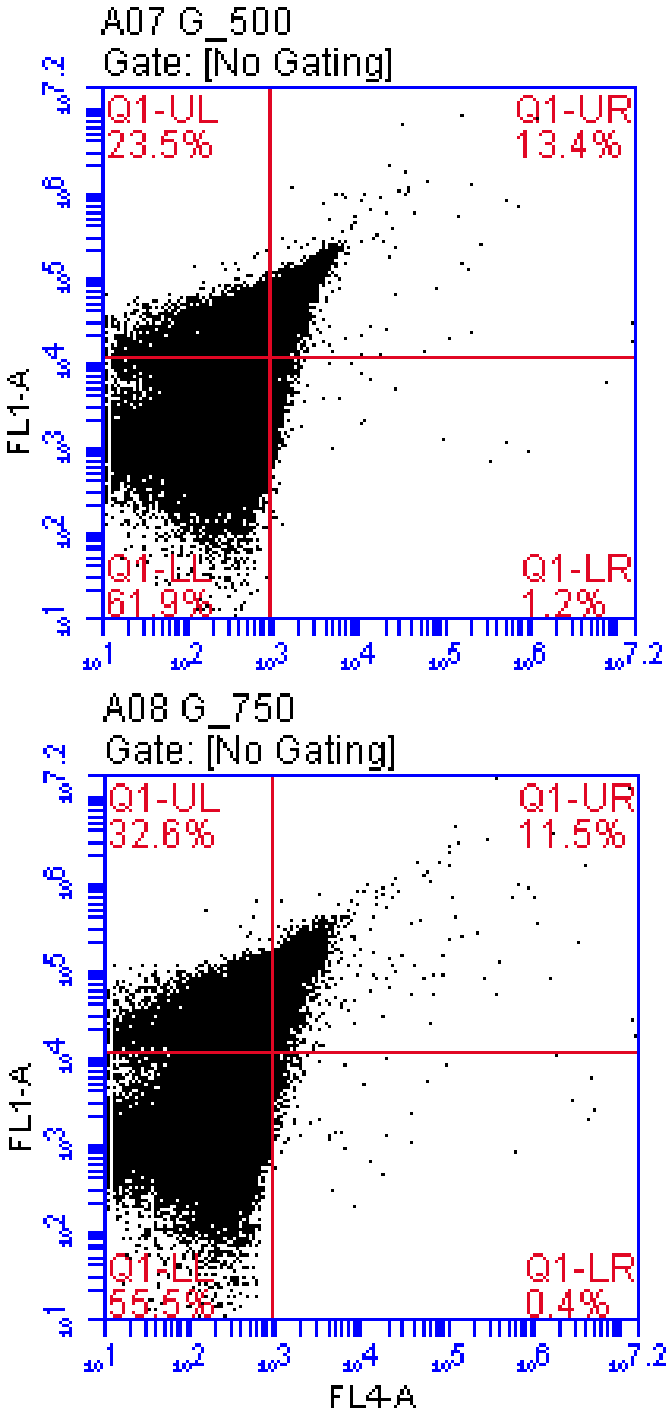

Figure A.10 Flow cytometry data showing binding populations of Fn3_G in the upper right quadrant (double positive) of the plots for 500nM(top) and 750nM (bottom) biotinylated lysozyme.

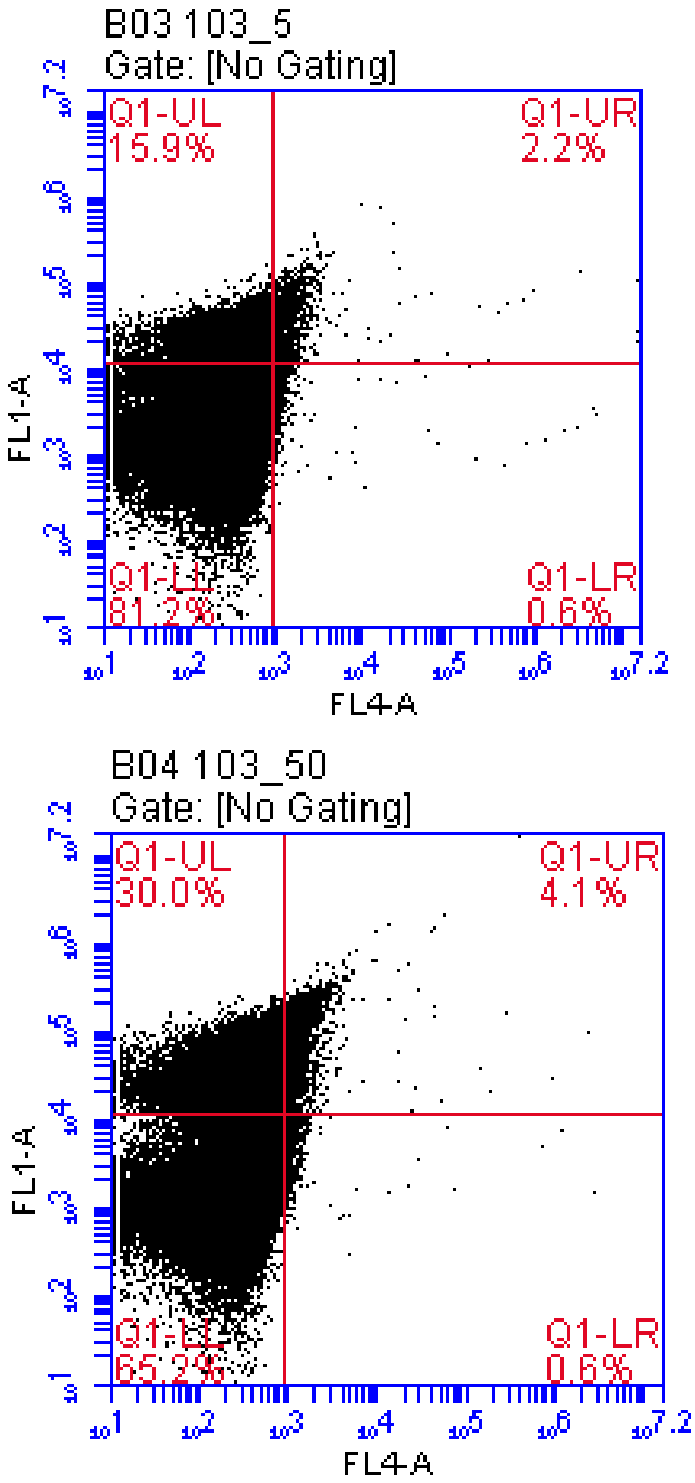

Figure A.11 Flow cytometry data showing binding populations of Fn3_103 in the upper right quadrant (double positive) of the plots for 5nM(top) and 50nM (bottom) biotinylated lysozyme.

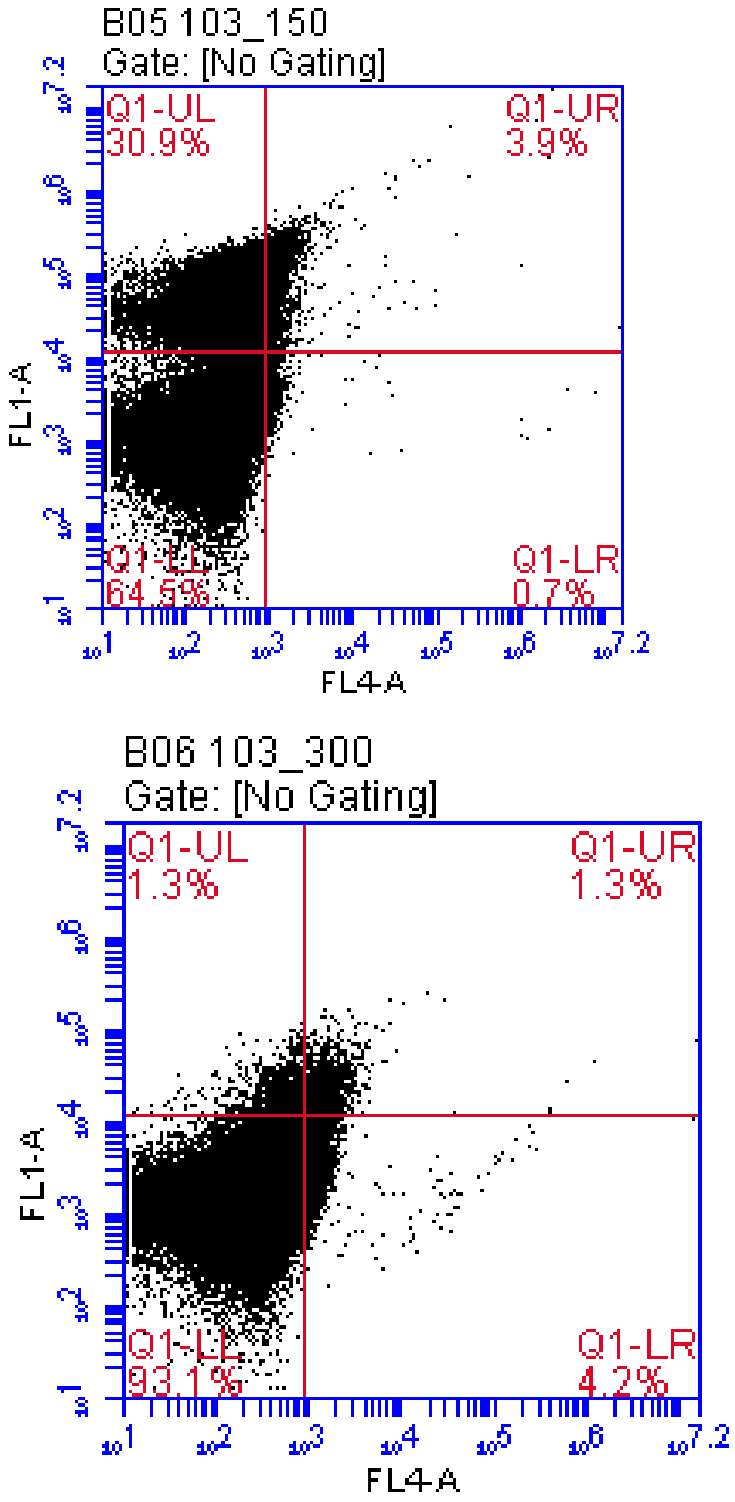

Figure A.12 Flow cytometry data showing binding populations of Fn3_103 in the upper right quadrant (double positive) of the plots for 150nM(top) and 300nM (bottom) biotinylated lysozyme.

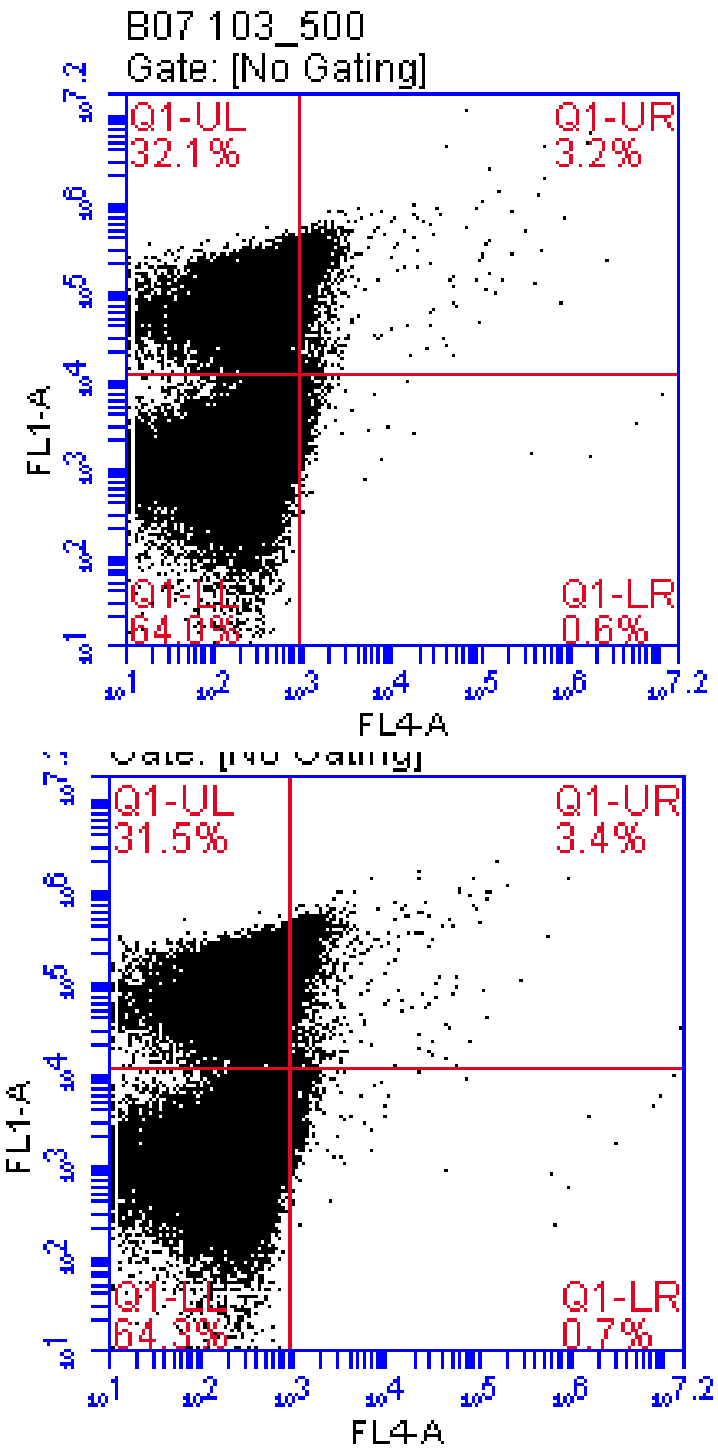

Figure A.13 Flow cytometry data showing binding populations of Fn3_103 in the upper right quadrant (double positive) of the plots for 500nM(top) and 750nM (bottom) biotinylated lysozyme.

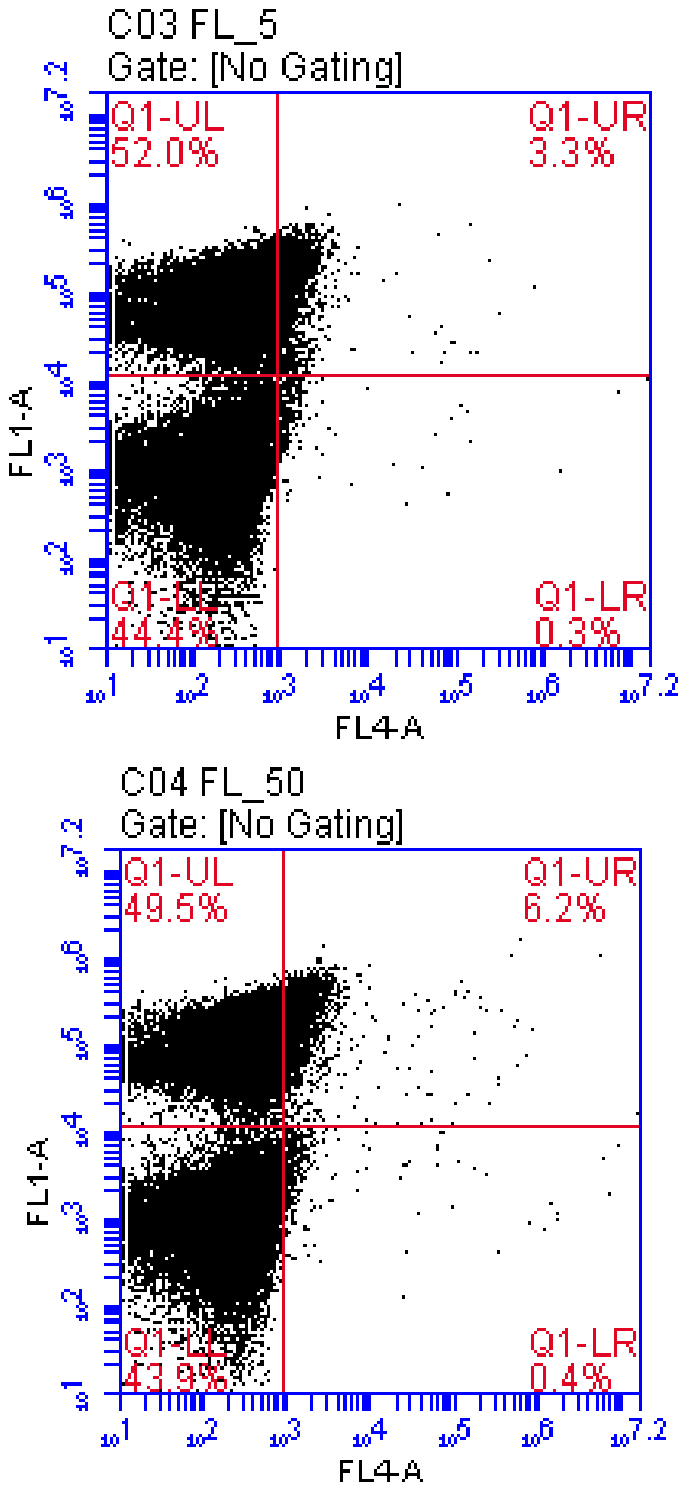

Figure A.14 Flow cytometry data showing binding populations of FL063 in the upper right quadrant (double positive) of the plots for 5nM(top) and 50nM (bottom) biotinylated lysozyme.

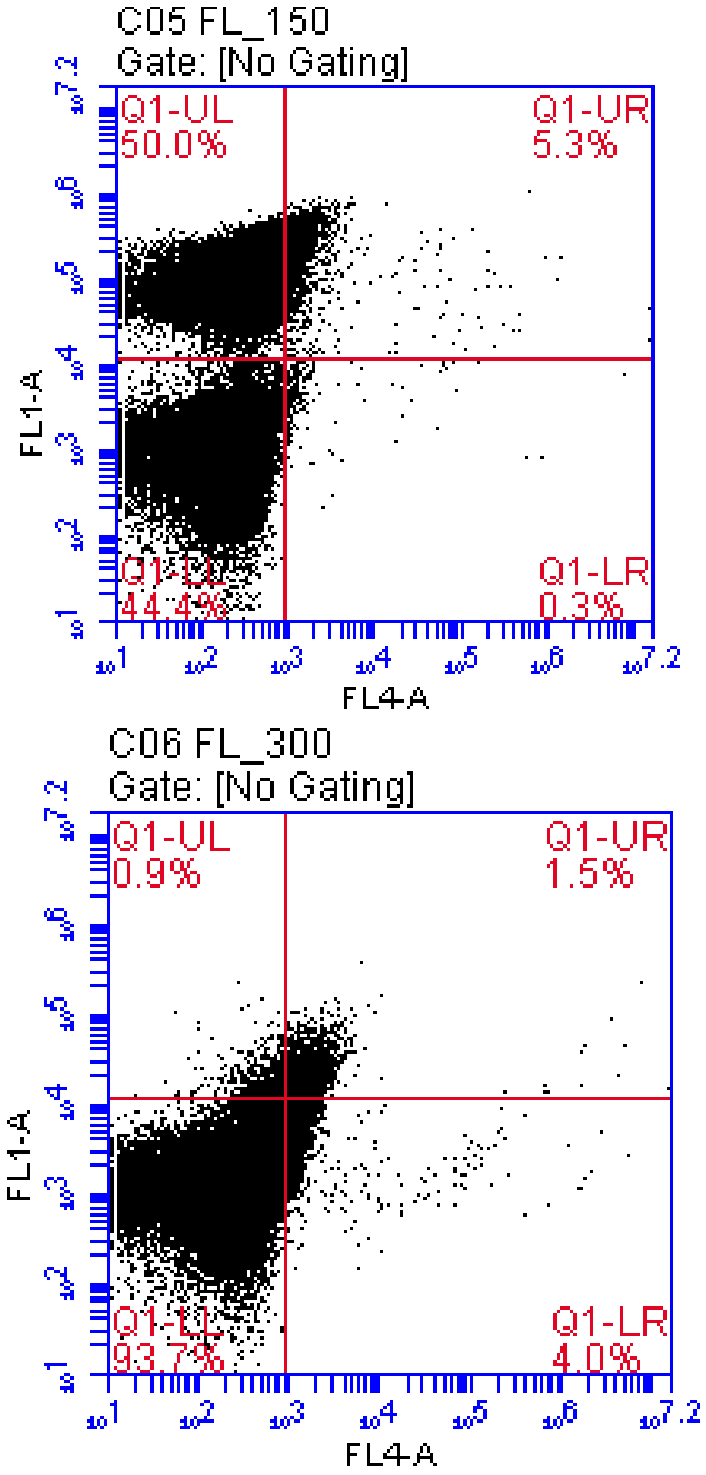

Figure A.15 Flow cytometry data showing binding populations of FL063 in the upper right quadrant (double positive) of the plots for 150nM(top) and 300nM (bottom) biotinylated lysozyme.

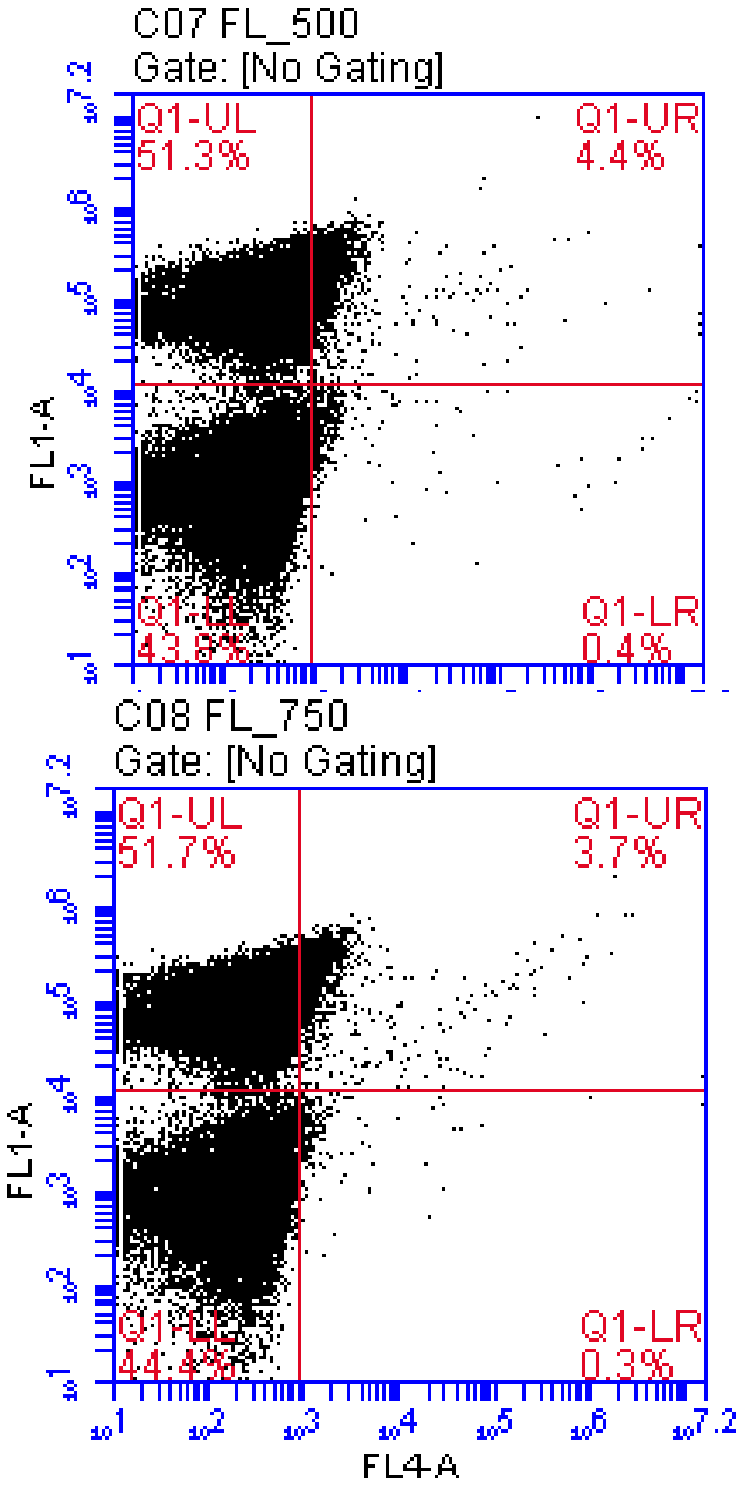

Figure A.16 Flow cytometry data showing binding populations of FL063 in the upper right quadrant (double positive) of the plots for 500nM(top) and 750nM (bottom) biotinylated lysozyme.

Table A.1 Binding Kinetics of Fn3_G using the mean fluorescence data obtained from flow cytometry.

Conc (nM)	G_FL1	Y_fit = A*(Fmin + (Fmax - Fmin)*(S/(S+KD)))	Residual	Residual^2
5	5210	484.9715775	-4725.028423	22325893.6
50	7217	4336.216353	-2880.783647	8298914.42
150	8115	10530.81112	2415.811124	5836143.39
500	17399	21061.62224	3662.622238	13414801.7
750	28145	24571.89261	-3573.10739	12767096.4
Constants				
Fmin	**Fmax**	**KD**	**SSR**	
1.32167E-05	36857.83892	375.0000002	62642849.48	

Table A.2 Binding Kinetics of Fn3_103 using the mean fluorescence data obtained from flow cytometry.

Conc (nM)	**G_FL 1**	**Y_fit = A*(Fmin + (Fmax - Fmin)*(S/(S+KD)))**	**Residual**	**Residual^ 2**
5	10968	12578.14653	1610.1465	2592571.86
50	29303.5	25687.44394	3616.05605	13075861.4
150	40071	42345.8397	2274.83970	5174895.67
500	61500	62551.0755	1051.0755	1104759.7
750	69078	67758.02249	1319.97751	1742340.63
Constants				
Fmin	Fmax	KD	SSR	
10735.5018	82,101	188.6498455	23690429.2	

Table A.3 Binding Kinetics of FL063 using the mean fluorescence data obtained from flow cytometry.

Conc (nM)	G_FL1	Y_fit = A*(Fmin + (Fmax Fmin)*(S/(S+KD)))	Residual	Residual^2
5	61148	62002.02548	854.0255	729359.5183
50	83812	79404.37731	-4407.62	19427137.75
150	84668.5	81090.29822	-3578.2	12803527.98
500	83481.5	81697.4106	-1784.09	3182974.989
750	72823	81784.88384	8961.884	80315361.88
Constants				
Fmin	**Fmax**	**KD**	**SSR**	
-6.97588E-05	81960.39346	1.609493222	1.16E+08	

Protein purification protocol (Adapted from Dr. Daniel R. Woldring's wet lab biochemistry protocols)

Timeline

- Bacterial transformation (1 day)
- Protein production in bacteria (2 days)
- Extraction, purification, and concentration of the protein (1 day)
- Check protein purification via SDS (1 day)

E. coli Transformation (In-house T7 Express)

*Typically for protein production

Prepare a water bath at 37˚C Prepare wet ice.

Once aliquots are prepared:

1. Thaw T7 Express cells in a vial on wet ice.
2. Pipette 0.5-5 μL of plasmid directly into cells.
3. Tap gently to mix.
4. Incubate on wet ice for 30 minutes.
5. Store extra plasmid at -20˚C.
6. Heat shock by placing in 37˚C water bath for exactly 90 seconds.
7. Remove from water bath and place on wet ice for 5 minutes.
8. Add 950 μL of room temperature SOB to the vial.
9. Shake the vial on an angle at 37˚C at 250 rpm for 1-2 h.
10. Spread 200 μL on an LB (+ appropriate antibiotic) agar plate.
11. Incubate the inverted plate overnight at 37˚C.
12. Store the remaining transformation at 4˚C.

Protein Production in Bacteria Grow Starter Culture

1. Add ~5 mL of LB+kan to a test tube.
2. Transfer a single colony of transformed E. coli (BL21(DE3) or T7 Express) + pET to the test tube.
3. Incubate culture at 37º, 250 rpm for 10-36h.

Grow and Induce Large Culture

Add 1L of LB (no antibiotics) to a 2L flask.

1. Add 1-5 mL of saturated culture to the flask.
2. Incubate at 37º, 250 rpm for until A600 ~1.0.

A600 of 0.5 – 1.0 is ok. Protein yields have been shown to drop as induction A600 approaches 2.

If 5 mL were added, this should take 3-4 h

3. If you are unsure of the production pattern for the given protein save 50 mL of culture. Spin down, remove LB, and resuspend in dH20 for SDS-PAGE comparison.

4. Add 1 mL of 0.5M IPTG to yield 0.5 mM IPTG.

5. Set the shaker to below 20º and leave it open for 5-10 minutes to allow for cooling. Place magnetic on sensor to continue shaking with the door ajar.

The goal here is to get as close to room temperature as possible. Typically, the shaker will hover around 25º.

6. Induce at room temp, 250 rpm for 1 hr. Optimal incubation time may be protein dependent.

7. If you are unsure of the production pattern of the given protein save 50 mL of culture.

{Spin down, remove LB, and resuspend in dH2O for SDS-PAGE comparison. }

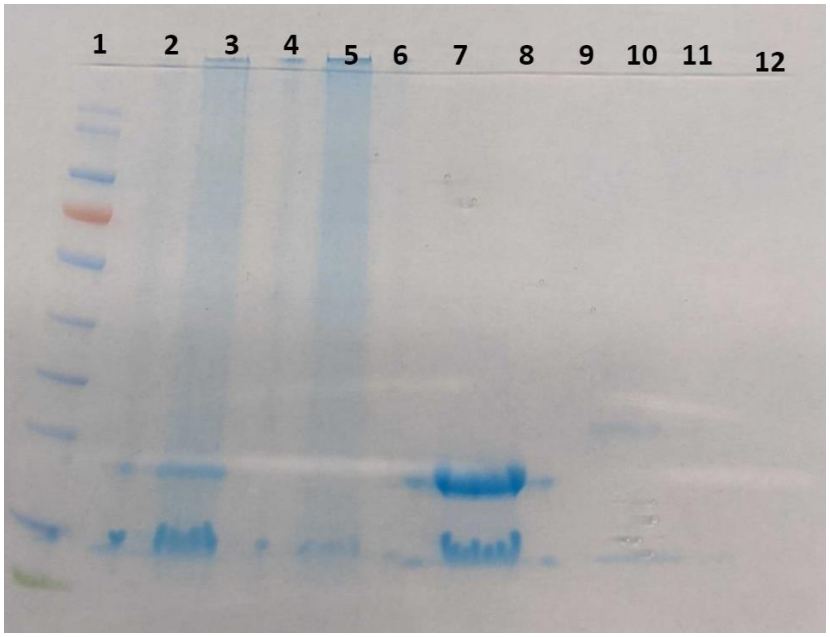

Figure A.17 SDS PAGE to optimize induction conditions for protein production in bacteria.

1: Ladder

2: FR041 w Cys before induction with IPTG 3: FL063 w Cys before induction with IPTG 4: FR041 induction for 45 minutes

5: FL063 induction for 45 minutes

6: FR041 induction for 90 minutes

7: FL063 induction for 90 minutes

8: FR041 induction for 360 minutes

9: FL063 induction for 360 minutes

10: FR041 induction for 150 minutes

11: FL063 induction for 150 minutes

12: 10 ug of Lysozyme <u>Prepare Lysate</u>

1. Pellet cells (e.g. 3200g for 15 min.). Remove supernatant. Perform sequential centrifugations to reduce the number of pellets. Cell pellet may be stored at -20º if pause is needed.

2. Resuspend the cell pellet in ~10 mL of lysis buffer w/ protease inhibitors.

Minimize bubble formation by not fully emptying the pipette or bottle.

3. Transfer cells and buffer to 15 mL conical.

4. Freeze/thaw four cycles.

5. Centrifuge at 12,000g for 10 min. at 10º.

6. Filter supernatant with 0.45 um filter. If filtering is not sufficient, filter a second time with a 0.2 um filter.

7. Store filtered product at 4º or continue to protein purification. IPTG (0.5 M)

Add IPTG to an empty conical

Add 8.4 mL of ddH2O per gram of IPTG Dissolve

Filter sterilize Lysis Buffer (1L)

9.38 g	Sodium Phosphate, Dibasic, Heptahydrate
2.07 g	Sodium Phosphate, Monobasic, Monohydrate
29.2 g	NaCl
50 mL	glycerol
3.1 g	CHAPS
1.7 g	imidazole
fill to 1L	water

Add protease inhibitors: Complete EDTA-free protease inhibitor pellet, 1 pellet/50 ml lysis buffer

Cell lysis using sonication:

- The samples were sonicated for 6 cycles (10 seconds on, 30 seconds off) with a pulse on for 0.8 seconds and a pulse off for 0.2 seconds.
- The samples were kept on ice to prevent overheating.

- They were then centrifuged at 4500 rpm for 1 hour and the supernatant was collected after filtering it through a 0.2 µM syringe filter.
- (Care should be taken that the filter does not touch the lid of the collecting tube/conical to avoid spilling!)

Figure A.18 Sonication probe for cell lysis in bacterial protein production.

Cell lysis using French Press Protocol for French Press Cell Lysis:

1. Preparation:

- Remove the closure plug from the cell body.

- Lubricate piston O-rings with water, silicone, glycerol, or other acceptable materials.

2. Piston Insertion:

- Insert the piston into the top of the cell body, aligned with the 'upright' label.

- Press the piston into the cell body until the max fill line aligns with the top of the piston.

3. Assembly:

- Flip the unit over and place it on the stand between three posts.

- Fill the cell suspension to about one inch from the top.

4. Sample Handling:

- For volumes less than 35 milliliters, proceed as normal; for greater volumes, perform multiple passes.

- Keep samples on ice and store the press in the fridge when not in use.

5. Closure Plug Adjustment:

- Slightly open the flow valve assembly on the closure plug.

- Ensure the sample outlet tube is directed away from the operator.

- Attach the closure plug to the cell body, allowing some liquid to drip out to avoid air pockets.

- Close the flow valve assembly snugly without over-tightening.

6. Final Assembly:

- Invert all parts as a set, ensuring the closure plug remains secure.

- Handle the assembled unit carefully as it weighs around 20 pounds (9 kilograms).

7. Set the pressure of the chamber to 1100 PSI to pop the E. coli cell walls and carefully collect the cell lysate. Centrifuge the cell lysate at 4500 rpm for 1 hour and collect the supernatant after filtering it through a 0.2 µM syringe filter

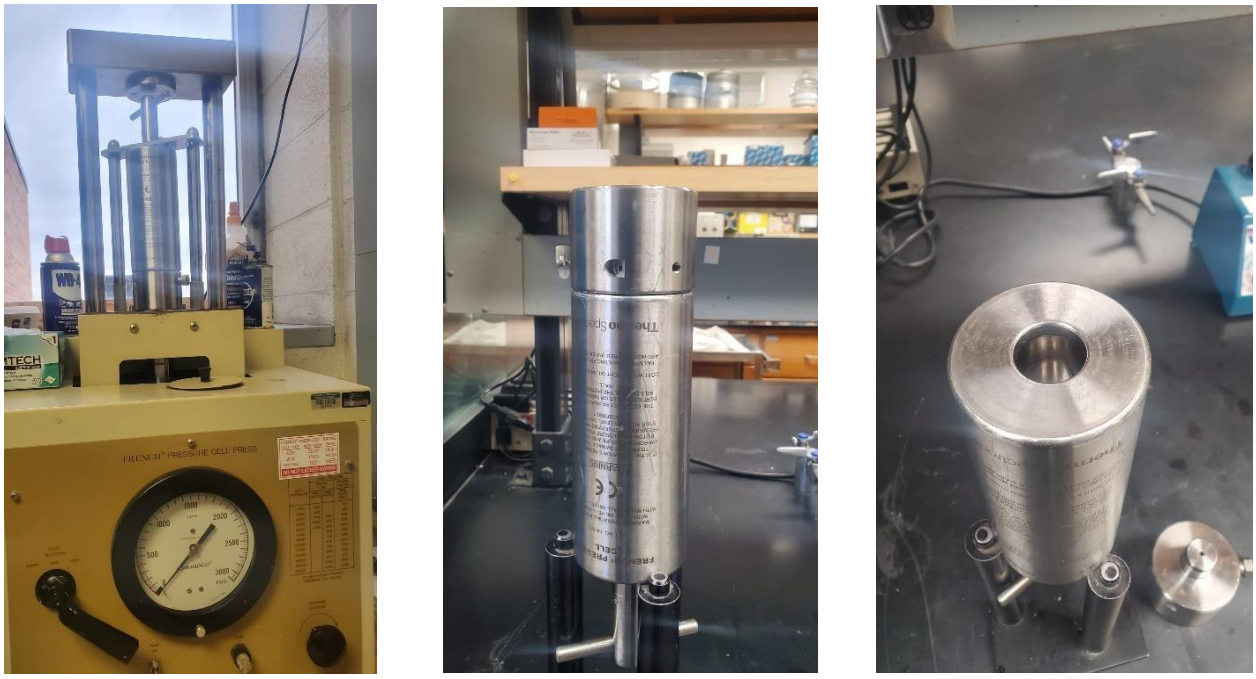

Figure A.19 French Press method for cell lysis in bacterial protein production.

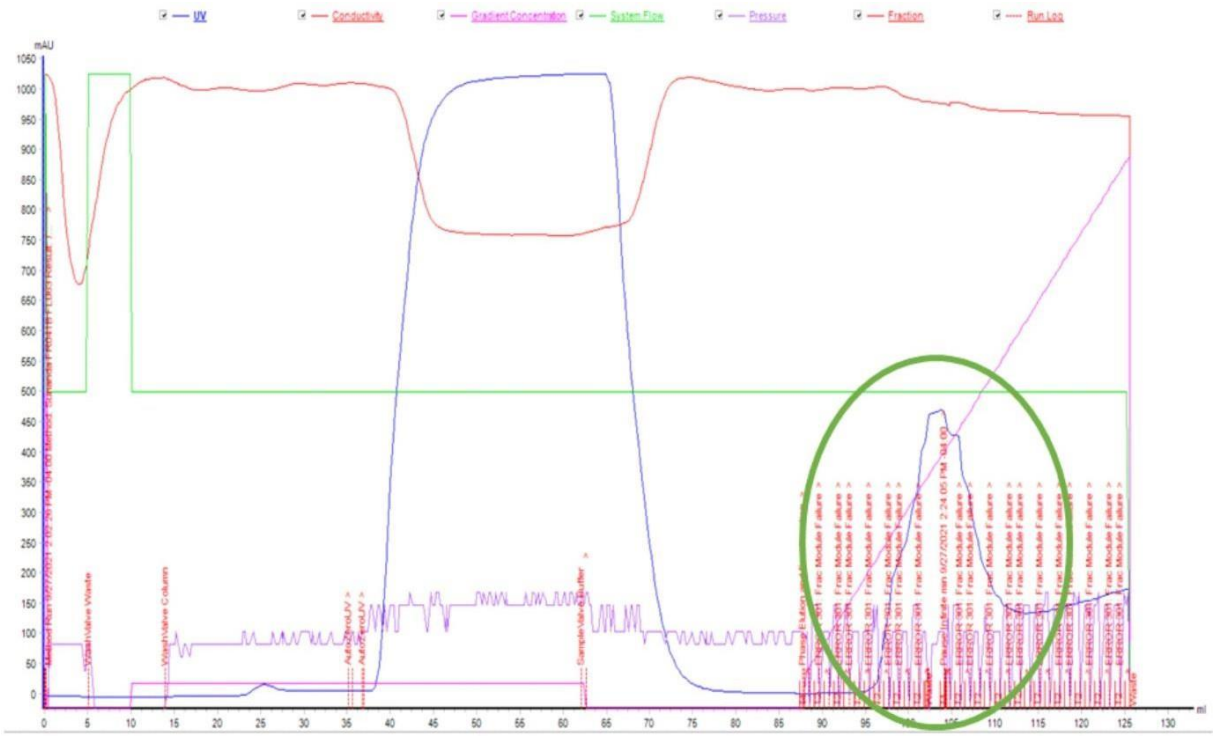

Figure A.20 FPLC data showing purified FL063 protein indicated by the green circle.

APPENDIX B: (CHAPTER 3)

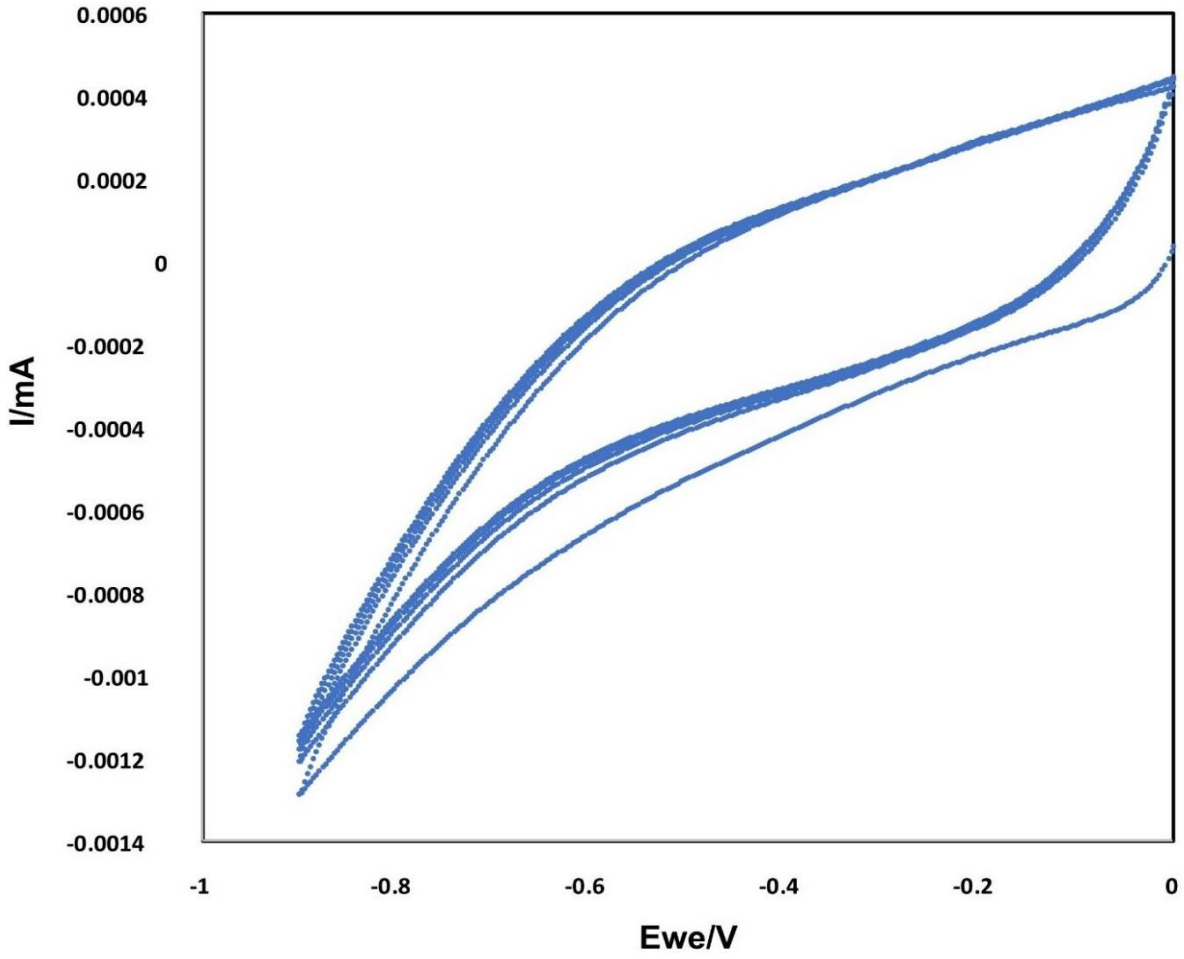

Figure B.1 Cyclic voltammogram showing electrochemical grafting NHS modified diazonium ester on the surface of GCE, using a Pt-wire counter electrode and Ag/AgNO3 reference electrode in DCM.

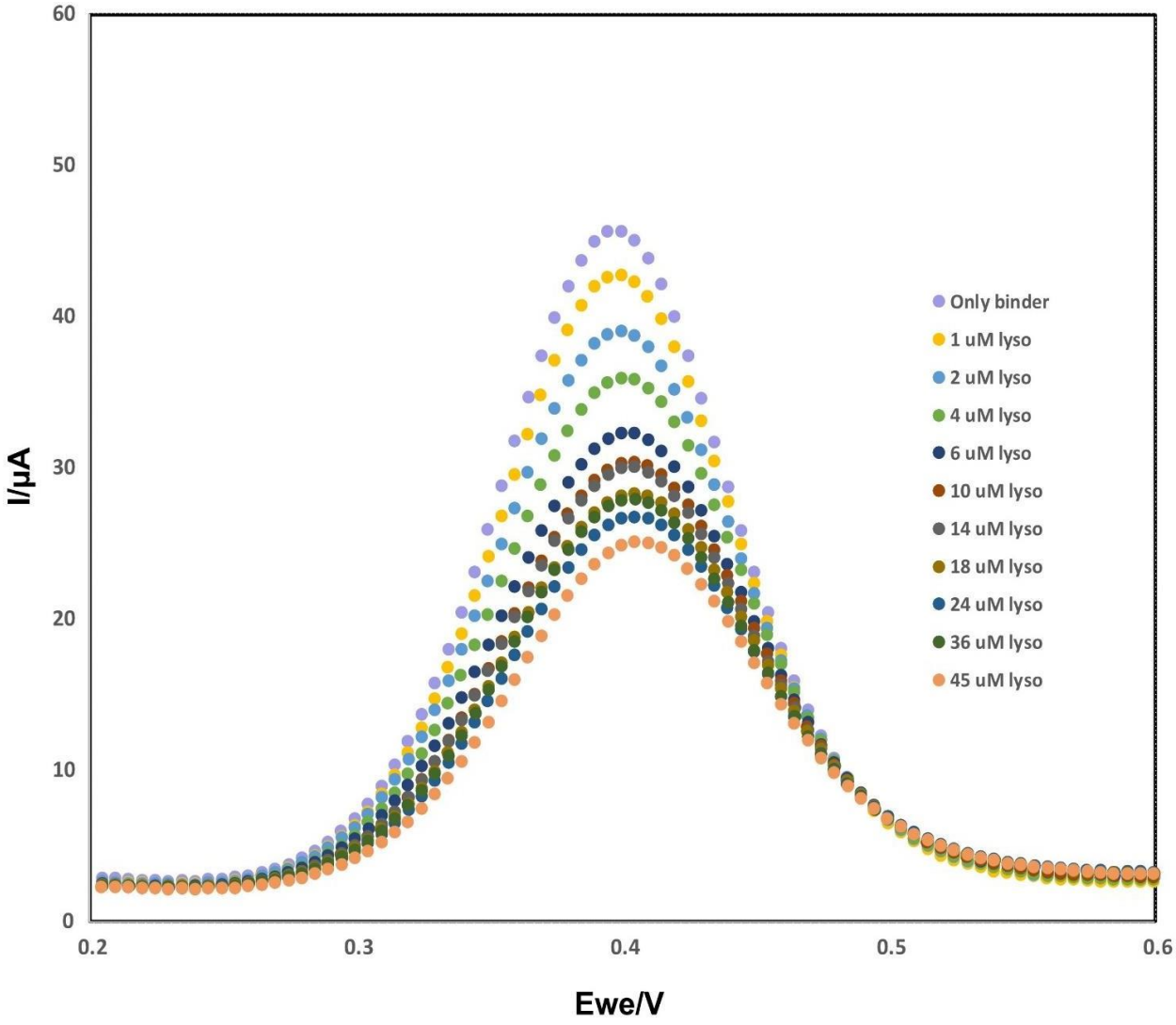

Figure B.2 Squarewave voltammogram showing concentration dependence of target lysozyme with signaling peak current. The measurements were taken using a 3 mm glassy carbon working electrode, Pt-wire counter electrode, SCE reference electrode, and 100 mM phosphate buffer at pH 7 and 25 °C.

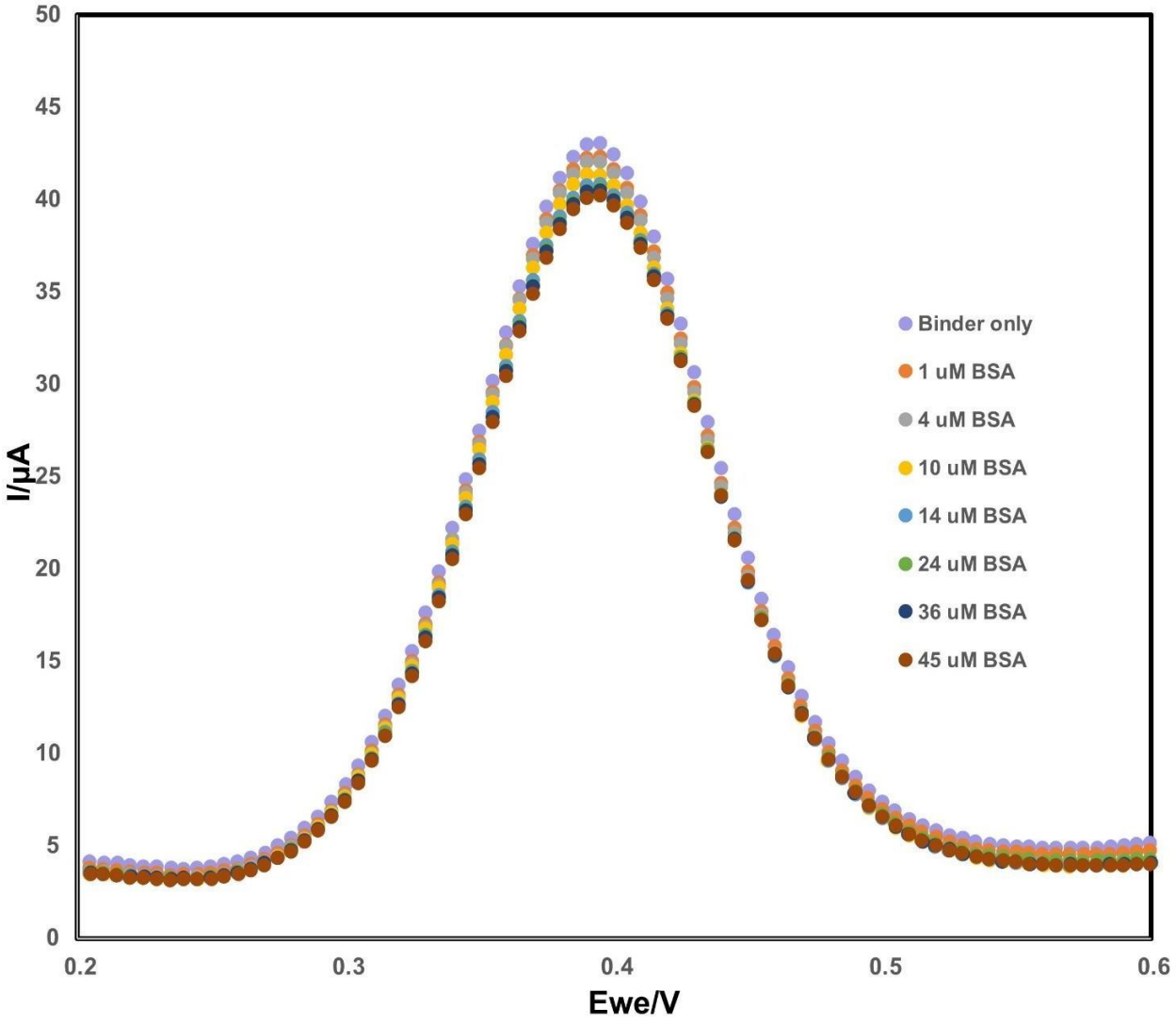

Figure B.3 Squarewave voltammogram of concentration dependence control using BSA. Unlike lysozyme interaction, no significant change in the peak current was seen with increasing concentration of BSA. All the measurements were taken using a 3 mm glassy carbon working electrode, Pt-wire counter electrode, SCE reference electrode, and 100 mM phosphate buffer at pH 7 and 25 °C.

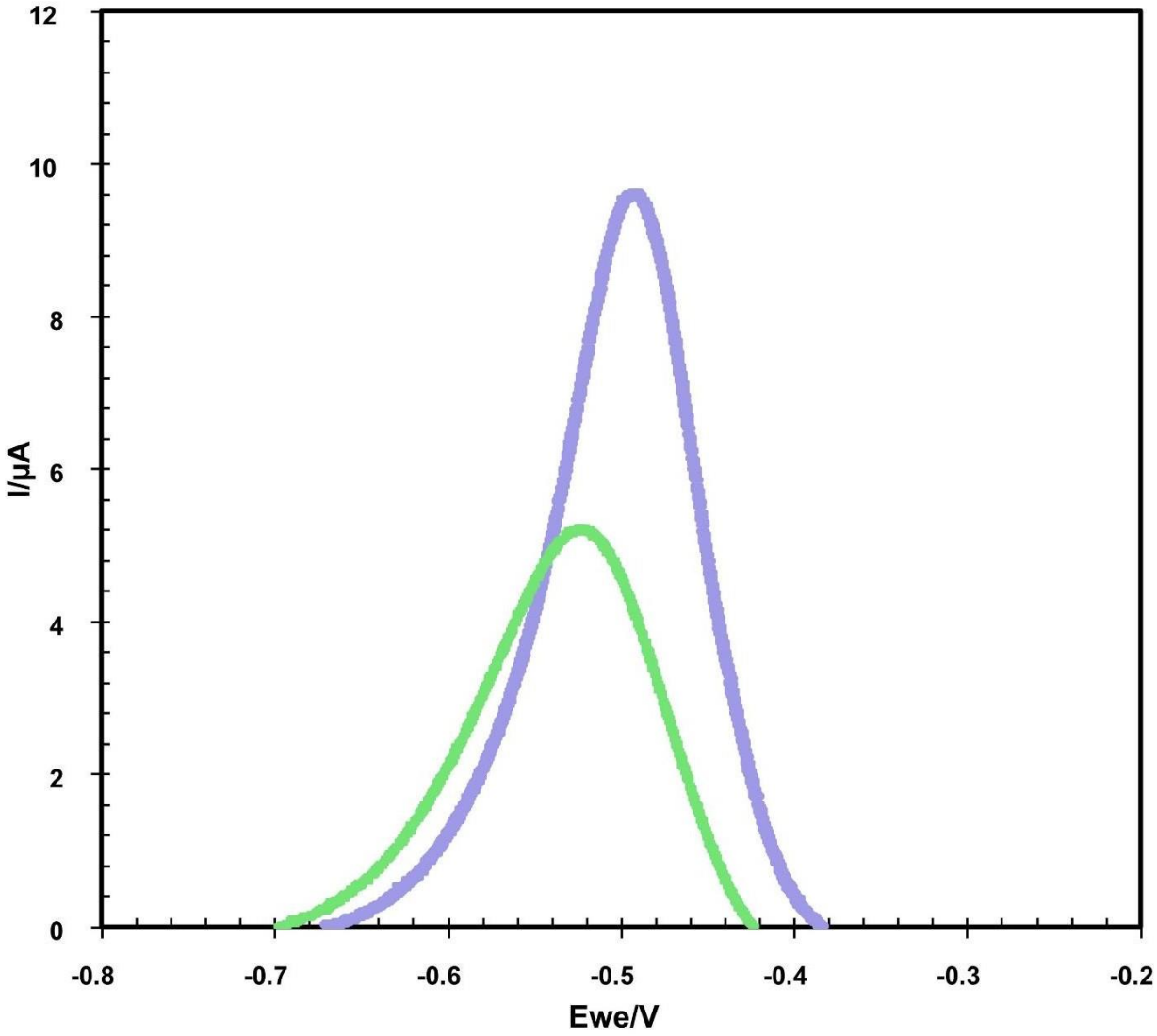

Figure B.4 Square wave voltammetry measurements of GCEs modified with FL063 (purple), FL063-Lysozyme (green), in 1mM AQS at a frequency of 10ms. Experiments were performed using a 3 mm glassy carbon working electrode, Pt-wire counter electrode, SCE reference electrode, and 100 mM phosphate buffer at pH 7 and 25 °C.

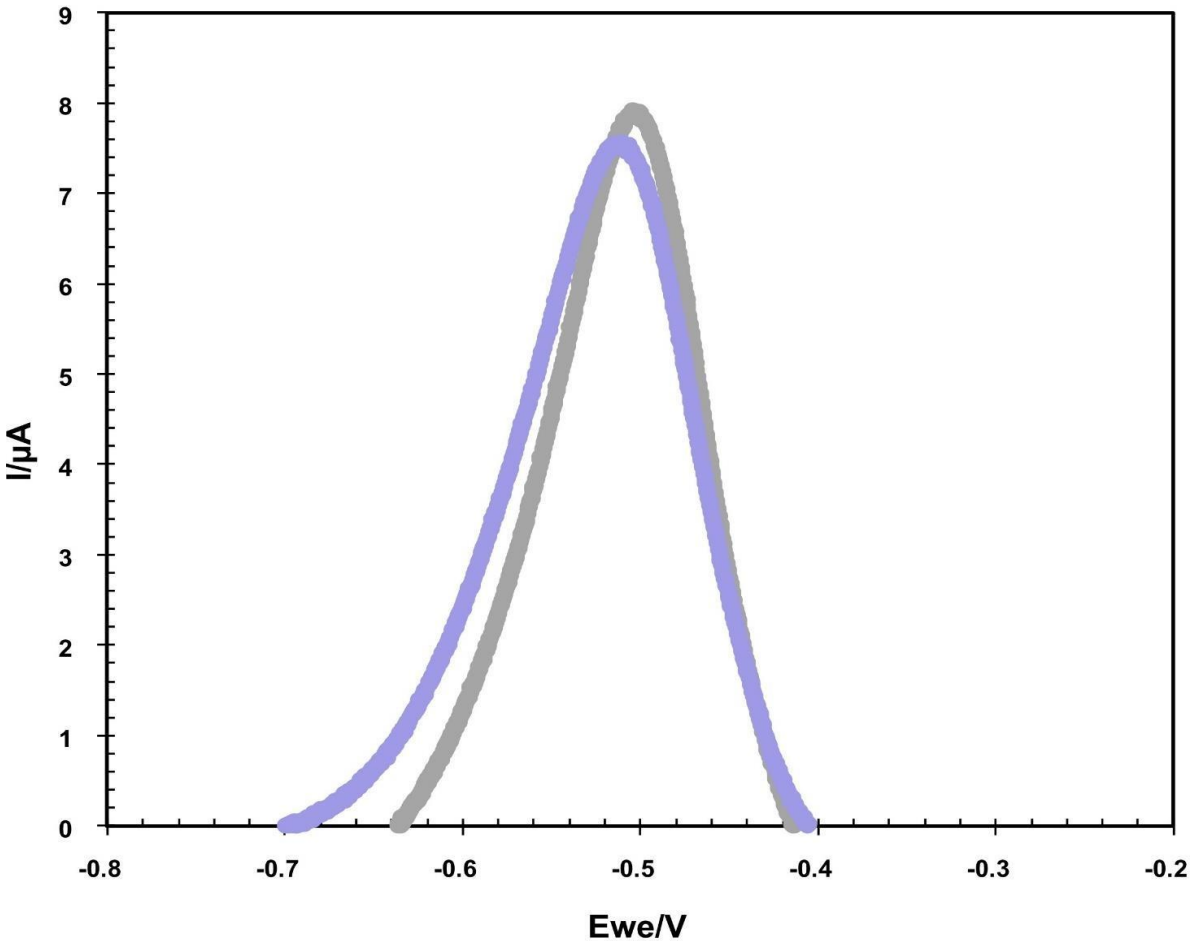

Figure B.5 Square wave voltammetry measurements of GCEs modified with FL063 (purple), BSA control (grey), in 1mM AQS at a frequency of 10ms. Experiments were performed using a 3 mm glassy carbon working electrode, Pt-wire counter electrode, SCE reference electrode, and 100 mM phosphate buffer at pH 7 and 25 °C.

APPENDIX C: (CHAPTER 4)

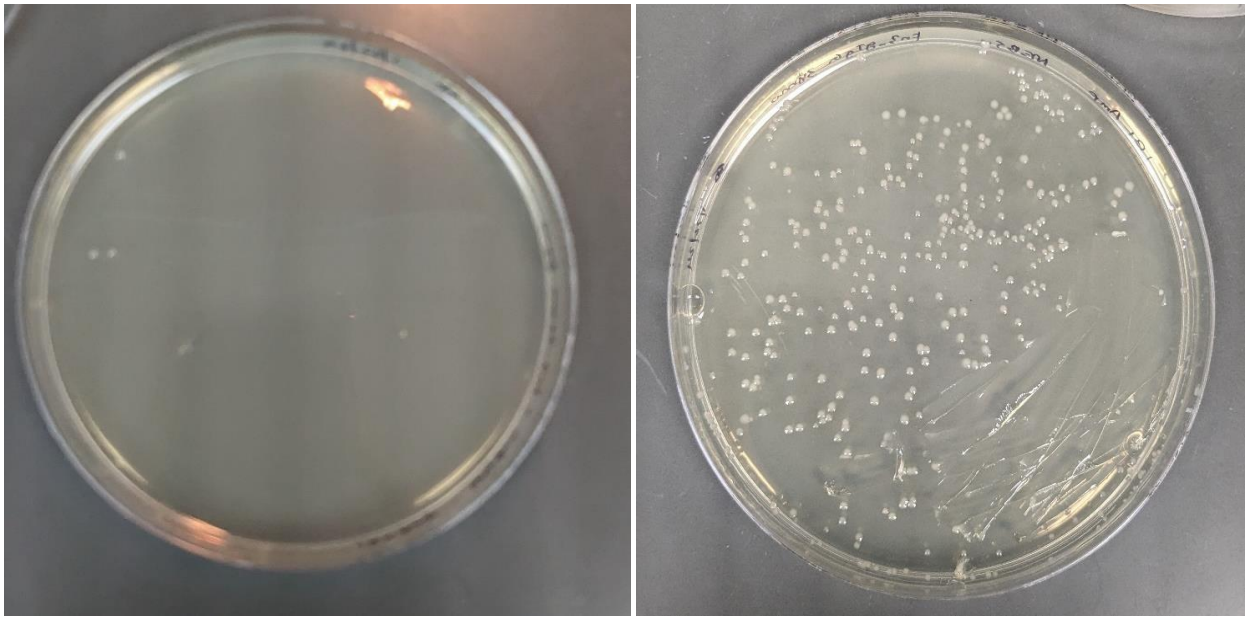

Figure C.1 *E. Coli* transformation of pCT plasmids containing human transferrin monobody plasmid (left) and goat IgG plasmid (right) prepared from zymoprep.

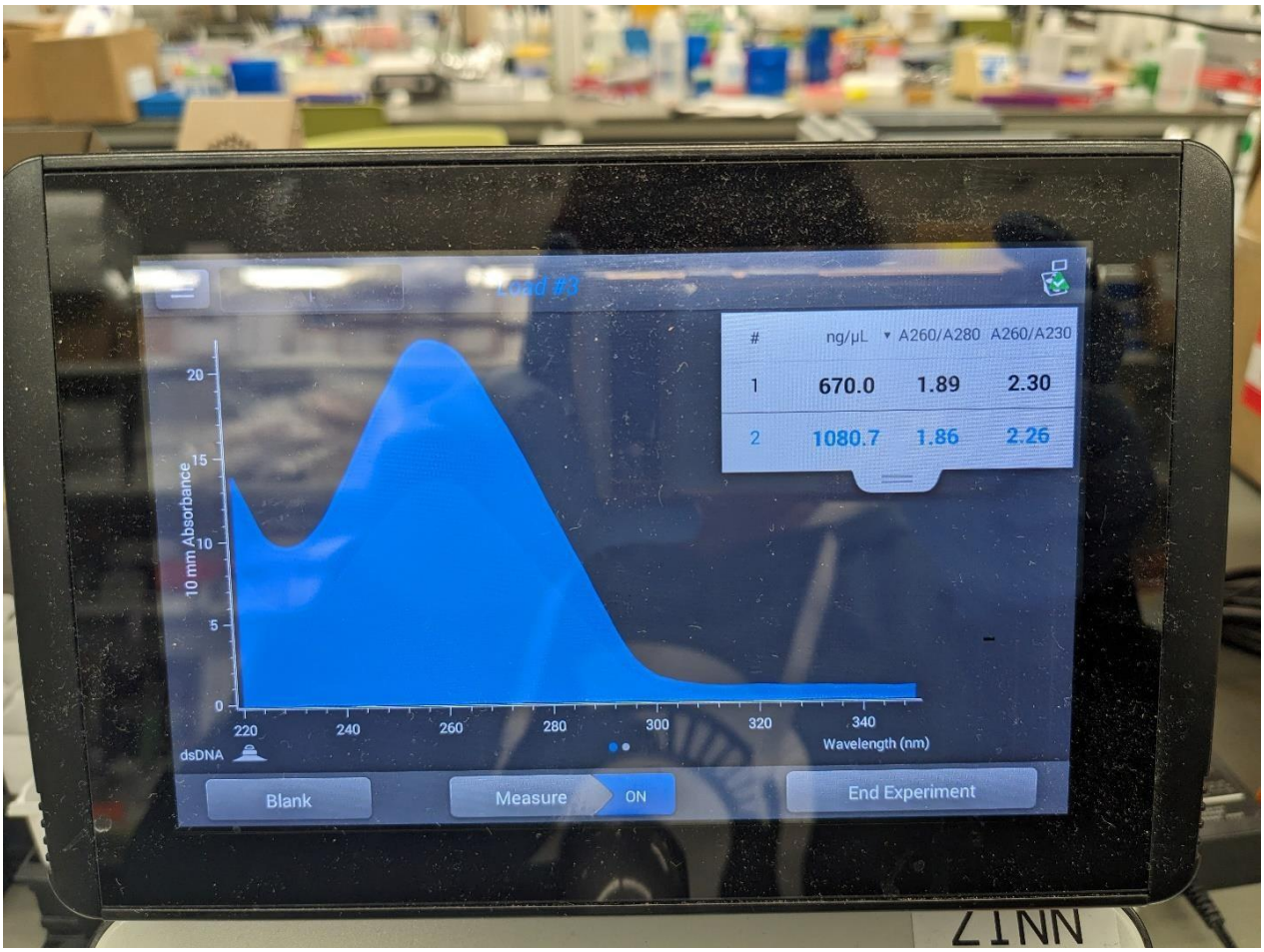

Figure C.2 Amplified DNA of pCT vector with goat IgG (1) and human transferrin (2) showing high purity.

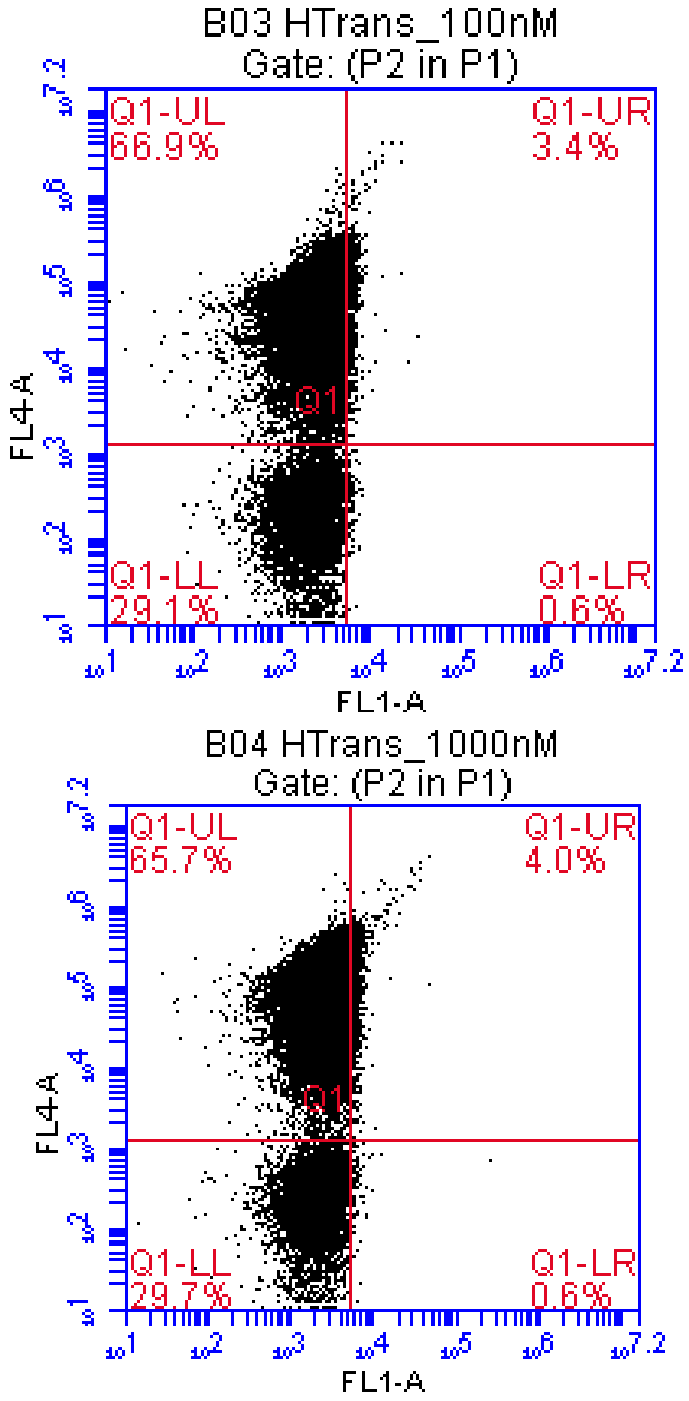

Figure C.3 No binding populations of monobody are observed in the upper right quadrant (double positive) of the plots for 1000nM (top) and 1000nM (bottom) biotinylated human transferrin target.

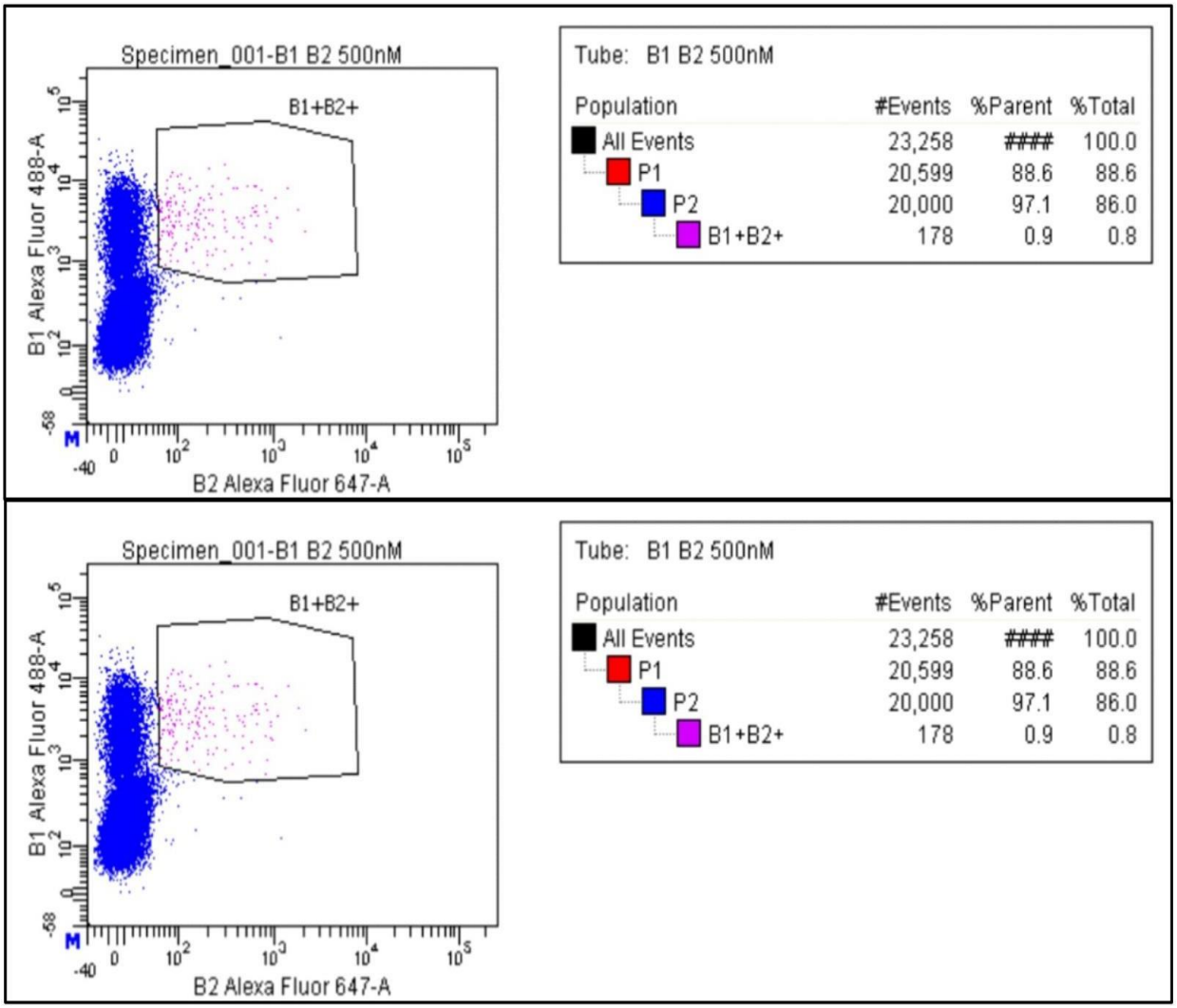

Figure C.4 Flow-assisted cell sorting data shows an increase in the non-competitive binding population of the cells expressing lysozyme binding monobodies from 0.9% in round 1 (A) to 2.9% in round 2(B).

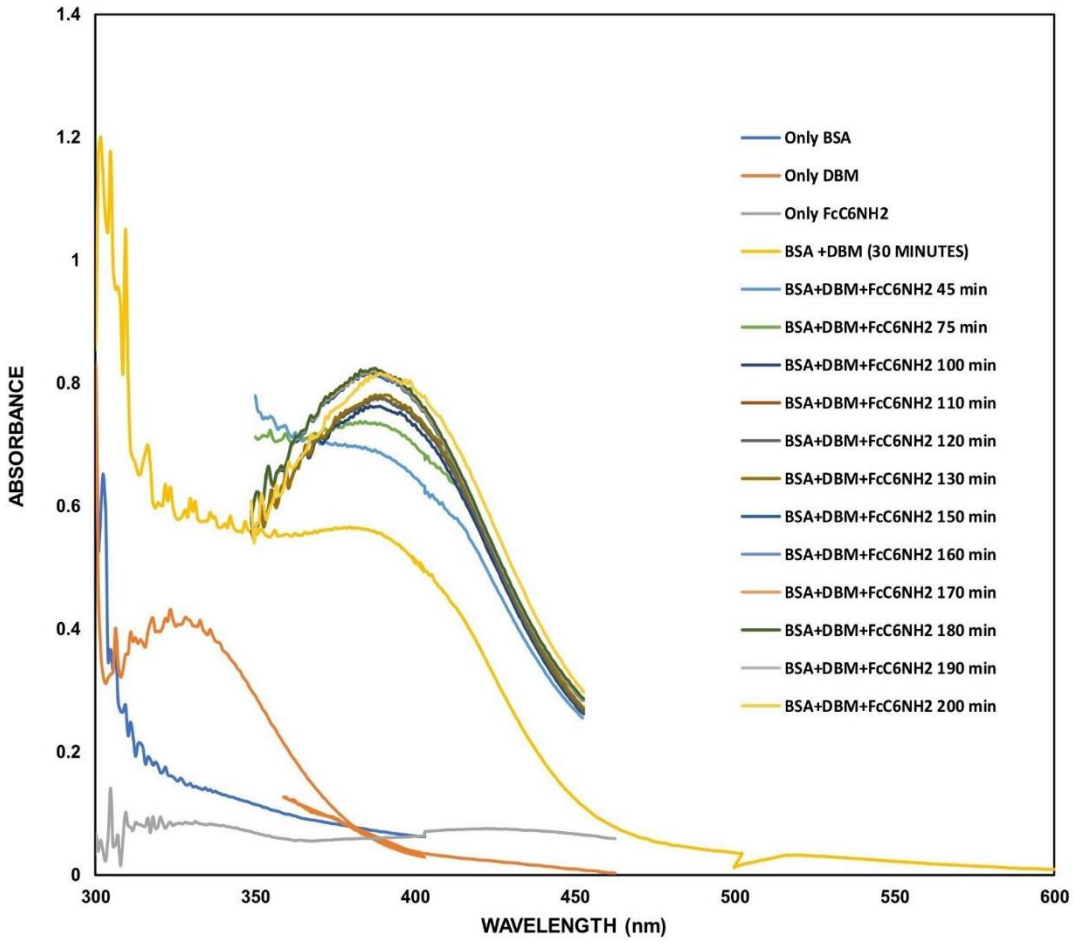

Figure C.5 Absorbance data showing BSA conjugation with ferrocene derivative using dibromomaleimide.